

2005

Large Scale Visualization of Pulsed Vortex Generator Jets

Kenneth Jay Moore Jr.
Wright State University

Follow this and additional works at: https://corescholar.libraries.wright.edu/etd_all



Part of the [Mechanical Engineering Commons](#)

Repository Citation

Moore, Kenneth Jay Jr., "Large Scale Visualization of Pulsed Vortex Generator Jets" (2005). *Browse all Theses and Dissertations*. 20.

https://corescholar.libraries.wright.edu/etd_all/20

This Thesis is brought to you for free and open access by the Theses and Dissertations at CORE Scholar. It has been accepted for inclusion in Browse all Theses and Dissertations by an authorized administrator of CORE Scholar. For more information, please contact library-corescholar@wright.edu.

LARGE SCALE VISUALIZATION OF
PULSED VORTEX GENERATOR JETS

A thesis submitted in partial fulfillment
of the requirements for the degree of
Master of Science

By

KENNETH JAY MOORE, JR.
B.S.M.E., Cedarville University, 2002

2005
Wright State University

WRIGHT STATE UNIVERSITY

SCHOOL OF GRADUATE STUDIES

April 14, 2005

I HEREBY RECOMMEND THAT THE THESIS PREPARED UNDER MY SUPERVISION BY Kenneth Jay Moore, Jr. ENTITLED Large Scale Visualization of Pulsed Vortex Generator Jets BE ACCEPTED IN PARTIAL FULFILLMENT OF THE REQUIREMENTS FOR THE DEGREE OF Master of Science

Mitch Wolff, Ph.D.
Thesis Director

Richard Bethke, Ph.D.
Department Chair

Committee on
Final Examination

Mitch Wolff, Ph.D.

David Johnston, Ph.D.

Scott Thomas, Ph.D.

Marc Polanka, Ph.D.

Rolf Sondergaard, Ph.D.

Joseph F. Thomas, Jr., Ph.D.
Dean, School of Graduate Studies

ABSTRACT

Moore, Kenneth Jay. M.S., Department of Mechanical and Materials Engineering, Wright State University, 2005. Large Scale Visualization of Pulsed Vortex Generator Jets.

The use of small jets of air has proven to be an effective means of flow control on low Reynolds number turbine blades. Pulsing of these jets has also shown benefits in reducing the amount of air needed to achieve the same level of flow control. An experiment using Hot Wire Anemometry and Particle Image Velocimetry (PIV) has been used to investigate how these pulsed jets interact with the boundary layer to help keep the flow attached. A 25x scaled jet in a flat plate has been utilized. The 25.4 mm diameter jet has a pitch angle of 30° and a skew angle of 90° . Pitch angle is defined as the angle the jet makes with the surface of the plate, and the skew angle is the angle that the projection of the jet on the surface makes with the crossflow. The jet was pulsed at both 0.5 Hz and 4 Hz with varying pulse durations (duty cycles), as well as various blowing ratios (ratio of the jet velocity to the freestream velocity). Duty cycles of 10, 25, 50, and 100 percent were implemented at a blowing ratio of unity. Blowing ratios of 0.5, 1, 2, and 4 were implemented at a 50% duty cycle and at 0.5 Hz. Velocity and vorticity planes were obtained at various spanwise locations and used in the characterization of the jet flow. Both the free jet as well as the jet in crossflow were studied. A calibration experiment was also performed using PIV on a rotating disk.

The calibration experiment was successful and the PIV results averaged a 1.56% error. The hot wire experiment with the free jet showed that the starting vortex is a key event at the beginning of each cycle, and the end of each cycle included a “kick-back” and a suction effect that could also have an influence on the boundary layer. The PIV

experiment was performed first on the free jet, and results were comparable to the hot wire results. When the PIV experiment was performed on the jet in crossflow, it was clear that both the beginning and ending events of the jet cycle were keys to eliminating or delaying flow separation. The effect of the beginning and ending events can be used to keep the flow attached for longer periods of time by increasing the frequency of the jet pulse. Due to limitations of the setup, higher frequency cases could not be studied. However, the experiment was successful in controlling a separated crossflow for blowing ratios greater than unity. The larger blowing ratios resulted in larger attachment size, and were able to sustain attachment for longer time periods.

TABLE OF CONTENTS

	<u>page</u>
1. INTRODUCTION	1
1.1 Background.....	1
1.2 Motivation.....	2
1.3 Parameter Matching.....	3
1.4 Literature Review	3
2. EXPERIMENTAL FACILITIES AND SETUP.....	10
2.1 Rotating Disk Experiment	10
2.2 Hot Wire Experiment.....	11
2.3 PIV Experiment	12
3. ROTATING DISK RESULTS AND ANALYSIS.....	15
3.1 $\omega = 35.5$ rad/s case.....	16
3.2 $\omega = 57.1$ rad/s case.....	22
3.3 $\omega = 161.1$ rad/s case.....	23
3.4 $\omega = 238.7$ rad/s case.....	25
3.5 $\omega = 123.2$ rad/s case.....	27
3.6 $\omega = 66.1$ rad/s case.....	29
3.7 $\omega = 140.6$ rad/s case.....	31
3.8 $\omega = 120.7$ rad/s case.....	33
3.9 Conclusions for the rotating disk experiment.....	35
4. FREE JET RESULTS AND ANALYSIS.....	39
4.1 Hot Wire Results.....	39
4.1.1 Conclusions for free jet hot wire experiment	47
4.2 PIV Results	48
4.2.1 Uncertainty and Verification of PIV Data	48
4.2.2 Steady Case ($\Delta = 100\%$).....	51
4.2.3 Unsteady 10% Duty Cycle Case.....	51
4.2.4 Unsteady 25% Duty Cycle Case.....	53
4.2.5 Unsteady 50% Duty Cycle Case.....	54
4.2.6 Conclusions for free jet PIV experiment	60
5. JET IN CROSSFLOW RESULTS AND ANALYSIS	62
5.1 Separated Flow Case (No Jet Blowing).....	62
5.2 Duty Cycle Comparison	63
5.3 Effect of Blowing Ratio.....	66

5.3.1 B = 4 Case ($f = 0.5$ Hz, $\Delta = 50\%$)	67
5.3.2 B = 2 Case ($f = 0.5$ Hz, $\Delta = 50\%$)	70
5.3.3 B = 1 Case ($f = 0.5$ Hz, $\Delta = 50\%$)	72
5.3.4 B = 0.5 Case ($f = 0.5$ Hz, $\Delta = 50\%$)	74
5.4 Conclusions for jet in crossflow experiment	75
6. SUMMARY AND CONCLUSIONS	82
APPENDIX A. Background to Particle Image Velocimetry	85
PIV Error Reduction	88
APPENDIX B. ROTATING DISK SETUP AND PROCEDURE	92
APPENDIX C. HOT WIRE EXPERIMENTAL SETUP AND PROCEDURE	105
APPENDIX D. PIV EXPERIMENTAL SETUP AND PROCEDURE	110
Free Jet	110
Jet in Crossflow	119
APPENDIX E. MatLab Code for Plotting Rotating Disk Data	127
Cont.m	127
APPENDIX F. MatLab and TecPlot Codes Used for Hot Wire Experiment	130
Hwplot.m	130
velvort.mcr	134
Aviexport.mcr	139
APPENDIX G. MatLab and TecPlot Codes Used for Free Jet PIV Experiment	141
imagesort.m	141
imagesortsteady.m	143
PIVplot.m	144
PIVplotsteady.m	150
velvort.mcr	155
aviexport.mcr	160
APPENDIX H. MatLab and TecPlot Codes Used for Jet in Crossflow PIV Experiment	162
velvort2.mcr	162
PIVplot3D.m	168
REFERENCES	171
BIOGRAPHICAL SKETCH	173

LIST OF FIGURES

<u>Figure</u>	<u>page</u>
Figure 1-1. Flat plate vortex generator jet.	2
Figure 2-1. Rotating disk experimental setup.	11
Figure 2-2. Picture of flat plate and hot wire traverse showing measurement plane.	12
Figure 2-3. Picture of free jet PIV setup.	13
Figure 2-4. Ramp location, axis information, and data plane measurement locations.	14
Figure 3-1. Sample PIV images of $\omega = 35.5$ rad/s rotating disk.	17
Figure 3-2. Exact velocity (m/s) based on known disk speed of $\omega = 35.5$ rad/s.	18
Figure 3-3. Velocity contours based on output from PIV correlation.	18
Figure 3-4. Contours showing comparison between “exact” and “calculated” velocities.	19
Figure 3-5. Contours showing percent error between experimental and known velocities.	19
Figure 3-6. Velocity comparison and percent error of $\omega = 57.1$ rad/s disk correlated with 32 x 32 pixel IR (top) and 64 x 64 pixel IR (bottom).	22
Figure 3-7. Velocity comparison and percent error of $\omega = 161.1$ rad/s disk correlated with 32 x 32 pixel IR (top), 64 x 64 pixel IR (middle), and 128 x 128 pixel IR (bottom).	24
Figure 3-8. Velocity comparison and percent error of $\omega = 238.7$ rad/s disk correlated with 32 x 32 pixel IR (top), 64 x 64 pixel IR (middle), and 128 x 128 pixel IR (bottom).	26
Figure 3-9. Velocity comparison and percent error of $\omega = 123.2$ rad/s disk correlated with 32 x 32 pixel IR (top), 64 x 64 pixel IR (middle), and 128 x 128 pixel IR (bottom).	28
Figure 3-10. Velocity comparison and percent error of $\omega = 66.1$ rad/s disk correlated with 32 x 32 pixel IR (top), 64 x 64 pixel IR (middle), and 128 x 128 pixel IR (bottom).	30

Figure 3-11. Velocity comparison and percent error of $\omega = 140.6$ rad/s disk correlated with 32 x 32 pixel IR (top), 64 x 64 pixel IR (middle), and 128 x 128 pixel IR (bottom).....	32
Figure 3-12. Velocity comparison and percent error of $\omega = 120.7$ rad/s disk correlated with 32 x 32 pixel IR (top), 64 x 64 pixel IR (middle), and 128 x 128 pixel IR (bottom).....	34
Figure 3-13. Percent error for the cases with 128 x 128 pixel IR.....	36
Figure 3-14. Percent error for the cases with 64 x 64 pixel IR.....	36
Figure 3-15. Percent error for the cases with 32 x 32 pixel IR.....	37
Figure 3-16. Effect of particle image displacement on PIV uncertainty. Taken from Raffel, et al [17].	38
Figure 4-1. Normalized vorticity plots (Hot-wire measurement). $f = 4$ Hz, $\Delta = 50\%$	40
Figure 4-2. Normalized velocity plots (Hot-wire measurement). $f = 4$ Hz, $\Delta = 50\%$	41
Figure 4-3. Normalized vorticity plots (Hot-wire measurement). $f = 4$ Hz, $\Delta = 25\%$	42
Figure 4-4. Normalized velocity plots (Hot-wire measurement). $f = 4$ Hz, $\Delta = 25\%$	43
Figure 4-5. Normalized vorticity plots (Hot-wire measurement). $f = 4$ Hz, $\Delta = 10\%$	44
Figure 4-6. Normalized velocity plots (Hot-wire measurement). $f = 4$ Hz, $\Delta = 10\%$	45
Figure 4-7. Centerpoint velocity of $f = 0.5$ Hz, 50% duty cycle jet.....	49
Figure 4-8. Normalized hot wire velocity data. $f = 4$ Hz, $\Delta = 50\%$	50
Figure 4-9. Normalized PIV velocity data. $f = 4$ Hz, $\Delta = 50\%$	50
Figure 4-10. Velocity (left), vorticity on wider scale (middle), and vorticity on narrower scale (right) of steady jet.	51
Figure 4-11. Normalized velocity plots (PIV measurement). $f = 0.5$ Hz, $\Delta = 10\%$	55
Figure 4-12. Normalized vorticity plots (PIV measurement). $f = 0.5$ Hz, $\Delta = 10\%$	56
Figure 4-13. Normalized velocity plots (PIV measurement). $f = 0.5$ Hz, $\Delta = 25\%$	57
Figure 4-14. Normalized vorticity plots (PIV measurement). $f = 0.5$ Hz, $\Delta = 25\%$	58
Figure 4-15. Normalized velocity plots (PIV measurement). $f = 0.5$ Hz, $\Delta = 25\%$	59

Figure 4-16. Normalized vorticity plots (PIV measurement). $f = 0.5$ Hz, $\Delta = 50\%$	60
Figure 5-1. Separated Flow ($B = 0$, $y = 2.25d$).....	63
Figure 5-2. Ramp location, axis information, and data plane measurement locations.....	64
Figure 5-3. First 10% of the $\Delta = 10\%$ case (a) and $\Delta = 50\%$ case (b), $F^+ = 0.004$, $B = 2$, $y = 5.25d$. The plots are velocity magnitude normalized by U_∞ (top), and in-plane vorticity normalized by U_∞/d (bottom).	65
Figure 5-4. First 10% after valve closure of the $\Delta = 10\%$ case (a) and $\Delta = 50\%$ case (b), $F^+ = 0.004$, $B = 2$, $y = 5.25d$. The plots are normalized as in Figure5-3.....	66
Figure 5-5. Normalized velocity plots (velocity magnitude divided by U_∞) for $B = 4$, $F^+ = 0.004$ Hz, $\Delta = 50\%$ case.....	69
Figure 5-6. Normalized velocity plots (velocity magnitude divided by U_∞) for $B = 2$, $F^+ = 0.004$ Hz, $\Delta = 50\%$ case.....	72
Figure 5-7. Normalized velocity plots (velocity magnitude divided by U_∞) for $B = 1$, $F^+ = 0.004$ Hz, $\Delta = 50\%$ case.....	74
Figure 5-8. Normalized velocity plots (velocity magnitude divided by U_∞) for $B = 0.5$, $F^+ = 0.004$ Hz, $\Delta = 50\%$ case.....	75
Figure 5-9. Maximum and minimum in-plane vorticity (averaged spanwise).	77
Figure 5-10. Attachment time and length (averaged spanwise).	77
Figure A-1. Basic PIV setup showing the different components of a PIV system.....	87
Figure A-2. Breakdown of images into interrogation regions that are correlated to give a velocity vector.	88
Figure B-1. Rotating disk with controller box.	93
Figure B-2. Rotating disk calibration curve.....	93
Figure B-3. Rotating disk experimental setup.	94
Figure B-4. Sketch of rotating disk setup. Dimensions are in meters.....	95
Figure B-5. Timing diagram for Kodak ES 4.0 camera.....	96
Figure B-6. Burn of Laser A (left) and Laser B (right).	98
Figure B-7. Sample PIV images of rotating disk (Image A left, Image B right).....	99
Figure B-8. Vector map (left) and contour plot (right) for 1153 RPM disk.	100

Figure B-9. Comparison of PIV “calculated” velocity values to expected “exact” values.	101
Figure B-10. Contours showing percent error between experimental and known velocities.	101
Figure C-1. TSI Model 1241 Standard "X" Probe (source: www.tsi.com).	106
Figure C-2. Schematic of hot wire experimental setup.	108
Figure C-3. Picture of flat plate and hot wire traverse showing measurement plane.	108
Figure D-1. Calibration curve for pressure transducer (Druck PDCR 22).	112
Figure D-2. Schematic of new hot wire traverse setup.	114
Figure D-3. Schematic of free jet PIV setup.	115
Figure D-4. Picture of free jet PIV setup.	116
Figure D-5. Ramp location, axis information, and data plane measurement locations.	122

LIST OF TABLES

<u>Table</u>	<u>page</u>
Table 3-1. Rotating Disk Test Cases.....	16
Table 3-2. Correlation settings and results for $\omega = 35.5$ rad/s case	21
Table 3-3. Correlation settings and results for $\omega = 57.1$ rad/s case	23
Table 3-4. Correlation settings and results for $\omega = 161.1$ rad/s case	25
Table 3-5. Correlation settings and results for $\omega = 238.7$ rad/s case	27
Table 3-6. Correlation settings and results for $\omega = 123.2$ rad/s case	29
Table 3-7. Correlation settings and results for $\omega = 66.1$ rad/s case	31
Table 3-8. Correlation settings and results for $\omega = 140.6$ rad/s case	33
Table 3-9. Correlation settings and results for $\omega = 120.7$ rad/s case	35
Table 5.1. Summary of attachment characteristics for the $B = 4$ case.....	68
Table 5.2. Summary of attachment characteristics for the $B = 2$ case.....	71
Table 5.3. Summary of attachment characteristics for the $B = 1$ case.....	73
Table 5.6. Summary of averaged attachment from each case plus max and min vorticity.....	76
Table D-1. Mass flux for each blowing ratio studied.	120

LIST OF SYMBOLS

A^*	=	choked area of jet feed line, m^2
B	=	jet blowing ratio, $\rho_j V_j / \rho_\infty U_\infty$
B_{mean}	=	mean blowing ratio
B_{max}	=	maximum blowing ratio
C_{roll}	=	roll coefficient
C_l	=	lift coefficient
C_x	=	chord length, m
d	=	diameter of jet, m
d_τ	=	particle image diameter, pixels
f	=	jet pulsing frequency, Hz
f_s	=	data sampling rate, Hz
F^+	=	reduced (non-dimensional) frequency, $f L / U_\infty$
G^*	=	mass flux, \dot{m} / A^* , $kg/s\cdot m^2$
L	=	characteristic length, m
M_∞	=	freestream Mach number
\dot{m}	=	mass flow in jet feed line, kg/s
P_0	=	stagnation pressure in jet feed line, Pa
r	=	radial dimension from rotating disk center, m
R	=	specific gas constant, 287.04 J/kg-K for air
Re_j	=	jet Reynolds number, $V_j d \rho_j / \mu$

s	=	jet spacing, m
Str_j	=	jet Strouhal number, $f d/V_j$
t	=	time normalized by period
T	=	period, seconds
T_0	=	stagnation temperature in jet feed line, K
U_∞	=	freestream velocity, m/s
V	=	velocity magnitude, m/s, or pressure transducer voltage, mV
V_j	=	jet velocity magnitude at center of jet exit, m/s
V_{avg}	=	average velocity across span of jet opening for entire cycle, m/s
x, y, z	=	Cartesian coordinates, m
α	=	pitch angle, the angle the jet makes with the surface in degrees
α_a	=	angle of attack in degrees
β	=	skew angle, the angle the projection of the jet on the surface makes with the crossflow in degrees
δ	=	boundary layer thickness, m
Δ	=	duty cycle, the percentage of the cycle that the jet is blowing
γ	=	specific heat ratio, 1.4 for air
μ	=	dynamic viscosity, Pa-s
ρ_j	=	density of jet air, kg/m^3
ρ_∞	=	density of freestream air, kg/m^3
ω	=	disk speed in radians per second
ω_i	=	in-plane vorticity (y-z plane) normalized by U_∞/d
ω_j	=	in-plane vorticity (x-z plane) normalized by U_∞/d

ACKNOWLEDGMENTS

The author would like to thank the Dayton Area Graduate Studies Institute (DAGSI), contract PRUC-01-07, and the Air Force Research Laboratory (AFRL), contract F33615-98-C-2895, for their financial support for this research. The author would also like to thank the AFRL for the use of their facilities in this project. Special thanks to Dr. Marc Polanka, Dr. Rolf Sondergaard, and Dr. Mitch Wolff for their involvement in this project, and to Dr. David Johnston and Dr. Scott Thomas for serving on the thesis defense committee. The assistance of Dr. Chuck Cross, Gary Terborg, Dr. Greg Minkiewicz, Dr. Campbell Carter, Dr. Richard Rivir, Dr. Andrew Lethander and others in the Propulsion Directorate of AFRL is also acknowledged.

1. INTRODUCTION

1.1 Background

A large scale flat-plate model of a vortex generator jet was studied with a goal of learning the mechanisms that result in control of boundary layer separation, and to investigate the jet interaction with the freestream flow. Boundary layer separation control is important in the low pressure turbine (LPT) because without control, the boundary layer flow can separate near the trailing edge of the blade suction surface. Boundary layer separation causes large aerodynamic losses in gas turbine engines. Lower density air at higher altitudes causes the Reynolds number of the flow to drop and these losses can increase dramatically. Associated with the increase in aerodynamic losses is a performance and efficiency decrease. By delaying flow separation, efficiency can be maintained at higher altitudes. These performance issues are what drive the desire to control boundary layer separation.

There are two main types of separation control: active and passive. Types of passive control include the use of dimples, slots, or grooves. Passive techniques permanently alter the blade design. What performs well at lower Reynolds numbers might be a detriment at higher Reynolds numbers. Active separation control has the benefit of the ability to be turned on or off, which provides more flexibility for optimization in a wider range of Reynolds numbers. Types of common active separation control techniques include the use of vortex generator jets (what this study is based on) and plasma actuators.

Flow control techniques studied at the Air Force Research Laboratory (AFRL) include the use of dimples, plasma actuators, and vortex generator jets (VGJs). Lake [1] was able to improve the loss coefficient by over 50% by applying dimples at 65% axial chord on a Pack-B blade geometry in the Low Speed Wind Tunnel (LSWT) facility. Current work is being done using plasma flow by Rivir et al. [2] at AFRL, while List et al. [3], have seen a reduction in loss coefficient of 14% at the Air Force Academy wind tunnel cascade (Langston blade geometry) using plasma actuators. VGJs have long been studied as a flow separation technique on airfoils, but recent studies by Bons et al. [4,5] in the LSWT have applied this technique to LPT blades. They successfully delayed flow separation on low Reynolds number turbine blades, reducing the loss coefficient by over 50%. In the Bons studies, pulsing the jets also proved to be effective, achieving the same benefits with up to an order of magnitude less mass flow.

1.2 Motivation

The physical reasons for separation delay using VGJs and the reasons pulsed jets are just as effective as steady jets are relatively unexplored. It would thus be desirable to visualize jet interaction with the boundary layer and to perform a detailed study of the resulting flow physics. A large scale flat plate model of the flow allows such a study. The work here is flat plate with a VGJ scaled 25x from the Pack-B VGJs studied in the LSWT. A picture of this flat plate jet is shown in Figure 1-1.



Figure 1-1. Flat plate vortex generator jet.

1.3 Parameter Matching

The flat plate jet is meant to be a scaled up version of the VGJs in the LSWT facility. That facility uses a PakB blade design, with one-millimeter diameter (0.04") jets, pitched at $\alpha = 30^\circ$ to the surface of the blade and skewed at $\beta = 90^\circ$ from the crossflow. The main blowing ratio (jet to freestream velocity ratio) studied there was $B = 2$, and the jets were typically pulsed at $f = 10$ Hz. With this configuration, the Reynolds number of the jet (based on the diameter of the jet) is $Re_j = 370$ and the reduced frequency of the pulsing is $F^+ = f l / U_\infty = 0.004$, where the characteristic length is the diameter of the VGJs ($L = d = 0.001$ m) and the freestream velocity is $U_\infty = 2.5$ m/s. Also, the approximate ratio of the boundary layer thickness to the jet diameter at the separation location was $\delta/d = 2.5$.

The flat plate jet in this study is scaled 25x to a one-inch (25.4 mm) diameter. It was also made with a $\alpha = 30^\circ$ pitch and $\beta = 90^\circ$ skew angle. The freestream velocity in the flat plate jet in crossflow experiment was $U_\infty = 3.15$ m/s. The reduced frequency is therefore matched at $F^+ = 0.004$ for the flat plate jet pulsed at $f = 0.5$ Hz if the characteristic length is again considered the jet diameter. The blowing ratio was also matched at $B = 2$, with other blowing ratios also studied ($B = 0.5, 1, 2, \text{ and } 4$). The boundary layer thickness at the jet location was approximately matched at 2.75 times the jet diameter ($\delta/d = 2.75$), without separation.

1.4 Literature Review

Johari and McManus [6] performed a flat plate experiment in a low-speed water tunnel, and found that the better performance of pulsed vortex generator jets (PVGJs) is attributed to the formation, stretching, and bending of the starting vortex ring, which

comes from the jet boundary layer fluid. The boundary layer shear of the crossflow amplifies the vorticity of the starting vortex and directs it in the streamwise direction. Separation control can be maximized within a certain frequency range at a low duty cycle. The trajectory of the jet in the far field scales with the blowing ratio. At an optimum pulsing frequency ($2.0 \leq f \leq 4.0$ Hz in water tunnel settings), the jet penetration can be increased by up to 100%. Important parameters that were studied were blowing ratio, jet diameter to boundary layer thickness ratio (d/δ), frequency, and duty cycle (Δ). The pitch angle of the jet was $\alpha = 45^\circ$, and the skew angle was $\beta = 90^\circ$. They found that the starting vortex grows in size and strength, then pinches off from the jet flow and proceeds ahead of the jet. Shortly after starting vortex separation, the jet begins to resemble a steady state jet. It is the separation of the starting vortex that is the cause of the improvement of pulsed VGJs over steady VGJs, therefore jet injection time should be limited to that of the starting vortex formation time (which can be estimated by $4d/V_j$), and the frequency should be optimized so that there is a prescribed distance between successive starting vortex rings (a maximum jet Strouhal number of $Str = 0.5*(1-\Delta)$). Increasing jet diameter would increase vortex ring circulation, however larger rings penetrate the boundary layer quicker and have less time for interaction. So there is an optimum jet diameter to maximize the effectiveness of streamwise vorticity augmentation. The source of streamwise vorticity is the boundary layer fluid of the jet rolling up into a vortex ring and getting deformed by the shear in the freestream boundary layer. A minimum jet diameter is required to form a starting vortex, and a minimum velocity ratio of unity is required to create starting vortex rings that remain coherent

within the boundary layer. The diameter of the VGJ should be smaller than the boundary layer thickness.

Compton and Johnston [7] found that the benefits of separation control are seen only if jets are pitched and skewed with respect to the main flow direction. Pitch angle is defined as the angle the jet makes with the surface of the plate, and the skew angle is the angle that the jet makes with the crossflow. The jet flow interacts with the main flow and generates a weak longitudinal vortex near the jet that persists well downstream and enhances cross-stream mixing. Maximum vorticity is strongly dependent on jet velocity and skew angle. Skew angles of $45^\circ \leq \beta \leq 90^\circ$ produce the strongest vortices. Studying the near field downstream of the jet may offer explanations for the interaction of the jet with the vorticity in the boundary layer. Important parameters studied were velocity ratio, and skew angle. The pitch angle was $\alpha = 45^\circ$, and only the steady jet was studied.

Bons et al. [8] performed a study with steady jet blowing at a chord location of $x/C_x = 73\%$ on an LPT blade model in a low-speed wind tunnel cascade. Both low and high freestream turbulence, as well as several blowing ratios were studied. It was found that above a minimum of $B = 0.6$, the wake loss is reduced by 65%. Boundary layer measurements were taken at $x/C_x = 67, 73, \text{ and } 79$ percent, and no significant adverse effects were seen when the jets are used at higher Reynolds numbers.

Milanovic and Zaman [9] studied a vortex generator jet in a turbulent boundary layer and looked at various blowing ratios ($1.22 \leq B \leq 4.47$), pitch angles ($\alpha = 20^\circ$ and 45°), and skew angles ($0^\circ \leq \beta \leq 90^\circ$). Larger velocity magnitudes occurred close to the wall for the $\alpha = 20^\circ$ case over the $\alpha = 45^\circ$ case. The larger pitch case had more upward penetration and more curvature. The skewed jet showed more spread than the unskewed

case. Peak streamwise vorticity occurred at $x/d = 3$ for $\beta = 15^\circ$ and 30° , and $x/d = 10$ for $\beta = 45^\circ$ and 60° (where x is the direction of the freestream and $x = 0$ is the location of the jet). For constant skew, smaller pitch results in larger peaks in the turbulence intensity of each of the three components of velocity.

Heinzen et al. [10], performed a PVGJ experiment on an Unmanned Air Vehicle (UAV) wing. The VGJs had $\alpha = \beta = 45^\circ$ pitch and skew angles. PVGJ effectiveness was measured by pressure distribution changes on the top surface, first in the wind tunnel and then in-flight. PVGJ were placed on the leading edge of the flap and delayed the onset of stall. The total weight of the UAV was still within design limits, but the blowing unit could only be installed on one wing (the right wing). The PVGJ system added 16.9 lbs to the 43.5 lb UAV. Reduced frequencies (based on flap chord length) near unity were most effective, but lower frequencies were also effective. They found significant increases in performance for PVGJs over steady VGJs for similar momentum flux. When implemented in flight, PVGJs caused increased lift on the right wing. Their conclusion was that PVGJs have application in high angle of attack control or in improving low speed performance.

McManus et al. [11] used a divergent lower wall in their test section to create separation, and placed three PVGJs upstream. The jets had diameters of $d = 2$ mm, were spaced $s = 1$ cm apart, and had $\alpha = 45^\circ$ pitch and $\beta = 90^\circ$ skew angles. They looked at freestream velocities of $U_\infty = 5.5$ and 11.5 m/s, blowing ratios of $0 \leq B \leq 10$, and frequencies of $0 \leq f \leq 500$ Hz. They found that PVGJs enhance cross-stream mixing in the boundary layer and delay separation. High speed flow in the freestream mixes with low speed boundary layer flow causing an increase in boundary layer momentum flux.

Flow-visualization suggested an optimum frequency of $f = 30$ Hz with a blowing ratio as low as $B = 2$ in order to control separation. Compared with steady VGJs, PVGJs showed significant improvements in separation control for a fixed mass flow rate.

McManus et al. [12] performed a PVGJ experiment on the leading edge flap of a flat plate airfoil model. Reduced frequency (based on wing chord length) was varied from $F^+ = 0.01$ to 3, and blowing ratio from $B = 0$ to 8. Stall was delayed by up to 5 degrees, and the optimal reduced frequency was $F^+ = 0.4$. An optimal jet diameter ($d = 3$ mm) and optimal jet spacing ($s = 12$ cm) was also found. Larger velocity ratios resulted in higher suction and a broader range of optimal frequency, although the peak was still at $F^+ = 0.4$. Lift was reduced for angles of attack of $12^\circ \leq \alpha_a \leq 18^\circ$, but above 18 degrees lift was increased, implying that lift is enhanced only at angles of attack above stall.

McManus and Magill [13] looked at PVGJs located at an airfoil leading edge. Freestream Mach number was varied from $M_\infty = 0.1$ to 0.5. The blowing ratio was kept at $B = 7.8$. At low Mach numbers, lift increases of up to 50% were observed with only small changes in drag. Modest lift enhancement was observed even at the highest Mach number. Reduced frequencies of $F^+ = 0.05$ to 2.0 were studied, with the characteristic length being the chord length of the wing ($L = C_x$). The optimal reduced frequency was $f = 0.6$, which was 30% higher than the optimal value for a flat plate model [12], implying that the optimal value is geometry dependent.

McManus and Magill [14] looked at a low-speed, Lambda-wing model, 7% scale, with PVGJs on the upper surface of the wing leading edge flaps. The VGJs were pitched 45° and skewed 90° . They found that PVGJs delayed flow separation and augmented lift. Control was optimized for reduced frequencies (based on wing chord length) near unity.

Control effectiveness monotonically increased with pulsing amplitude. The lift coefficient increased up to $C_l = 7\%$, and a roll coefficient of up to $C_{roll} = 0.011$ could be produced when applying PVGJs to one wing only.

Bons et al. [15] studied an LPT blade with Reynolds number matched to high-altitude aircraft engines and aft stages of industrial turbine engines with elevated turbine inlet temperatures. The PVGJs had $\alpha = 30^\circ$ pitch and $\beta = 90^\circ$ skew angles. Their frequency was $f = 10$ Hz and blowing ratios up to $B = 4$ were studied. Boundary layer separation was almost completely eliminated with pulsed blowing. Wake loss reductions of over 50% were measured. They concluded that the key mechanism is the starting and stopping of the pulses rather than the injection itself. PVGJs were applied at $x/C_x = 45$ and 63 percent, and were effective at both positions. Freestream turbulence was less than 1%, and the boundary layer was laminar. At $x/C_x = 45\%$, effective control was observed as low as $B_{mean} = 0.5$ for the pulsed jets (with duty cycle of $\Delta = 50\%$). For the steady jets this required $B_{mean} = 2$ to achieve the same control. At $x/C_x = 63\%$, control was achieved at $B_{mean} = 2$ for steady and $B_{mean} = 0.2$ for pulsed jets. That is an order of magnitude less mass flow in the pulsed case, and a mere 0.02% additional massflow to the LPT throughflow. The boundary layer thickness was $\delta = 2.5$ mm (2.5d). For constant B_{max} , pulsing was still effective as low as 1% duty cycle ($B_{mean} = 0.05$). At 63% chord (near the natural separation point), PVGJs influence separation by initiating early boundary layer transition. At 45% chord, PVGJs influence separation by drawing free-stream momentum down to the wall. Frequencies ranging from $10 \leq f \leq 100$ Hz produced similar results. Steady jets influence separation by a shedding instability as well as by

free-stream momentum entrainment. Pulsing may play a reduced role at higher Re since the boundary layer may already be turbulent.

Bons et al. [16] again looked at the LPT blade and found PVGJ control effectiveness with up to a 60% wake loss reduction for reduced frequencies as low as $F^+ = 0.1$ and duty cycles as low as $\Delta = 10\%$ ($B_{\text{mean}} = 0.2$). Separation control at low frequencies is a result of the relaxation period of the boundary layer after being influenced by the jet flow. Relaxation time is an inherent property of the flow, therefore lower duty cycles are also effective.

2. EXPERIMENTAL FACILITIES AND SETUP

This study was divided into three phases. The first phase was a rotating disk experiment performed in order to become familiar with the equipment involved in the Particle Image Velocimetry (PIV) measurement technique. This also served as a calibration experiment. This was done using a rotating disk because the disk speed could be measured separately and compared to the PIV results. The second phase was a free jet experiment. In that experiment, hot wire measurements were taken to serve as a baseline for the PIV data that was also taken. In the final phase, the jet in crossflow was studied using PIV. This chapter describes the setup and facilities for each experiment.

2.1 Rotating Disk Experiment

The purpose of the rotating disk experiment was mainly to become more familiar to the PIV technique. A background study on PIV was also performed, and is included as Appendix A. The rotating disk experiment was performed on a tabletop in a small laboratory setting in Building 252 of Wright-Patterson Air Force Base, near the Low Speed Wind Tunnel (LSWT) facility. A picture of this setup is shown in Figure 2-1, with the green lines indicating the path of the laser beam. The disk speed was measured with an optical sensor, and this “exact” value was used to compare to the measured velocities gathered from the PIV method. Several tests were run using various laser timings and disk speeds until satisfactory results were obtained. Detailed setup procedures and the experimental process for the rotating disk experiment are shown in Appendix B.

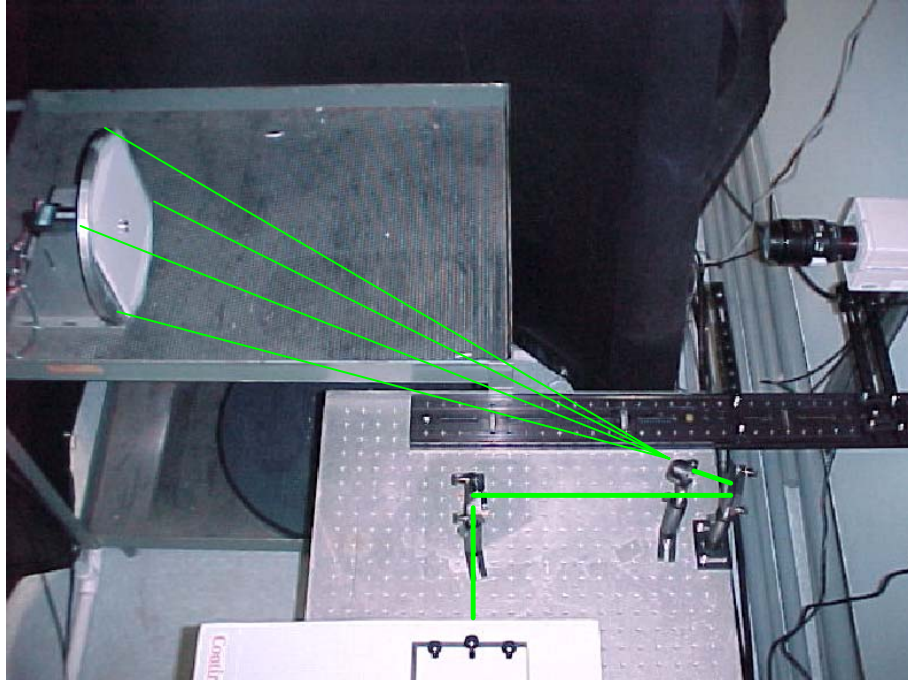


Figure 2-1. Rotating disk experimental setup.

2.2 Hot Wire Experiment

After verifying the ability to use PIV to gather accurate velocity measurements with the rotating disk experiment, the PIV method could be used on the vortex generator jet. But before making PIV measurements, a more familiar technique was used to measure the VGJ. This hot wire anemometry experiment would also provide a mode of comparison to the later PIV measurements. The hot wire experiment was set up on a bench top next to the Low Speed Wind Tunnel. A picture of this bench top hot wire traverse is shown in Figure 2-2. The red rectangular area shows the measurement plane traversed by the hot wire probe. The probe was mounted on a two-dimensional traverse also shown in Figure 2-2. The velocity data from the hot wire probe and the position data from the traverse were recorded using a LabView program, and the results were plotted using TecPlot. Three different cases were studied, with duty cycles of $\Delta = 10$, 25, and 50

percent, and used as a baseline for comparison to the PIV data to come later. Detailed setup procedures for the hot wire experiment are included in Appendix C.

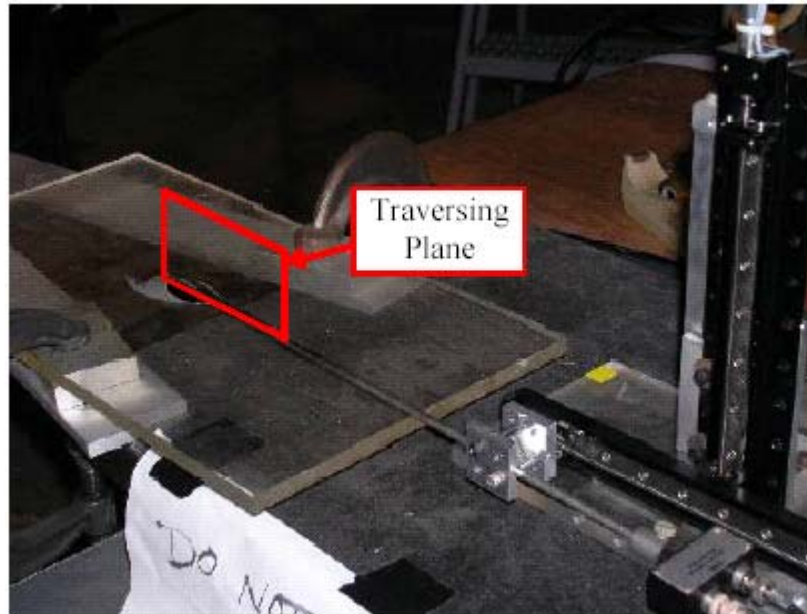


Figure 2-2. Picture of flat plate and hot wire traverse showing measurement plane.

2.3 PIV Experiment

2.3.1 Free Jet

The jet in the flat plate used in the hot wire experiment was duplicated for the PIV setup. It was placed at the end of the Boundary Layer Tunnel (BLT, another AFRL facility in Building 18C, Room 21), which is set on a table. This tunnel allowed the development of a crossflow when that became necessary. A picture of the setup used for this experiment is shown in Figure 2-3. This setup was different than that used in the previous hot wire experiment, so a baseline case was run using both the hotwire and the PIV methods in the BLT setup. After a satisfactory comparison of the PIV data to the hot wire data, the free jet PIV experiment was run using the same three cases as before, with $\Delta = 10, 25, \text{ and } 50\%$. A more detailed description of the setup and procedure for this experiment is shown in Appendix D.

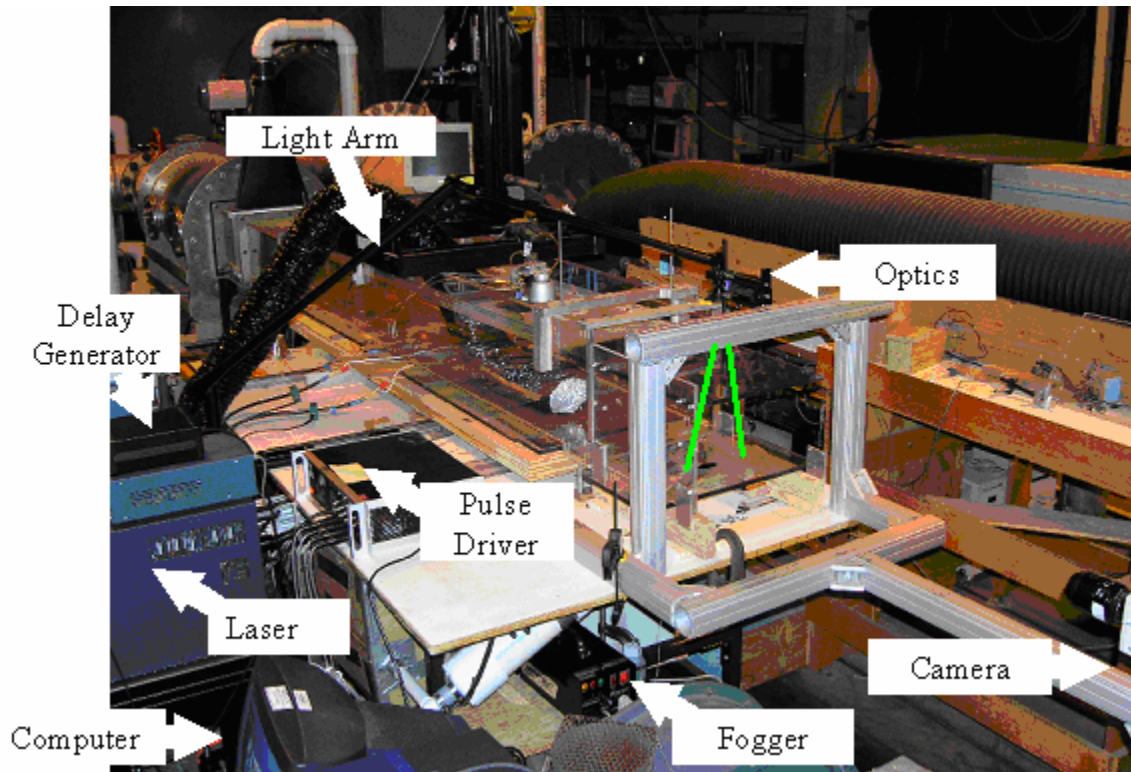


Figure 2-3. Picture of free jet PIV setup.

2.3.2 Jet in Crossflow

The setup for the jet in crossflow experiment was much the same as the free jet experiment. Of course the major difference is the added crossflow from the Boundary Layer Tunnel. The same facility was used and the setup is the same except the camera and light sheet are rotated 90° to measure the major (streamwise) velocity components in the x-z plane. Also, a ramp was added to the tunnel just upstream of the jet to create a separation region. A sketch of the jet in crossflow showing the data planes taken as well as the coordinate system is shown in Figure 2-4. Note the seven different planes of data indicated in the figure. These seven planes were combined to create three dimensional plots of the data, which helped in visualizing the jet interaction with the crossflow. The jet's effectiveness was determined by how well it mitigated the separation caused by the ramp. Two cases were run with different duty cycles ($\Delta = 10\%$ and 50%) at a fixed

frequency and blowing ratio ($f = 0.5$ Hz, $B = 1$). Then four more cases were run with different blowing ratios ($B = 0.5, 1, 2,$ and 4) at a fixed frequency and duty cycle ($f = 0.5$ Hz, $\Delta = 50\%$). Appendix D includes the detailed description of the setup and procedures for this jet in crossflow experiment.

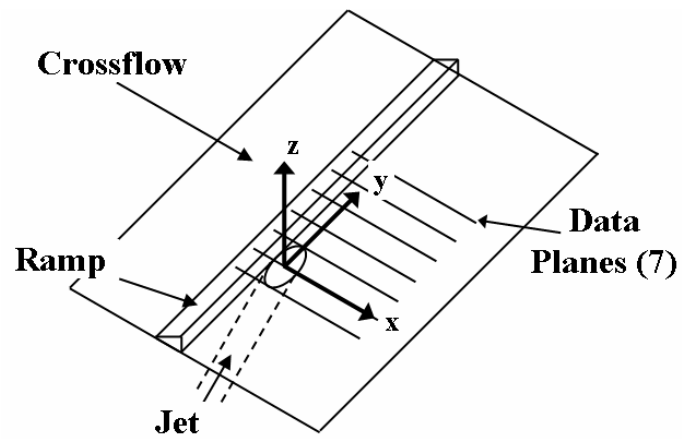


Figure 2-4. Ramp location, axis information, and data plane measurement locations.

3. ROTATING DISK RESULTS AND ANALYSIS

The procedure discussed in Appendix B was carried out for different speeds of the rotating disk. These speeds were $\omega = 35.5, 57.1, 161.1, 238.7, 123.2, 66.1, 140.6,$ and 120.7 rad/s (details of the calculation of disk speed are also in Appendix B). In addition, each case was analyzed with three different correlation techniques. Each was done with an adaptive correlation with different finishing interrogation region (IR) sizes of 128×128 pixels, 64×64 , and 32×32 pixels. A summary of the cases run is shown in Table 3-1. The three different correlation techniques were done in the final six cases, but only one was done in the first case, and two in the second case. In order for FlowManager (PIV processing software from Dantec Dynamics) to calculate velocity, it must know the width or height of the image (in millimeters) as well as the time between images. This information is shown in Table 3-1 for each case. FlowManager calculates the actual displacement by dividing the displacement of the particle (in pixels) by the width of the image (2048 pixels), then multiplying by the width of the image in millimeters. The velocity is then calculated by dividing the displacement (in millimeters) by the time between images (in microseconds), and then multiplying by 1000 to make the units meters per second.

Table 3-1. Rotating Disk Test Cases.

Disk Speed (rad/s)	Width (mm)	Δt (μ s)	Final IR (pixels)
35.5	143	10.2	128 x 128
57.1	143	10	64 x 64, 32 x 32
161.1	143	10	128 x 128, 64 x 64, 32 x 32
238.7	142.8	10	128 x 128, 64 x 64, 32 x 32
123.2	142.8	10	128 x 128, 64 x 64, 32 x 32
66.1	142.8	10	128 x 128, 64 x 64, 32 x 32
140.6	142.8	30	128 x 128, 64 x 64, 32 x 32
120.7	142.8	30	128 x 128, 64 x 64, 32 x 32

3.1 $\omega = 35.5$ rad/s case

Ninety-eight images (49 image pairs) were captured with the disk spinning at $\omega = 35.5$ rad/s. A sample of these image pairs is shown in Figure 3-1. These images were imported into FlowManager and correlated using an adaptive correlation. The adaptive correlation started with a correlation of 512 x 512 pixel interrogation regions, followed by four passes with 256 x 256 pixel interrogation regions, and finally four passes with 128 x 128 pixel interrogation regions. Each interrogation region was correlated with a 25% overlap. Each resulting vector map was filtered with a range validation where all vectors with a magnitude higher than 6 m/s were rejected. After the range validation, the vector map was applied with a moving average validation, where each vector was compared to those around it (in a 3 x 3 array) based on an acceptance factor of 0.01. If a vector was found outside the range of acceptance, it would be replaced by a more valid vector (eliminating erroneous vectors without losing data). After the moving average, the vector map would be sent through an average filter, which averages each vector based on those around it in a 3 x 3 vector array. Finally, all the vector maps (49) were averaged, and the scalar values of the velocities were exported to a spreadsheet, where the average

error and standard deviation of error were calculated based on the exact known velocities. MatLab was used to read in the exact and PIV calculated velocities from the spreadsheet, and used to plot contours for comparing the known to the calculated velocities and to create a scalar map of the percent error. The MatLab code used to create these plots is included as Appendix A. Figure 3-2 shows the exact velocity of the disk based on the known disk speed of $\omega = 35.5$ rad/s. Figure 3-3 shows the calculated velocity of the PIV correlation. Figure 3-4 shows a direct comparison of the two contour plots, and Figure 3-5 shows the percent error of the calculated velocity. A mask has been added in the error plot to indicate the location of the taped area where the extruded aluminum part of the disk was.

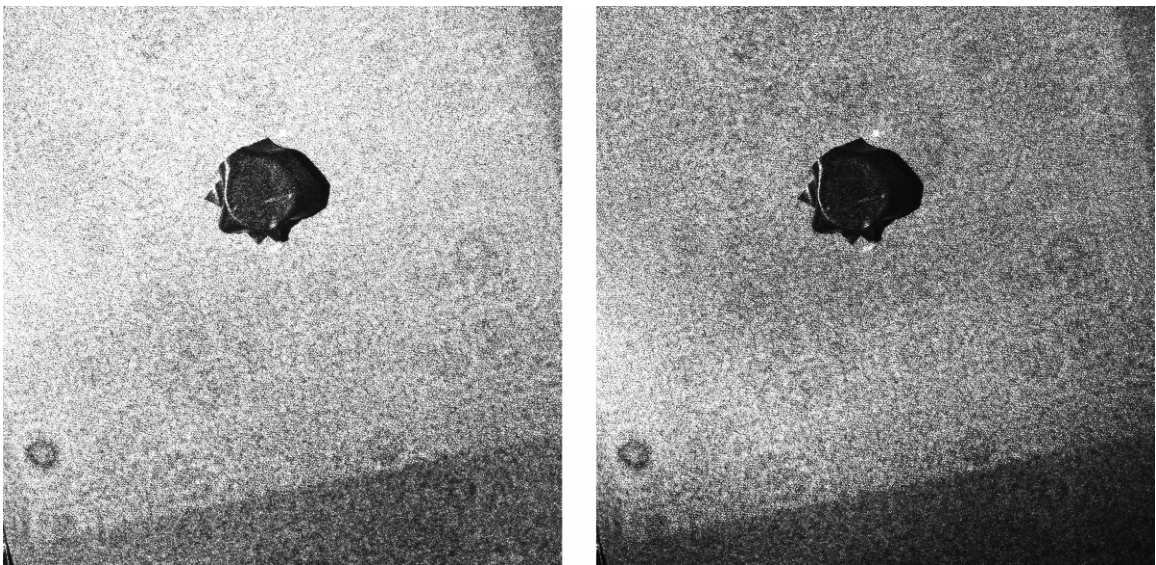


Figure 3-1. Sample PIV images of $\omega = 35.5$ rad/s rotating disk.

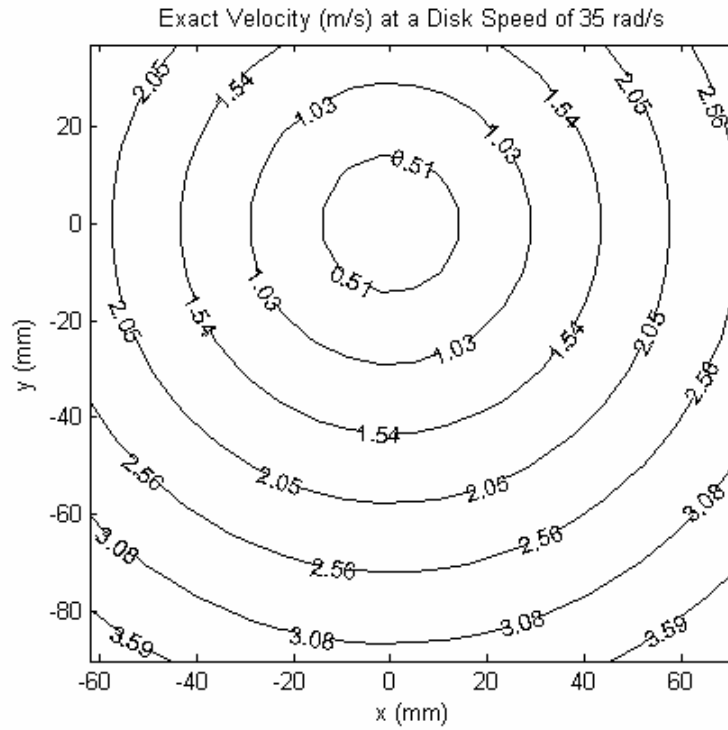


Figure 3-2. Exact velocity (m/s) based on known disk speed of $\omega = 35.5$ rad/s.

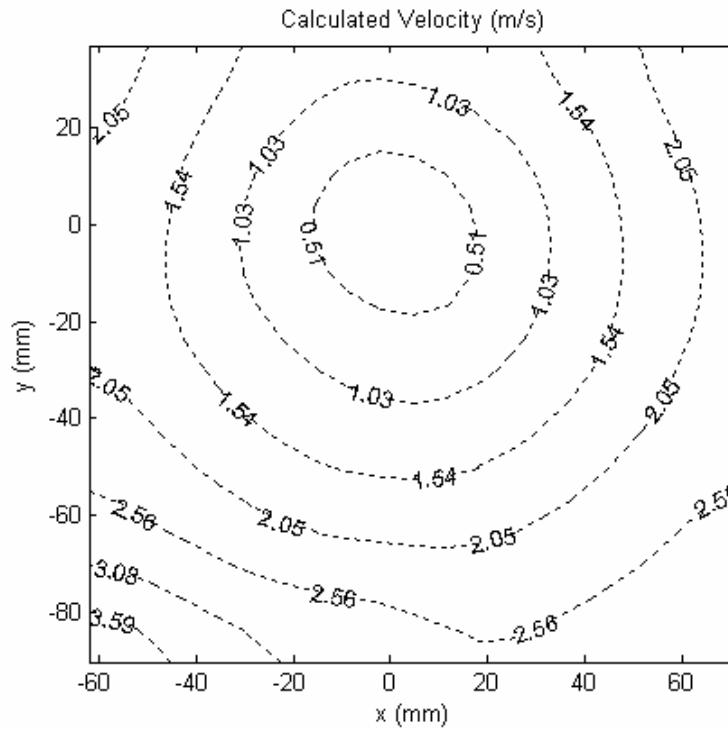


Figure 3-3. Velocity contours based on output from PIV correlation

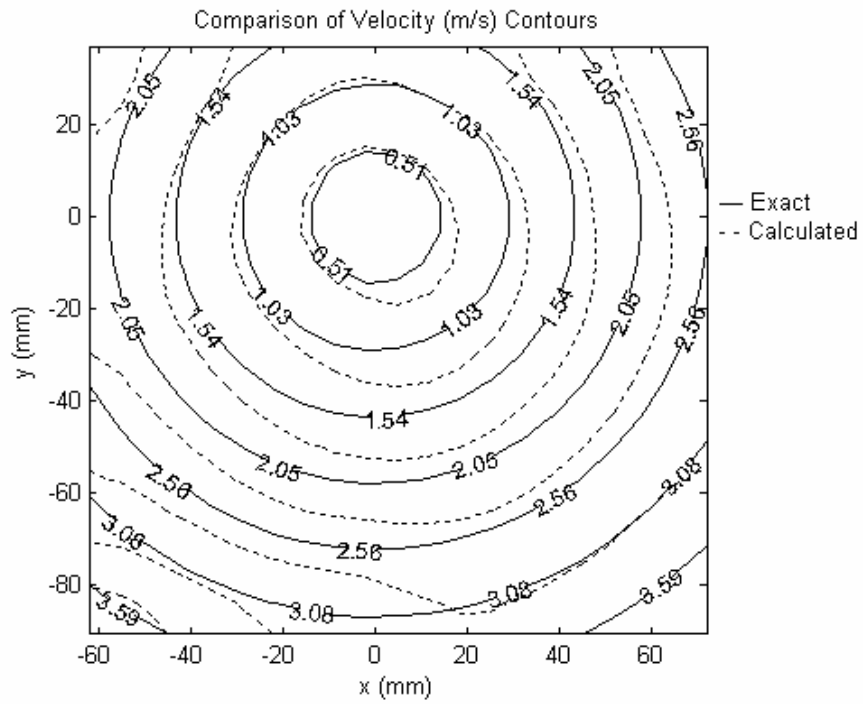


Figure 3-4. Contours showing comparison between “exact” and “calculated” velocities.

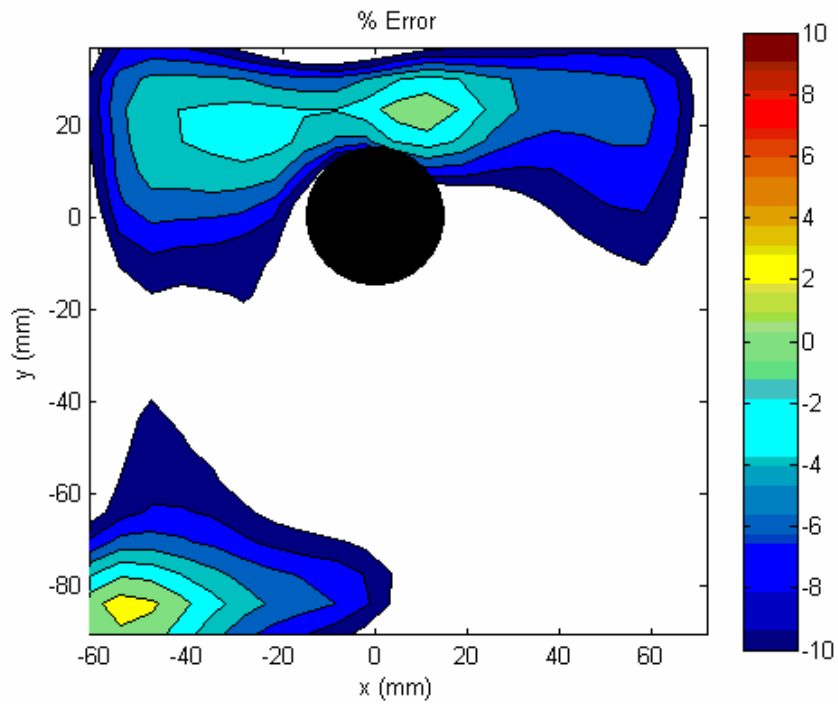


Figure 3-5. Contours showing percent error between experimental and known velocities.

The white areas of Figure 3-5 are where the percent error is greater than $\pm 10\%$. The average magnitude of the error in Figure 3-5 is 11.65% with a standard deviation of 6.17%. This error does not include the shaded area of Figure 3-5, which is a 14 mm circle centered at the origin. This case is summarized in Table 3-2. The first entry in the table is initial interrogation region (IR) size. The second is the number of refinement steps (two refinement steps with an initial IR size of 512 x 512 pixels means the second step in the adaptive correlation had 256 x 256 pixel IR sizes, and the third step had the final IR size of 128 x 128 pixels). The third entry is the final IR size. The fourth through sixth entries are the number of initial step passes (how many times the initial IR size was used before moving to the next step), intermediate step passes (how many times each subsequent IR size was used before moving to the final step), and final step passes (how many times the final IR size was used). The next two entries are the vertical overlap (the percentage of the IR that overlaps the IR directly below it) and the horizontal overlap (the percentage of the IR that overlaps the IR directly to the left). The ninth entry is the differencing method used to determine the correlation (either forward or central). The tenth entry is the method used to correlate the boundary (either move the second IR inside or substitute). The next entry is the range limit of velocity magnitude (above which velocity vectors would be rejected). The twelfth entry contains the moving average settings that were used, the thirteenth entry contains the average filter settings that were used, and the fourteenth entry indicates the radius that was used to reject the results from the center of the disk. The average velocity (based on the known disk speed), the average displacement (in pixels, based on the above mentioned average velocity), the average error, and the standard deviation of the error are each listed at the

end of the table. The application of the moving average and the average filter is the same for all cases, so those entries are eliminated from subsequent tables.

Table 3-2. Correlation settings and results for $\omega = 35.5$ rad/s case

Initial IR size (pixels)	512 x 512
Number of refinement steps	2
Final IR size (pixels)	128 x 128
Initial step passes	1
Intermediate step passes	4
Final step passes	4
Vertical overlap	25%
Horizontal overlap	25%
Differencing	Forward
Boundary	Move 2nd IR inside
Range (m/s)	6
Moving average	3 x 3 vector averaging area, 0.01 acceptance factor, one iteration, substitute invalidated, don't substitute previous invalidations, validate on boundary
Average filter	3 x 3 vector averaging area
Protrusion radius (mm)	14
Average velocity (m/s)	2.09
Avg displacement (pix)	0.31
Average error	11.65%
Std Dev of error	6.17%

3.2 $\omega = 57.1$ rad/s case

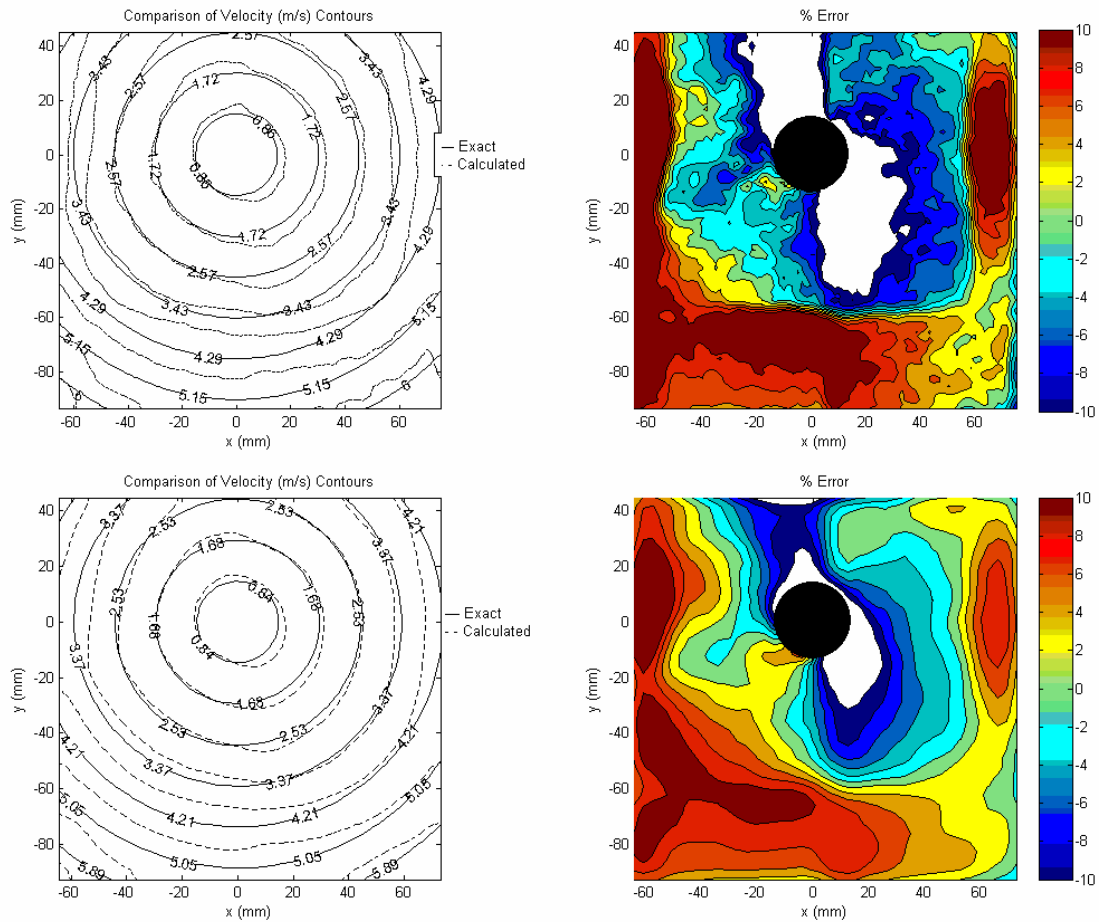


Figure 3-6. Velocity comparison and percent error of $\omega = 57.1$ rad/s disk correlated with 32 x 32 pixel IR (top) and 64 x 64 pixel IR (bottom).

Figure 3-6 shows the $\omega = 57.1$ rad/s case correlated with both 32 x 32 pixel and 64 x 64 pixel interrogation regions. The figures have been reduced in size to provide an easier comparison between the correlation methods. Table 3-3 shows the settings and results for both correlations. The average percent error is down from the previous case, and the 64 x 64 pixel interrogation regions resulted in smaller errors than the 32 x 32 pixel IR.

Table 3-3. Correlation settings and results for $\omega = 57.1$ rad/s case

Initial IR size (pixels)	512 x 512	512 x 512
Number of refinement steps	4	3
Final IR size (pixels)	32 x 32	64 x 64
Initial step passes	1	1
Intermediate step passes	4	4
Final step passes	1	3
Vertical overlap	25%	25%
Horizontal overlap	25%	25%
Differencing	Forward	Forward
Boundary	Move 2 nd IR inside	Move 2 nd IR inside
Range (m/s)	10	10
Protrusion radius (mm)	14	14
Average velocity (m/s)	3.40	3.37
Avg displacement (pix)	0.49	0.48
Average error	7.31%	5.60%
Std Dev of error	4.83%	3.77%

3.3 $\omega = 161.1$ rad/s case

Figure 3-7 shows the results of the $\omega = 161.1$ rad/s case, and the correlation methods and results are summarized in Table 3-4. Notice that the 32 x 32 pixel IR correlation method results in a noisier plot than the 64 x 64 pixel IR correlation method, and the 64 x 64 pixel IR method results in a noisier plot than the 128 x 128 pixel IR method. This is simply due to the higher resolution cases being able to show more points in the plot. The 64 x 64 IR correlation resulted in less error, but the combined percent error and standard deviation of error is least in the 128 x 128 IR correlation results. Note that the overall error and standard deviation are much lower than the previous two cases.

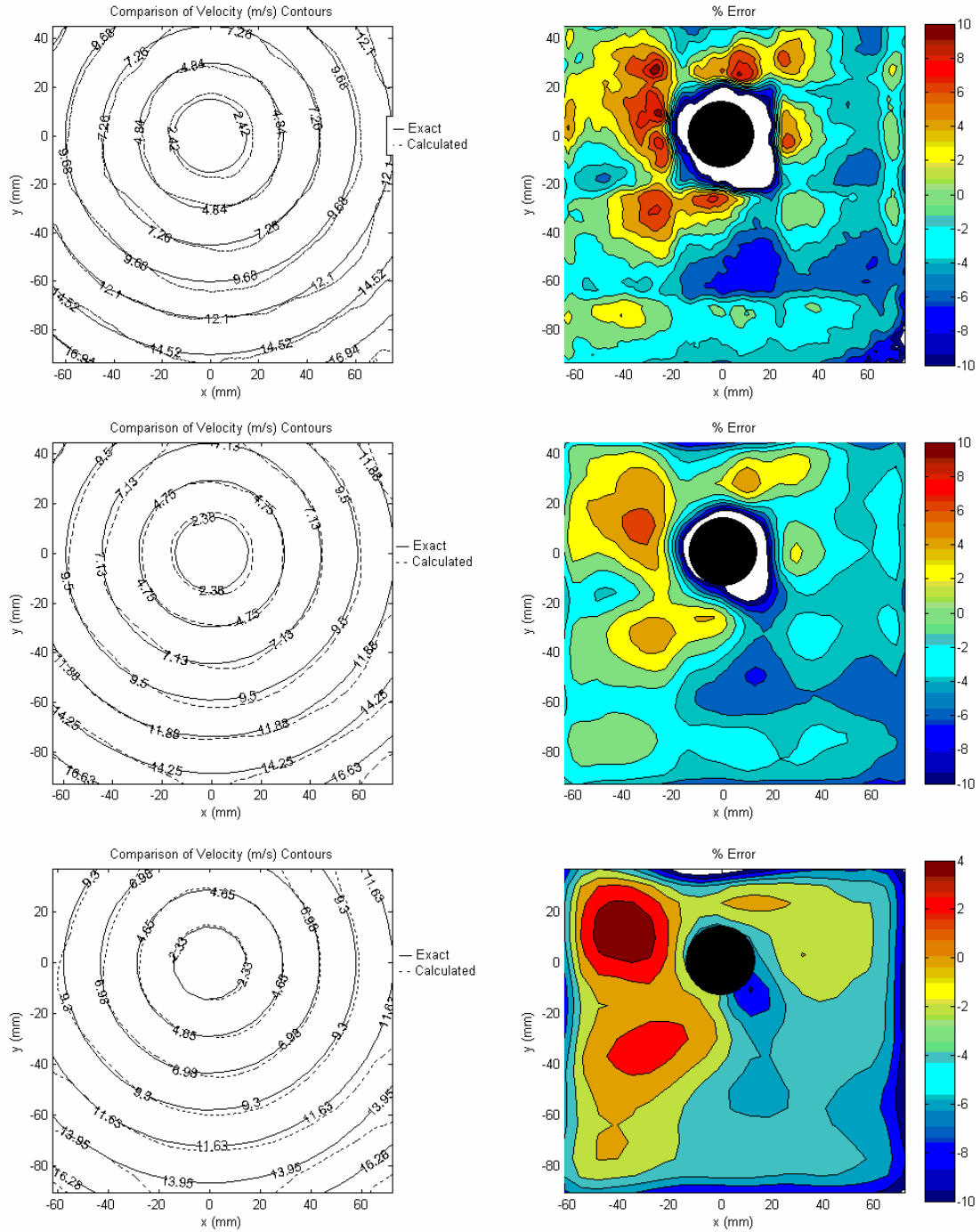


Figure 3-7. Velocity comparison and percent error of $\omega = 161.1$ rad/s disk correlated with 32 x 32 pixel IR (top), 64 x 64 pixel IR (middle), and 128 x 128 pixel IR (bottom).

Table 3-4. Correlation settings and results for $\omega = 161.1$ rad/s case

Initial IR size (pixels)	512 x 512	512 x 512	512 x 512
Number of refinement steps	4	3	2
Final IR size (pixels)	32 x 32	64 x 64	128 x 128
Initial step passes	1	1	1
Intermediate step passes	4	4	4
Final step passes	1	3	4
Vertical overlap	25%	25%	25%
Horizontal overlap	25%	25%	25%
Differencing	Forward	Forward	Forward
Boundary	Move 2nd IR inside	Move 2nd IR inside	Move 2nd IR inside
Range (m/s)	30	30	20
Protrusion radius (mm)	14	14	14
Average velocity (m/s)	9.59	9.52	9.50
Avg displacement (pix)	1.37	1.36	1.36
Average error	3.37%	2.82%	3.40%
Std Dev of error	3.32%	3.25%	2.56%

3.4 $\omega = 238.7$ rad/s case

Figure 3-8 shows the results of the $\omega = 238.7$ rad/s case, and the correlation methods and results are summarized in Table 3-5. The errors have decreased again with the increase in disk speed, however, the improvement is not as drastic this time. However, the standard deviation of error is down considerably from the previous case for the 64 x 64 and 32 x 32 IR methods.

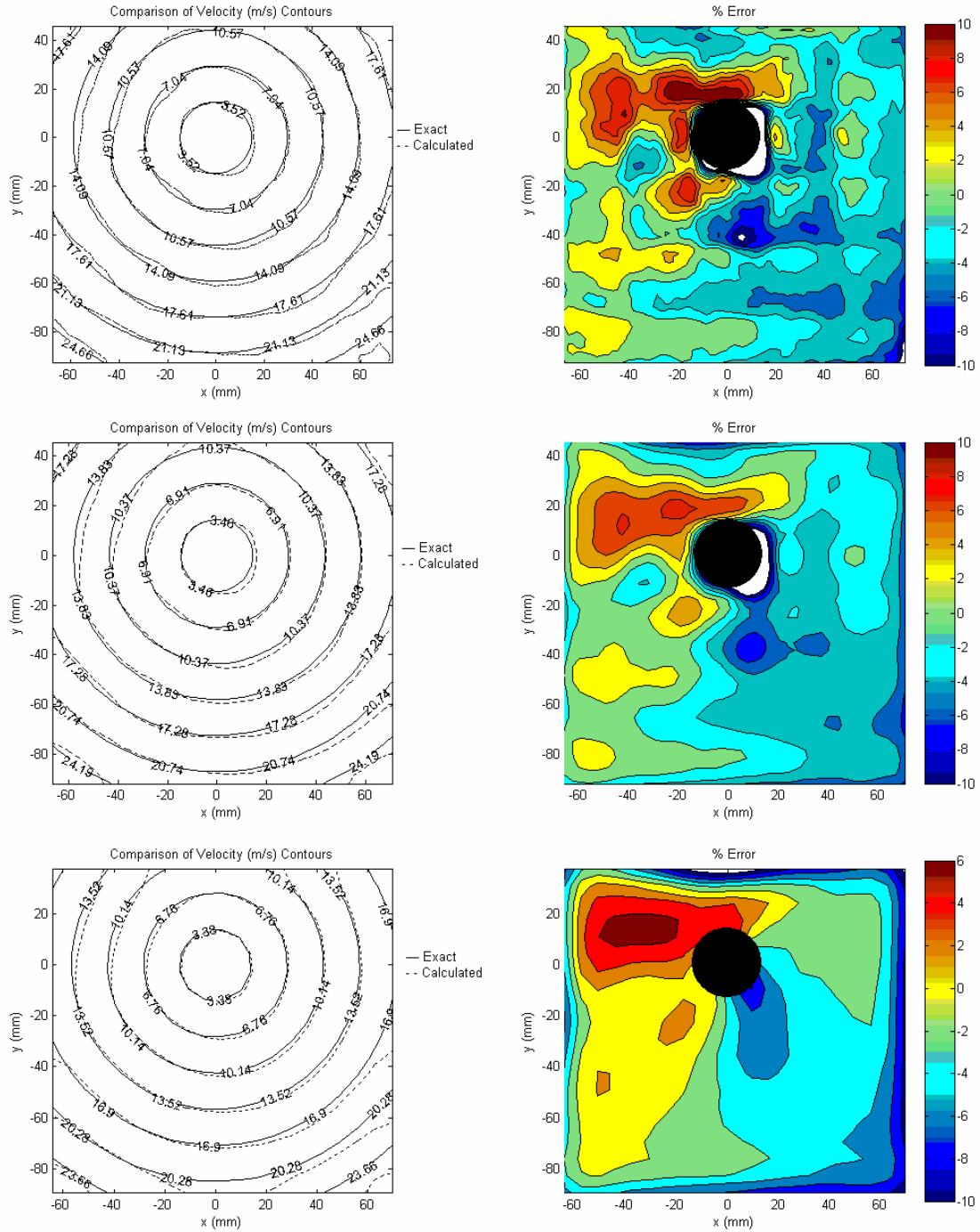


Figure 3-8. Velocity comparison and percent error of $\omega = 238.7$ rad/s disk correlated with 32 x 32 pixel IR (top), 64 x 64 pixel IR (middle), and 128 x 128 pixel IR (bottom).

Table 3-5. Correlation settings and results for $\omega = 238.7$ rad/s case

Initial IR size (pixels)	512 x 512	512 x 512	512 x 512
Number of refinement steps	4	3	2
Final IR size (pixels)	32 x 32	64 x 64	128 x 128
Initial step passes	1	1	1
Intermediate step passes	4	4	4
Final step passes	1	3	4
Vertical overlap	25%	25%	25%
Horizontal overlap	25%	25%	25%
Differencing	Forward	Forward	Forward
Boundary	Move 2nd IR inside	Move 2nd IR inside	Move 2nd IR inside
Range (m/s)	40	40	40
Protrusion radius (mm)	14	14	14
Average velocity (m/s)	14.10	14.02	13.94
Avg displacement (pix)	2.02	2.01	2.00
Average error	2.92%	2.64%	3.26%
Std Dev of error	2.55%	2.03%	2.39%

3.5 $\omega = 123.2$ rad/s case

Figure 3-9 shows the results of the $\omega = 123.2$ rad/s case, and the correlation methods and results are summarized in Table 3-6. In this case, the errors have increased to make the results worse than the previous two cases, but still better than the first two. This case has a higher velocity than the first two cases and a lower velocity than the previous two. The best results for this case are for the 128 x 128 pixel IR method, with an error approximately equal to that of the 64 x 64 pixel IR case, but a standard deviation much smaller.

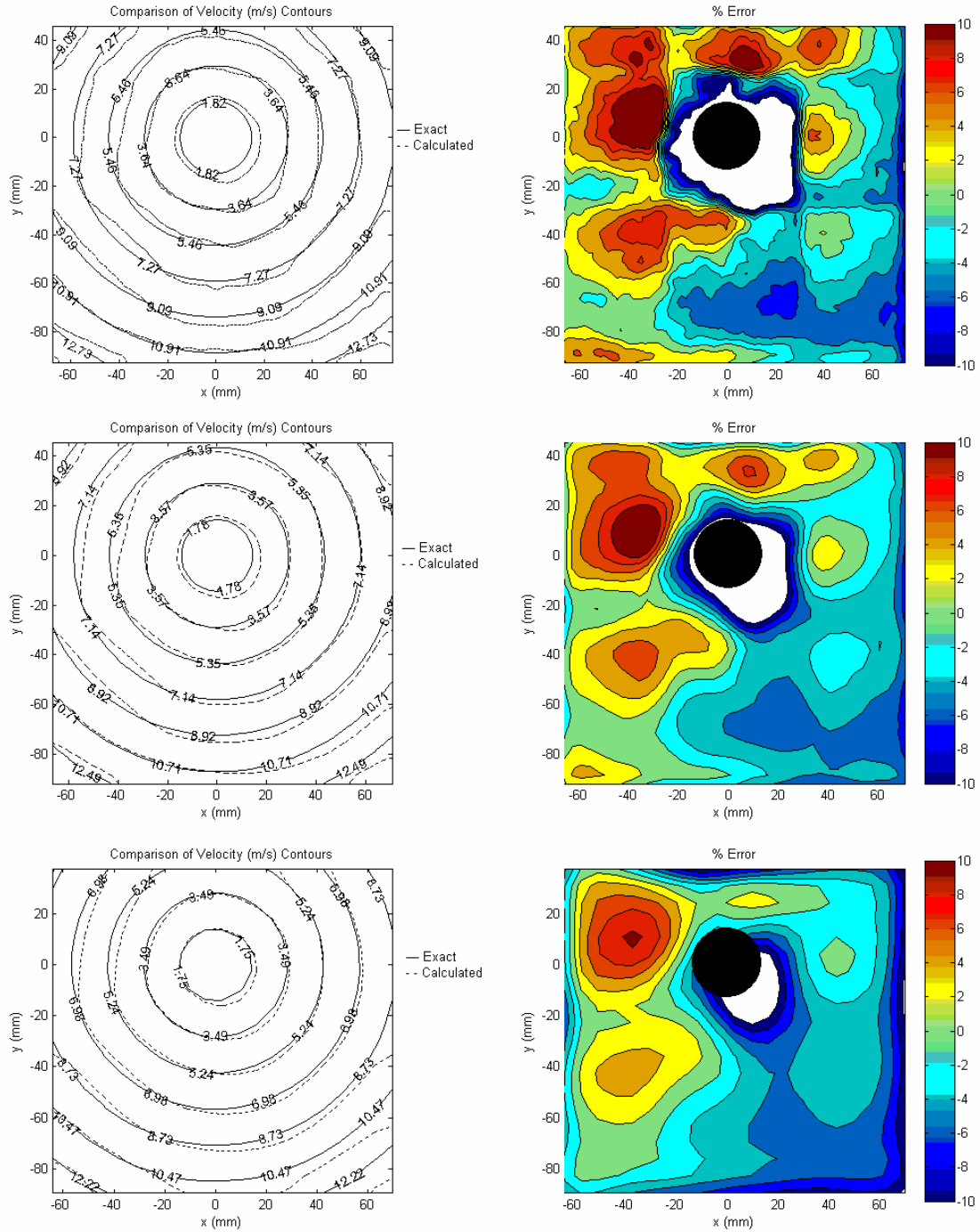


Figure 3-9. Velocity comparison and percent error of $\omega = 123.2$ rad/s disk correlated with 32 x 32 pixel IR (top), 64 x 64 pixel IR (middle), and 128 x 128 pixel IR (bottom).

Table 3-6. Correlation settings and results for $\omega = 123.2$ rad/s case

Initial IR size (pixels)	512 x 512	512 x 512	512 x 512
Number of refinement steps	4	3	2
Final IR size (pixels)	32 x 32	64 x 64	128 x 128
Initial step passes	1	1	1
Intermediate step passes	4	4	4
Final step passes	1	3	4
Vertical overlap	25%	25%	25%
Horizontal overlap	25%	25%	25%
Differencing	Forward	Forward	Forward
Boundary	Move 2nd IR inside	Move 2nd IR inside	Move 2nd IR inside
Range (m/s)	20	20	20
Protrusion radius (mm)	14	14	14
Average velocity (m/s)	7.23	7.24	7.20
Avg displacement (pix)	1.04	1.04	1.03
Average error	4.91%	3.86%	3.90%
Std Dev of error	4.36%	4.09%	2.87%

3.6 $\omega = 66.1$ rad/s case

Figure 3-10 shows the results of the $\omega = 66.1$ rad/s case, and the correlation methods and results are summarized in Table 3-7. In this case, like the previous one, the 128 x 128 pixel IR method gave the best results, with the least amount of error and the least standard deviation of error. Also like the previous case, the error is the worst in the 32 x 32 pixel IR method. However, all errors are greater in this case than the previous ones, except the very first case ($\omega = 35.5$ rad/s).

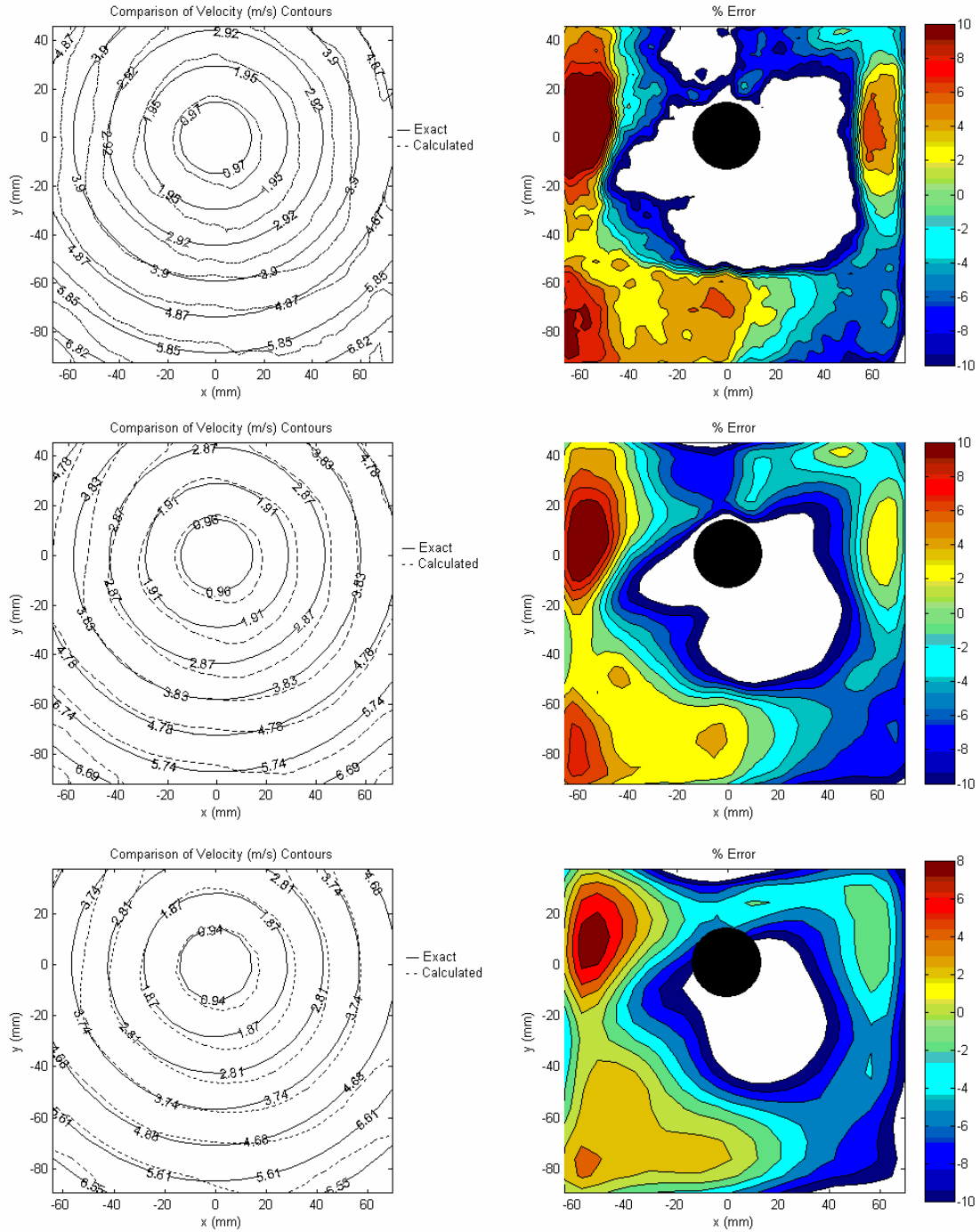


Table 3-7. Correlation settings and results for $\omega = 66.1$ rad/s case

Initial IR size (pixels)	512 x 512	512 x 512	512 x 512
Number of refinement steps	4	3	2
Final IR size (pixels)	32 x 32	64 x 64	128 x 128
Initial step passes	1	1	1
Intermediate step passes	4	4	4
Final step passes	1	3	4
Vertical overlap	25%	25%	25%
Horizontal overlap	25%	25%	25%
Differencing	Forward	Forward	Forward
Boundary	Move 2nd IR inside	Move 2nd IR inside	Move 2nd IR inside
Range (m/s)	20	20	20
Protrusion radius (mm)	14	14	14
Average velocity (m/s)	3.90	3.88	3.86
Avg displacement (pix)	0.56	0.56	0.55
Average error	8.50%	6.30%	5.70%
Std Dev of error	6.36%	5.23%	4.59%

3.7 $\omega = 140.6$ rad/s case

Figure 3-11 shows the results of the $\omega = 140.6$ rad/s case, and the correlation methods and results are summarized in Table 3-8. In this case, the errors remain large for the 32 x 32 and the 128 x 128 pixel IR methods. However, the 64 x 64 pixel IR method gave much better results, better than any case thus far, with only 1.57% average error and 1.73% standard deviation of error. The average displacement is up in this case because the time between images was changed from 10 μ s to 30 μ s, effectively tripling the displacement of a similar speed disk.

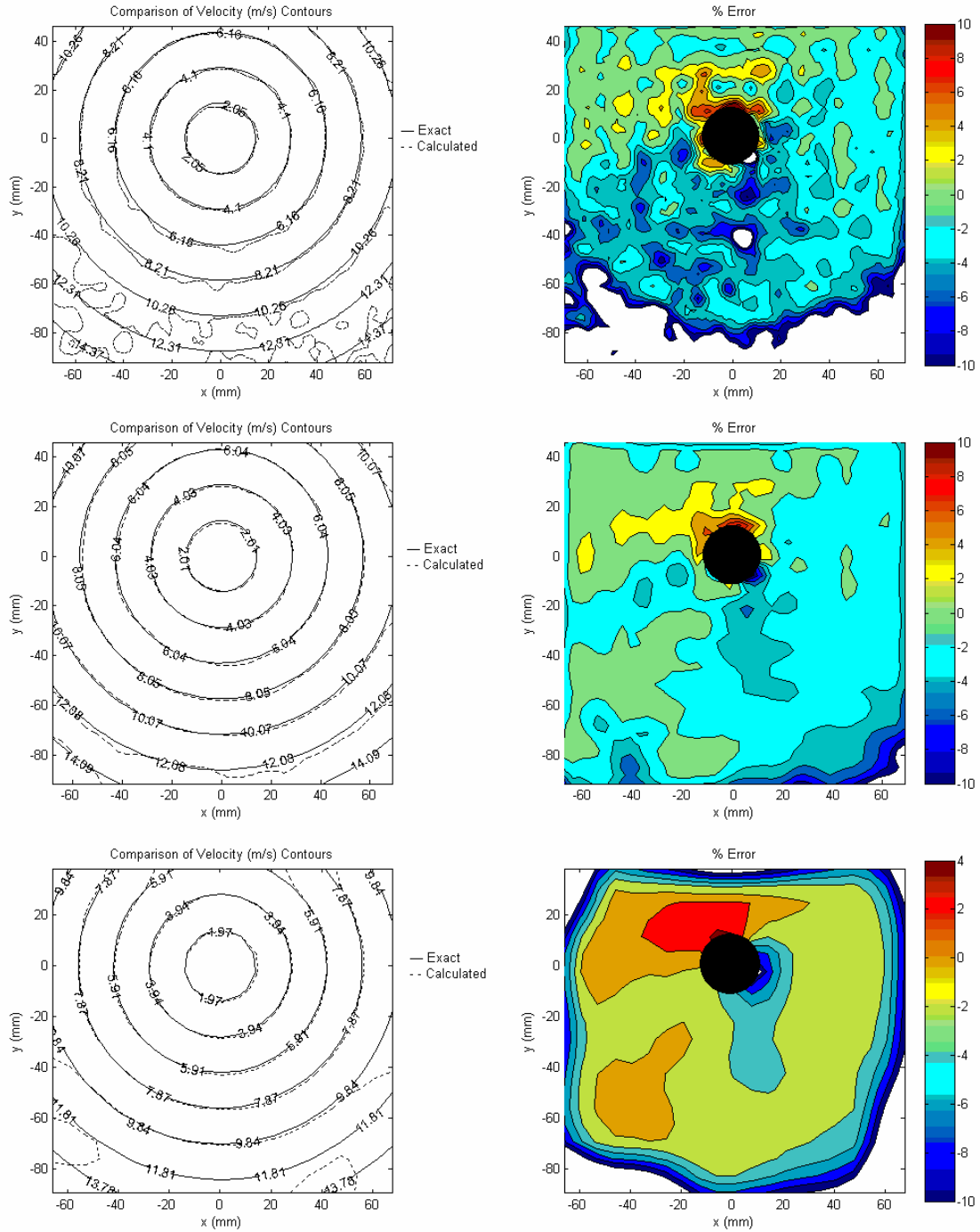


Figure 3-11. Velocity comparison and percent error of $\omega = 140.6$ rad/s disk correlated with 32 x 32 pixel IR (top), 64 x 64 pixel IR (middle), and 128 x 128 pixel IR (bottom).

Table 3-8. Correlation settings and results for $\omega = 140.6$ rad/s case

Initial IR size (pixels)	512 x 512	512 x 512	1024 x 1024
Number of refinement steps	4	3	3
Final IR size (pixels)	32 x 32	64 x 64	128 x 128
Initial step passes	1	1	2
Intermediate step passes	4	4	3
Final step passes	1	3	2
Vertical overlap	25%	25%	25%
Horizontal overlap	25%	25%	25%
Differencing	Forward	Forward	Central
Boundary	Move 2nd IR inside	Move 2nd IR inside	Substitute
Range (m/s)	20	20	20
Protrusion radius (mm)	12	12	12
Average velocity (m/s)	8.24	8.17	8.15
Avg displacement (pix)	3.54	3.52	3.51
Average error	4.93%	1.57%	4.29%
Std Dev of error	7.25%	1.73%	5.90%

3.8 $\omega = 120.7$ rad/s case

Figure 3-12 shows the results of the $\omega = 120.7$ rad/s case, and the correlation methods and results are summarized in Table 3-9. Both the percent error and the standard deviation of error for the 32 x 32 and the 64 x 64 pixel IR methods is the least for any case. The percent error for the 128 x 128 pixel IR method is lower than most cases, but the standard deviation of error is still fairly high. The time between images in this case was also 30 μ s, making the displacements larger than the cases previous to the $\omega = 140.6$ rad/s case even though the disk speed is not necessarily higher.

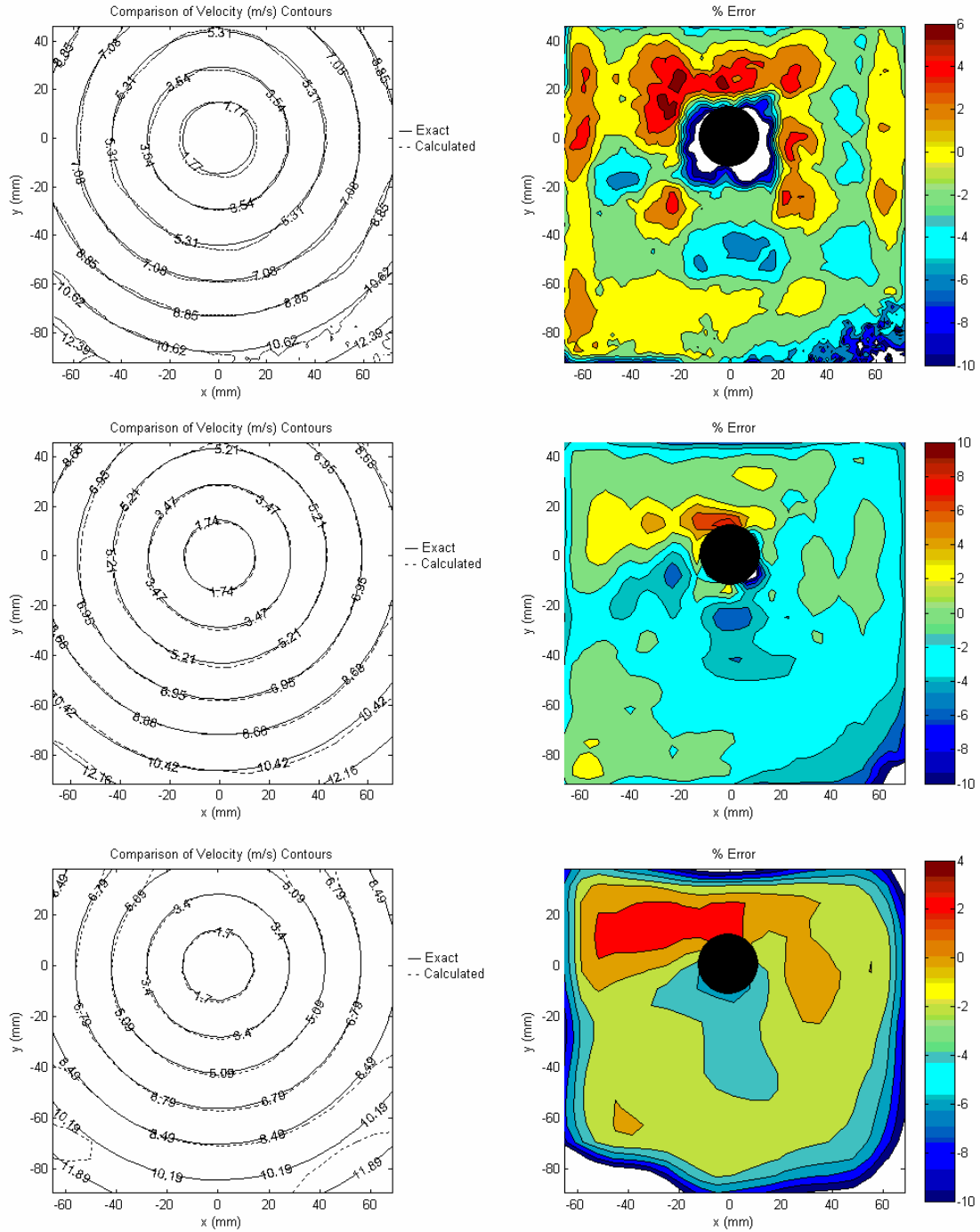


Figure 3-12. Velocity comparison and percent error of $\omega = 120.7$ rad/s disk correlated with 32 x 32 pixel IR (top), 64 x 64 pixel IR (middle), and 128 x 128 pixel IR (bottom).

Table 3-9. Correlation settings and results for $\omega = 120.7$ rad/s case

Initial IR size (pixels)	256 x 256	512 x 512	1024 x 1024
Number of refinement steps	3	3	3
Final IR size (pixels)	32 x 32	64 x 64	128 x 128
Initial step passes	1	4	4
Intermediate step passes	4	4	4
Final step passes	1	1	4
Vertical overlap	25%	25%	25%
Horizontal overlap	25%	25%	25%
Differencing	Central	Forward	Central
Boundary	Substitute	Move 2nd IR inside	Substitute
Range (m/s)	20	20	20
Protrusion radius (mm)	12	12	12
Average velocity (m/s)	7.08	7.03	6.98
Avg displacement (pix)	3.04	3.02	3.01
Average error	2.31%	1.56%	3.58%
Std Dev of error	2.51%	1.62%	4.77%

3.9 Conclusions for the rotating disk experiment

The important thing to note for each of the cases is the average percent error. This gives a good representation of how the results compared overall to the known velocities. Another thing to note is the average displacement. While the average velocity is informative, it doesn't tell the whole story. Just because the $\omega = 120.7$ rad/s case is slower than the $\omega = 123.2$ rad/s case, doesn't necessarily mean that the displacements were lower. Remember from Table 3-1 that the $\omega = 120.7$ rad/s case (as well as the $\omega = 140.6$ rad/s case) has 30 μ s between images, while the other cases had 10 μ s between images. The longer time in between images causes the displacement to be larger. So the more important parameter is the average displacement. The percent error is plotted against this value for each of the cases in Figures 3-13 through 3-15. Note that in these figures the percent error has not been reduced due to the disk protrusion as it was in the tables. The figures have been divided up based on the final interrogation region size of the correlations.

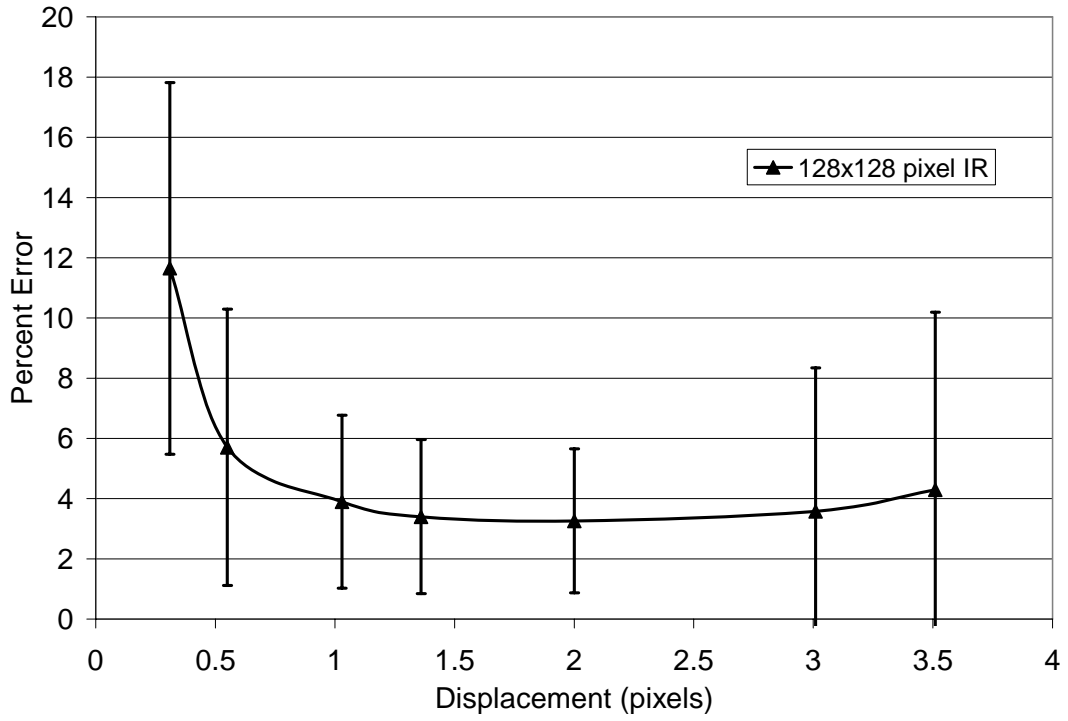


Figure 3-13. Percent error for the cases with 128 x 128 pixel IR.

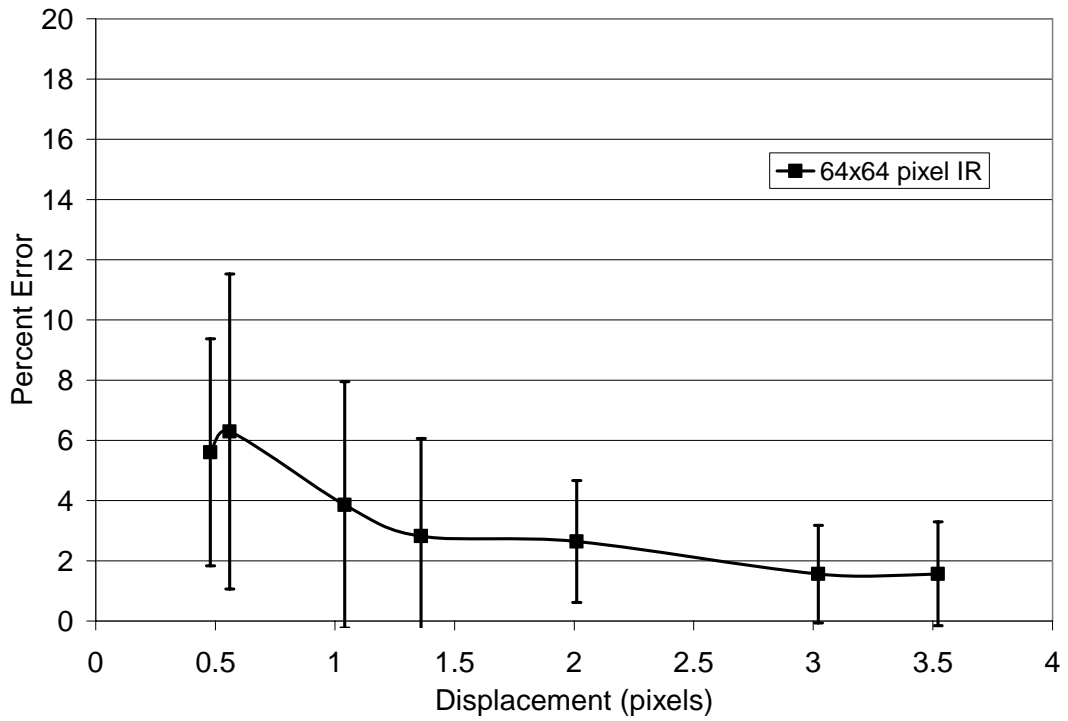


Figure 3-14. Percent error for the cases with 64 x 64 pixel IR.

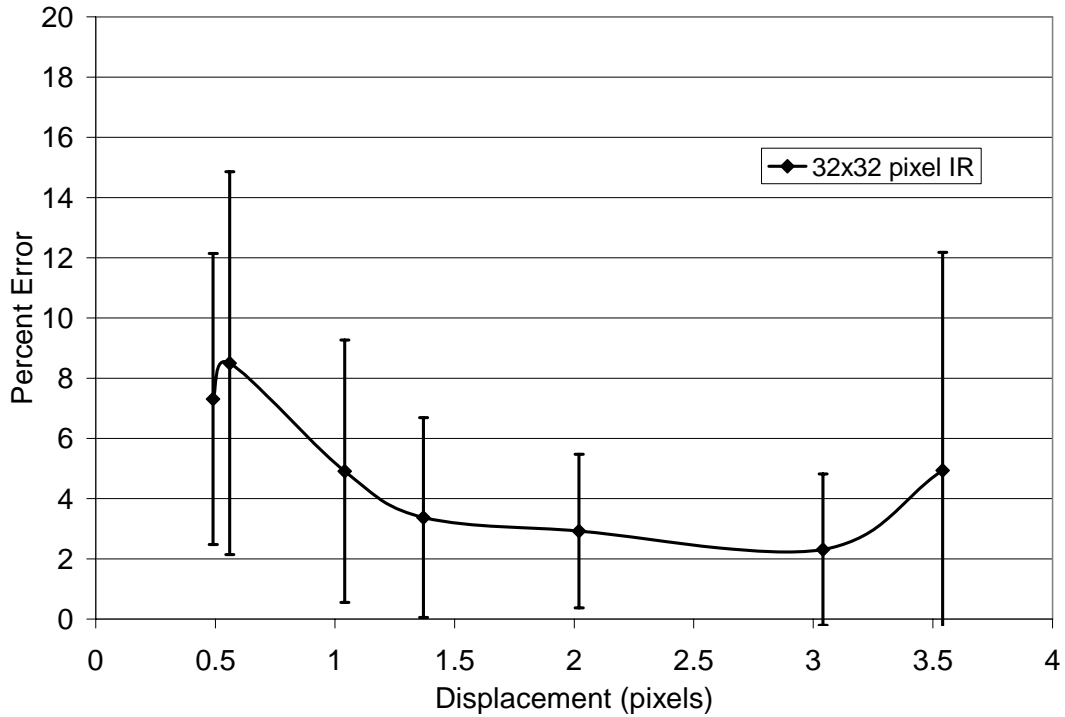


Figure 3-15. Percent error for the cases with 32 x 32 pixel IR.

Note that the error generally decreases for the larger displacements. This is consistent with Raffel et al [17], who ran a Monte Carlo simulation for measurement uncertainty in PIV. Their graph of RMS uncertainty with particle image displacement is shown in Figure 3-16. The d_{τ} parameter in the figure is the particle image diameter in pixels, and the “window” they are referring to is the size of the interrogation region. In this rotating disk experiment, the particle image diameter is typically about 5 pixels. The optimal particle image diameter is slightly over 2.0 pixels [17]. Keep in mind that the uncertainty in Figure 3-16 is given in pixels, and that if it were given as a percentage of the displacement the error would actually be decreasing with larger displacement. Also note from Figures 3-13 through 3-15 the importance of the interrogation region size. For each case other than the 66.1 rad/s case the average error was the least when using a final interrogation region size of 64 x 64 pixels. From the graph in Figure 3-16 one can see the

increase in error going from a 64 x 64 pixel window to a 32 x 32 pixel window for a given particle image diameter. This could be due to a fewer number of particles in a given IR or more particles leaving the IR between images. The error increase going from 64 x 64 pixel IR to 128 x 128 pixel IR can be attributed to the larger range in velocity in the larger IR.

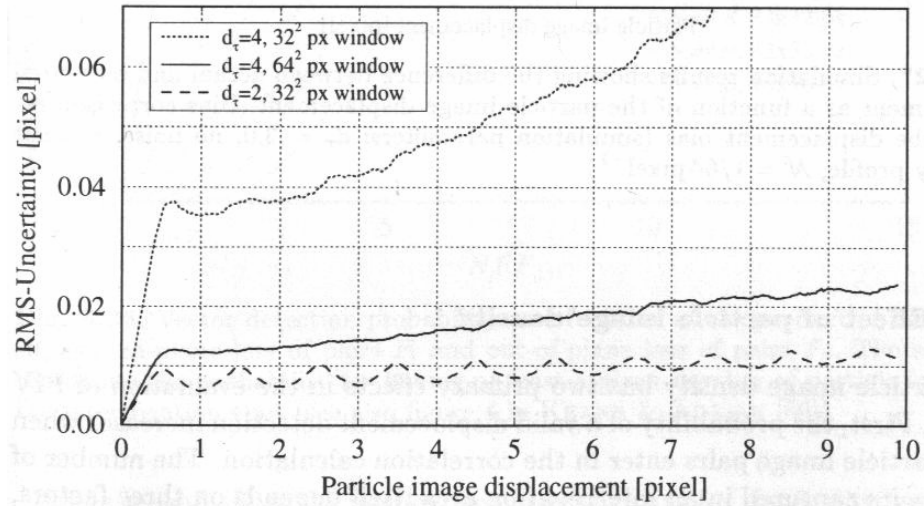


Figure 3-16. Effect of particle image displacement on PIV uncertainty. Taken from Raffel, et al [17].

The conclusion drawn from this experiment is that one should be careful to ensure that the displacement of the image particles is large enough. Of course, too large of an image displacement will result in particles leaving the IR. The best way to adjust the displacement of the image particle in most situations would be to change the time between images (as was done here in going from 10 μ s to 30 μ s). In this particular experiment, the displacement could also be changed by adjusting the disk speed, but in many experiments the velocity of the testing medium cannot necessarily be changed. Also, multiple attempts at correlating the images should be done to assure that the best possible resulting vector map is attained.

4. FREE JET RESULTS AND ANALYSIS

4.1 Hot Wire Results

Before trying to apply PIV to the free jet, a hot wire experiment was performed to provide a baseline for PIV data comparison. The setup and procedure of the experiment was detailed in section 2.2. The data collected from the Labview program “Phs Lckd Grid Data Auto X-wire.vi” contained velocity magnitudes at 2 mm increments, in a 160 mm long by 100 mm tall plane, at 1 ms time intervals (sampling rate of $f_s = 1$ kHz). Due to the physical constraint of the hot wire probe and probe holder thickness, each plane has a 4 mm offset from the surface of the plate. The velocity data was the ensemble average of 59 cycles (15 seconds of data at a 4 Hz pulse rate). With 4,000 samples taking 15 seconds, one plane of data would typically take about 17 hours to complete. A MatLab code (“PIVplot.m” in Appendix G) was written to format the data into a TecPlot readable file, as well as include the calculation of vorticity. TecPlot macros (“velvort.mcr” and “aviexport.mcr” in Appendix G) were then used to create animated contour plots of the velocity and vorticity. The velocity contour plots are overlaid by plots of the velocity vectors. For clarity, only every other velocity vector is shown. The position of the jet relative to the data plane is indicated on each plot by the parallel lines under the horizontal axis that are pitched 30° to the surface. Selected frames from the 50%, 25%, and 10% duty cycle centerline traverses are shown in Figures 4-1 through 4-6. The time (normalized by the period, $T = 0.25$ s) of each frame relative to the start of the cycle is shown at the top of each frame. The velocity is normalized by the nominal jet velocity

that will correspond to a blowing ratio of $B = 1.0$ in the jet in crossflow experiment. This velocity is $V_j = 3.15$ m/s. The vorticity is normalized by $V_j/d = 3.15/0.0254 = 124$ s⁻¹.

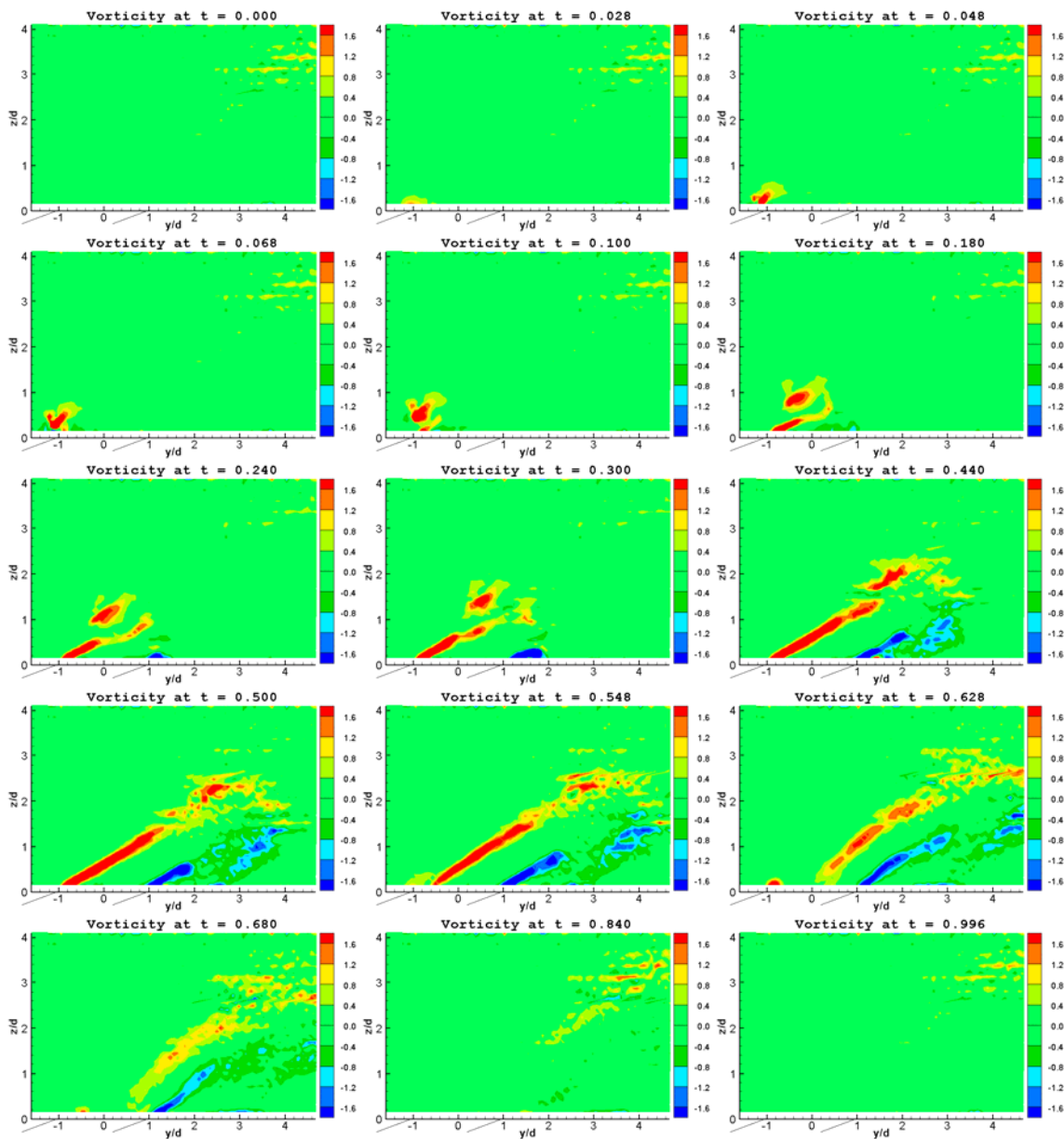


Figure 4-1. Normalized vorticity plots (Hot-wire measurement). $f = 4$ Hz, $\Delta = 50\%$.

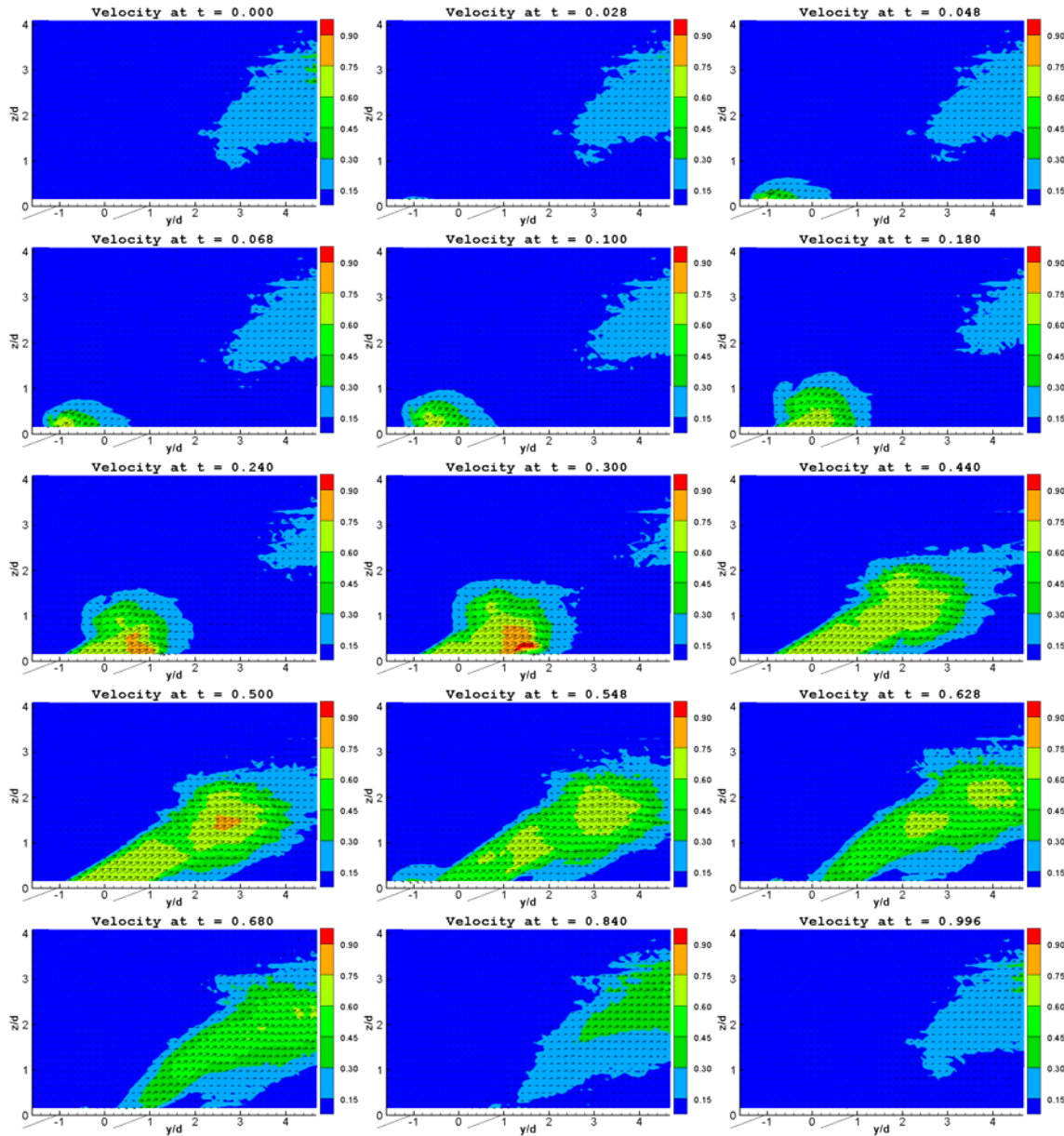


Figure 4-2. Normalized velocity plots (Hot-wire measurement). $f = 4$ Hz, $\Delta = 50\%$.

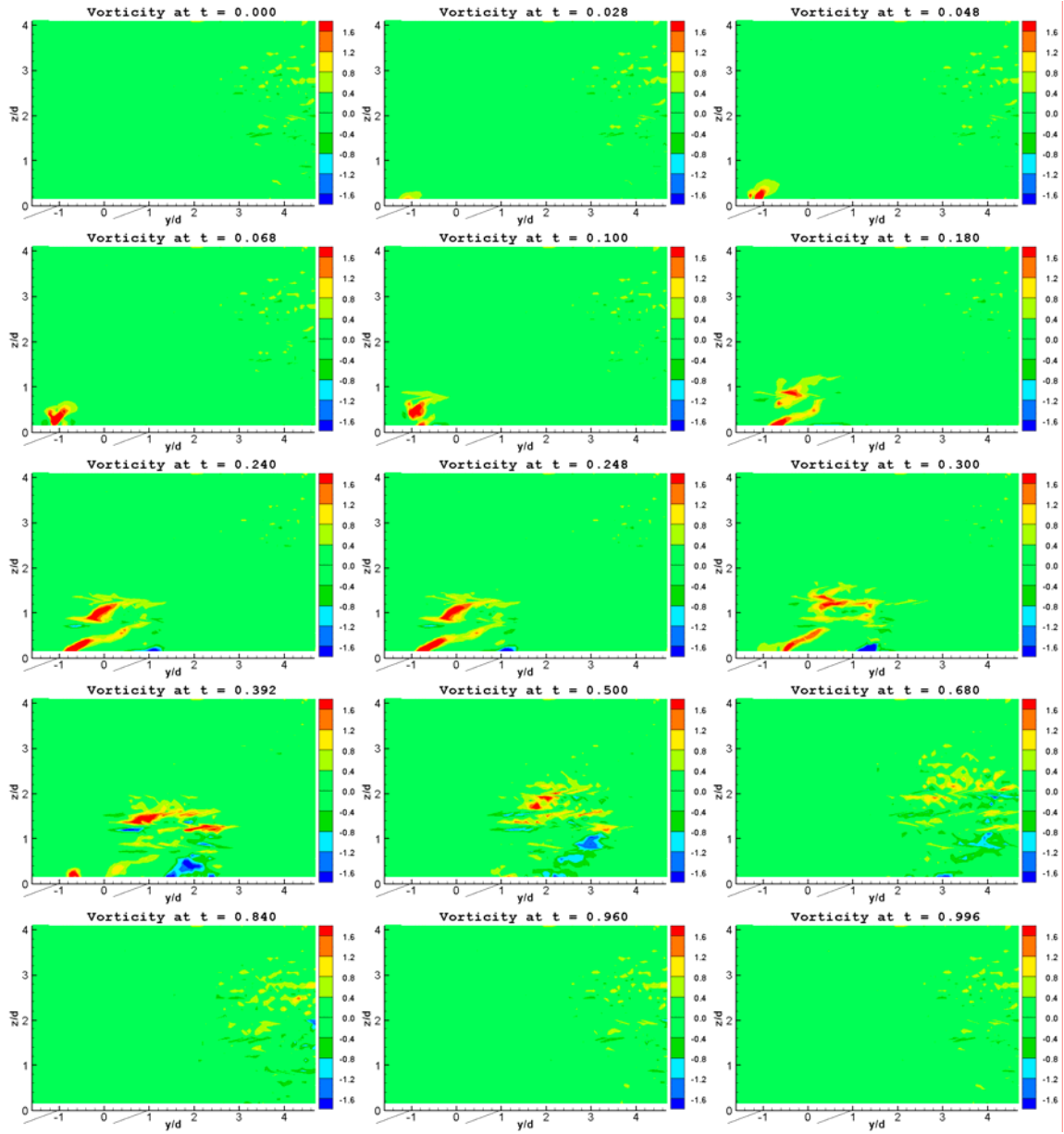


Figure 4-3. Normalized vorticity plots (Hot-wire measurement). $f = 4$ Hz, $\Delta = 25\%$.

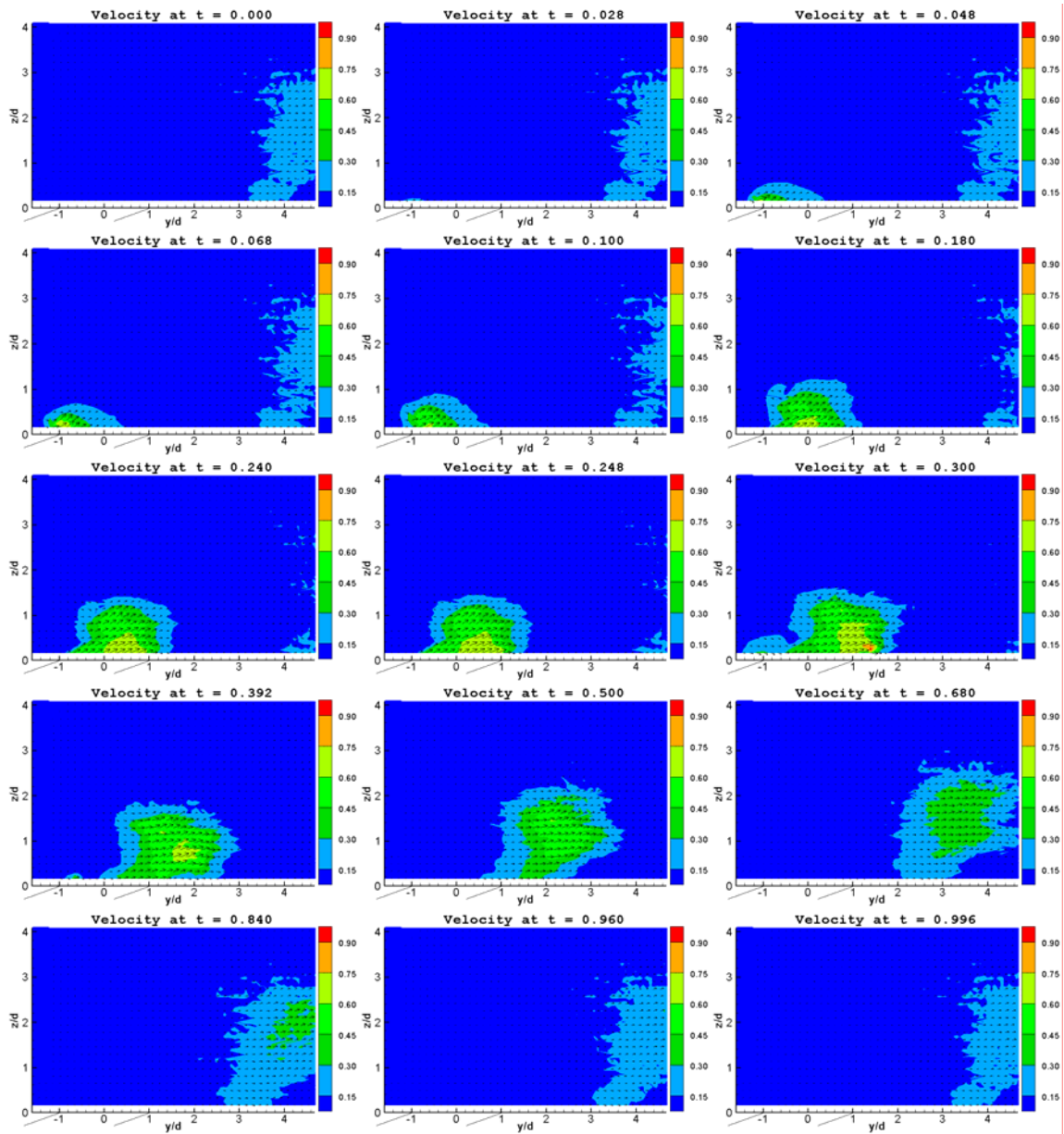


Figure 4-4. Normalized velocity plots (Hot-wire measurement). $f = 4$ Hz, $\Delta = 25\%$.

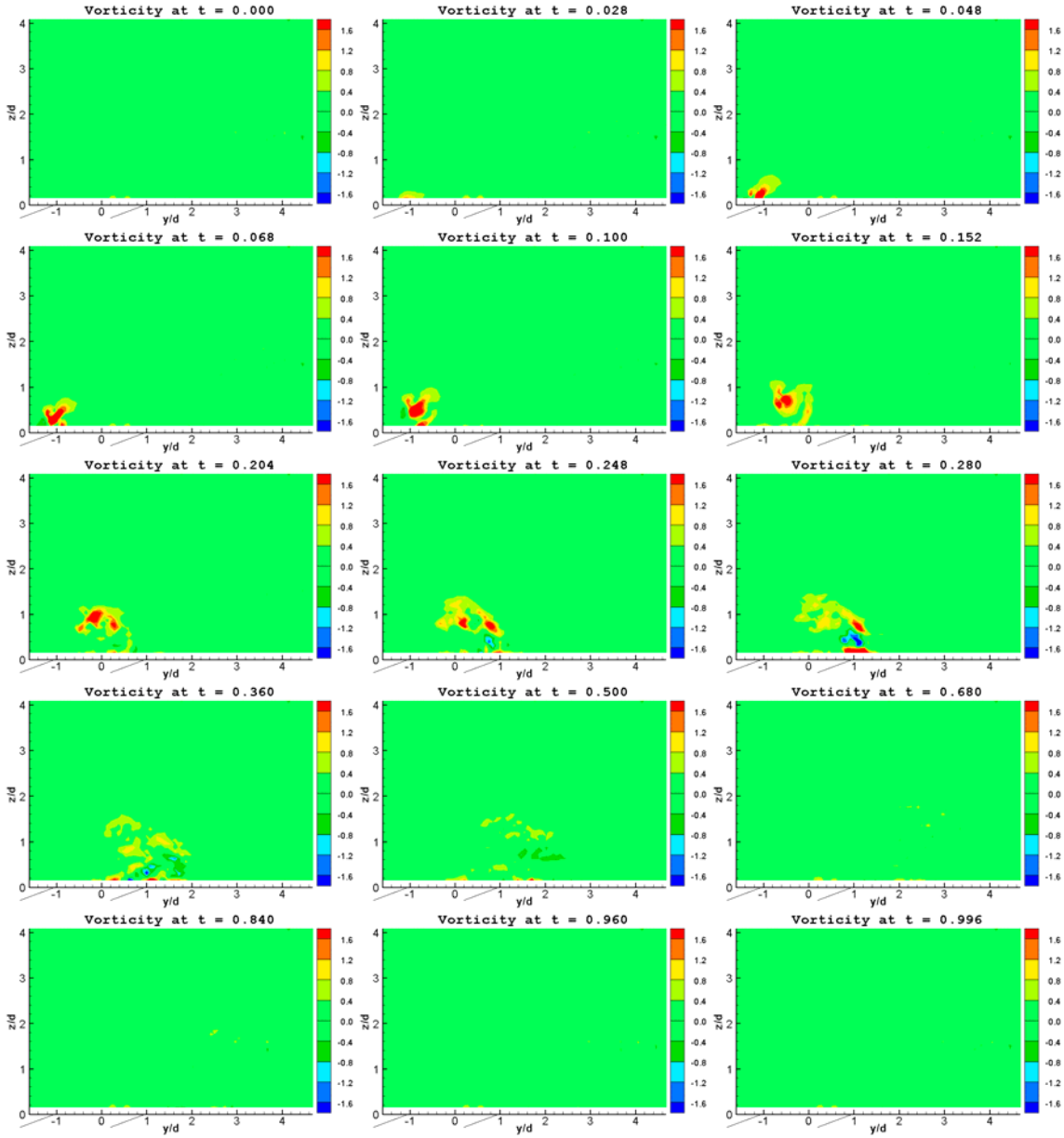


Figure 4-5. Normalized vorticity plots (Hot-wire measurement). $f = 4$ Hz, $\Delta = 10\%$.

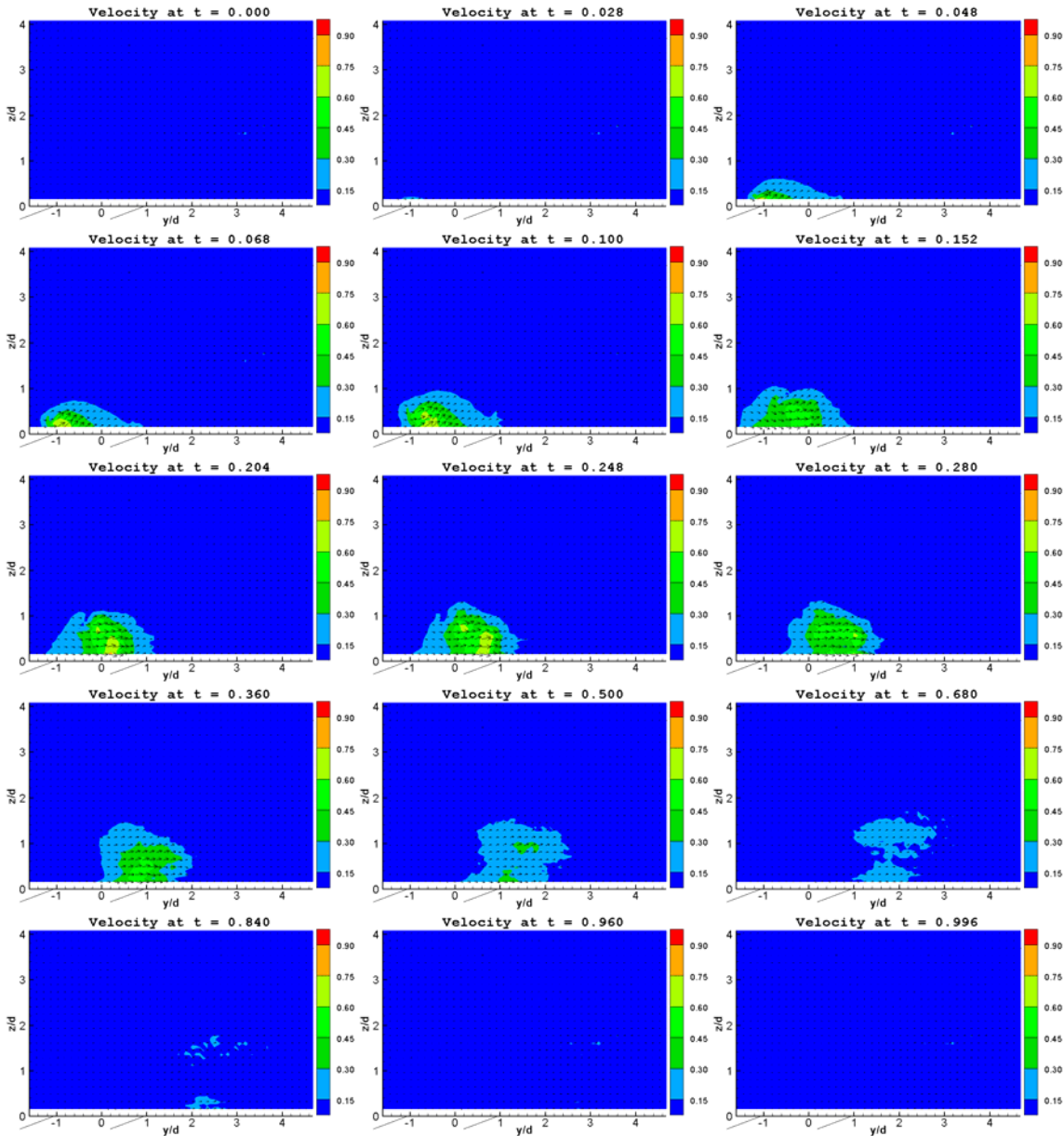


Figure 4-6. Normalized velocity plots (Hot-wire measurement). $f = 4$ Hz, $\Delta = 10\%$.

As the cycle first begins, there is a delay as the flow must travel through the feed plenum and the jet cylinder before exiting the jet. As the air reaches the leading edge of the jet (around $t = 0.028$), a starting vortex begins to form. After about $t = 0.068$, the starting vortex moves away from the jet, and another leading edge vortex begins to form as the jet begins flowing across its span. At $t = 0.100$, the starting vortex begins to pull

away from the main jet flow. This is how each cycle begins for each of the different cases, the shortest of which (10% duty cycle) has the jet on until $t = 0.100$.

For the 50% duty cycle case (Figures 4-1 and 4-2), the air does not reach the trailing edge of the jet (the lip of the jet on the right side when looking at these figures) until around $t = 0.180$, because the jet is pitched with respect to the plate surface. At $t = 0.240$, the initial pulse of the jet flow approaches the trailing edge, and creates a clockwise vortex at that point. By $t = 0.300$, the initial pulse of jet flow has nearly completely pulled away from the jet, and it begins to lose strength. At $t = 0.440$, the initial pulse has lost most of its strength, and the starting vortex has started to diffuse. At $t = 0.500$, the jet flow becomes more developed and mixed into the leading pulse of the flow, approaching the look of a steady jet. This is the point where the valve shuts off for the 50% duty cycle case, cutting off the air supply to the jet. From $t = 0.532$ to 0.572 , ambient air is entrained into the jet in reaction to the valve shutting off, as the main jet flow begins to lose momentum. From $t = 0.580$ to 0.680 , that entrained air exits the jet, and after 210 ms there is no more air leaving the jet. The starting vortex has almost completely diffused by $t = 0.680$, and gets mixed up in the diffusion of the main jet flow. The air from the jet remains in the field of view until the end of the cycle, and through the first $t = 0.400$ of the next cycle.

The first $t = 0.248$ of the 25% duty cycle case is the same as the 50% duty cycle case. In this 25% duty cycle case (Figures 4-3 and 4-4), the valve shuts off at $t = 0.250$, and the outside air is entrained from $t = 0.284$ to 0.324 . The entrained air exits from $t = 0.336$ to 0.448 . The initial pulse of jet air again loses strength after $t = 0.300$. As in the 50% duty cycle case, the starting vortex is almost completely diffused at $t = 0.680$, but

this time it is easier to see that the diffuse vortices are actually from the starting vortex. Air from the jet stays in the field of view until $t = 0.288$ into the following cycle.

The first $t = 0.100$ of the 10% duty cycle case is the same as the other two cases. In this 10% duty cycle case (Figures 4-5 and 4-6), the valve shuts off at $t = 0.100$, and the outside air is entrained from $t = 0.128$ to 0.168 . The entrained air exits from $t = 0.188$ to 0.216 . The jet impulse is its strongest at $t = 0.224$, after which it diffuses quickly. The starting vortex begins to break up at $t = 0.152$, and is the only vortex that gets propagated away from the jet. It is interesting to note that the vortex formed after the starting vortex actually propagates across the jet, and picks up strength as it reaches the trailing edge at around $t = 0.280$. This creates an opposing clockwise vortex that appears just below the starting vortex, leaving a series of three vortices in a vertical row. However, the vortices lose strength quickly, and are almost completely diffused by around $t = 0.360$. The air from the jet, along with the starting vortex, does not completely dissipate until 0.960 .

4.1.1 Conclusions for free jet hot wire experiment

The 50% duty cycle case gives the deepest and most sustained penetration into the quiescent air. The 25% case has similar penetration, but does not carry quite as much momentum. The 10% case has relatively no penetration, but does show some effect for almost the entire cycle. The common denominator for all three cases is that the starting vortex had time to develop and get pushed away from the jet. The results from the Bons study, where the loss coefficient was reduced by over 50% for duty cycles as low as 10%, would imply that this starting vortex is the key to separation control for pulsed jets. In fact, since the starting vortex is significant only 3 ms after starting to form, it may indicate that duty cycles as low as 1% (2.5 ms at 4 Hz) can still have an effect on

boundary layer separation. This would also be consistent with the Bons study, in which the loss coefficient was reduced by 45% for a 1% duty cycle case. The fact that the lower duty cycles do not have as much penetration may not matter, but it would have to depend on the boundary layer thickness or size of separation region.

4.2 PIV Results

4.2.1 Uncertainty and Verification of PIV Data

In order to get an idea of the variability in the PIV results, one case ($f = 4$ Hz, $\Delta = 50\%$ duty cycle, $V_j = 3.15$ m/s) was run six times. Each of the six cases was ensemble averaged over 13 cycles of data. The average velocity over the entire cycle over the expanse of the jet exit (averaging in space and time) was compared for each of the six cases. The mean velocity was $V_{\text{avg}} = 0.78$ m/s, with a standard deviation of 0.022 m/s. The percent error could be thus estimated as 2.8%. There is also a measurement error to consider, combining bias and RMS errors, which is typically about 0.1 pixels [24]. In this setup, 0.1 pixels is equivalent to 0.035 m/s. As a percentage of $V_{\text{avg}} = 0.78$ m/s, this error is 4.5%. The root sum of squares of these two errors is 5.3%.

A hot wire experiment was performed for this case to further verify these PIV results. The previous hot wire experiment was done with a different setup, so it was critical that at least one case be re-run to be able to compare it to the PIV results. The hot wire probe was traversed in the same 2D plane represented by the PIV data (offset 4 mm in the vertical direction to allow room for the hot wire probe), in increments of 2 mm in both the vertical and horizontal directions. Each point was sampled at $f_s = 1$ kHz, and was ensemble averaged over 59 cycles. Since this amounts to almost 20 hours of data collection at a pulsing frequency of $f = 4$ Hz, taking hot wire measurements at $f = 0.5$ Hz was not attempted, as it would have taken nearly a week to obtain a full 2D plane of data.

A frequency of $f = 0.5$ Hz was desired as mentioned before in order to match the reduced frequency of the LSWT facility. But a frequency of $f = 4$ Hz was not practical for looking at smaller duty cycles due to the highly damped effect of adding the smoke box. This effect can be seen by looking at Figure 4-7, which is a centerpoint trace of the velocity of the jet measured with a hot wire. A 10% duty cycle jet at $f = 4$ Hz would only be on for 25 ms, which would correspond to almost no velocity output at all when looking at Figure 4-7 (the velocity at 25 ms is only 0.63 m/s). To obtain a velocity output that closely resembles a square wave, a frequency of $f = 0.5$ Hz is preferred over $f = 4$ Hz. This was not the case before adding the smoke box (such as the previous set of hot wire data), when the damping was not as strong. It is resonance that causes the two humps (one after the valve opens, one after it closes) in Figure 4-7. Without damping, these “humps” would be tall and narrow spikes, and the overall look of the plot would be as a square wave with very short rise and fall times.

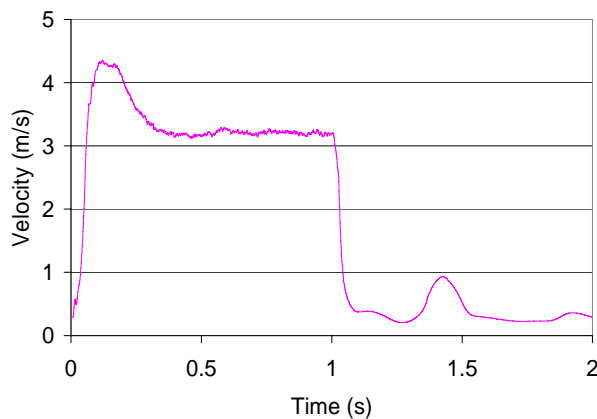


Figure 4-7. Centerpoint velocity of $f = 0.5$ Hz, 50% duty cycle jet.

For the PIV measurements, data was taken at $f_s = 400$ Hz, and was ensemble averaged over 13 cycles. The comparison between the hot wire and PIV data is shown in the series of images in Figures 4-8 and 4-9 (comparing the hot wire data in Figure 4-8 to the PIV data in Figure 4-9). The velocity is normalized by $V_j = 3.15$ m/s as it was in the

hot wire experiment. Each velocity contour plot is overlaid with velocity vectors, with only every other vector plotted for the hot wire data and every fourth vector plotted for the PIV data. The hot wire will output a voltage even when there is no velocity, and so at lower velocities the hot wire data will appear slightly high. Also, at very low velocities the averaging of PIV data will tend toward zero, so the PIV data will appear slightly low. However, the PIV data is much smoother due to these averaging techniques within the correlation algorithm. In observing the main flow of the jet, the plots compare very well, so the PIV data can be taken with confidence.

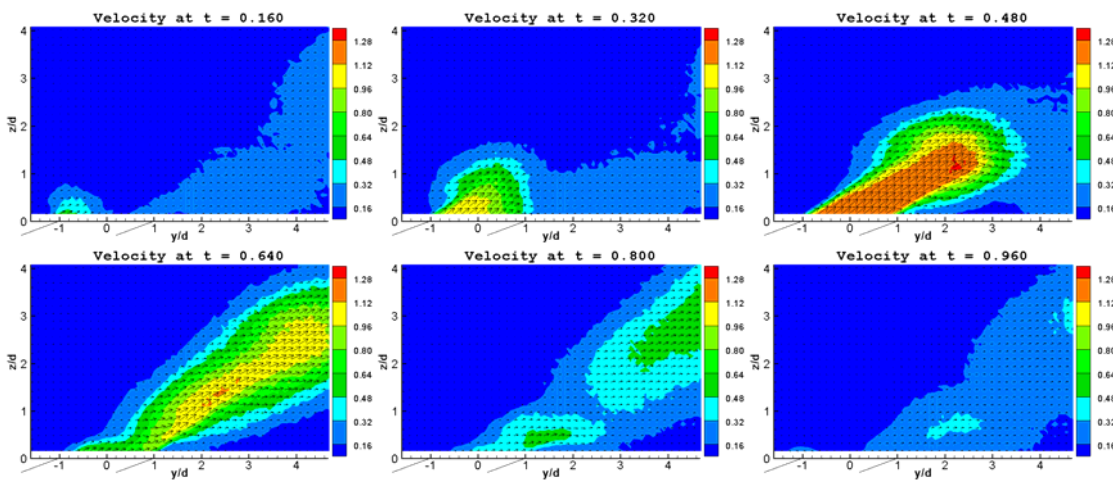


Figure 4-8. Normalized hot wire velocity data. $f = 4 \text{ Hz}$, $\Delta = 50\%$.

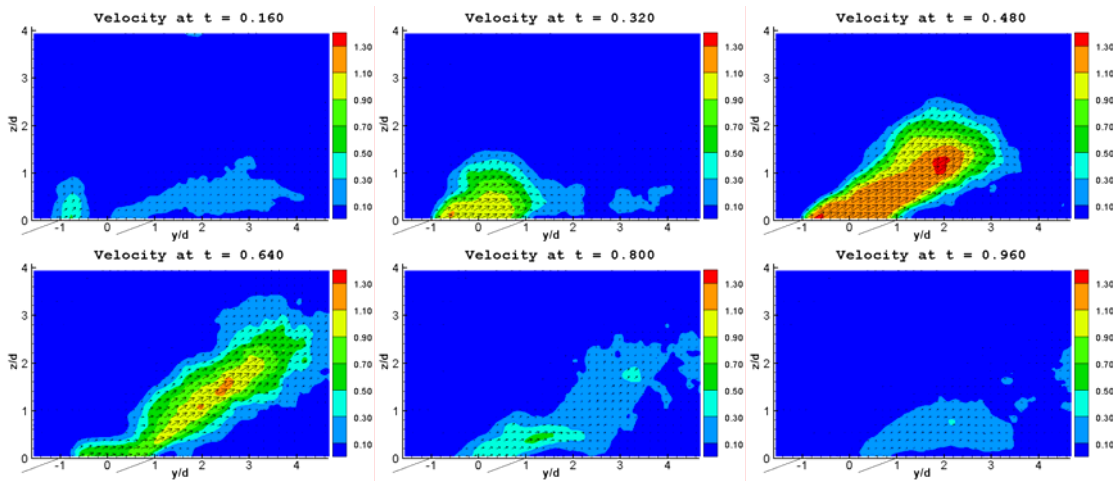


Figure 4-9. Normalized PIV velocity data. $f = 4 \text{ Hz}$, $\Delta = 50\%$.

4.2.2 Steady Case ($\Delta = 100\%$)

Figure 4-10 shows the velocity and vorticity plots for the steady case. The normalization is the same as for the hot wire experiment. The data is the average of 1300 images pairs taken at 400 Hz. The velocity at the center of the jet ($y = 0.27d$, $z = 0.16d$) is $V_j = 3.52$ m/s. The velocity profile does not appear to spread out very much as it gets further from the jet, and maintains its $\alpha = 30^\circ$ pitch angle until it reaches the extent of the field of view. The maximum velocity is 3.56 m/s and occurred at $y = 1.22d$ and $z = 0.08d$. The maximum positive (counterclockwise) vorticity is $\omega_i = 5.30$ and occurred at $y = 0.87d$ and $z = 0.24d$. The maximum negative (clockwise) vorticity is $\omega_i = -4.50$ and occurred at $y = 2.83d$ and $z = 0.28d$. Because the vorticity range is so wide, the contour levels were adjusted so the lower-range vortex contours could be observed more easily. This adjusted scale is shown in the rightmost plot of Figure 4-10. This makes it especially easier to view the progression of the starting vortex in the unsteady cases, and is why this scale is used for all future plots. For the steady case only, the vorticity is plotted on an expanded scale (middle of Figure 4-10).

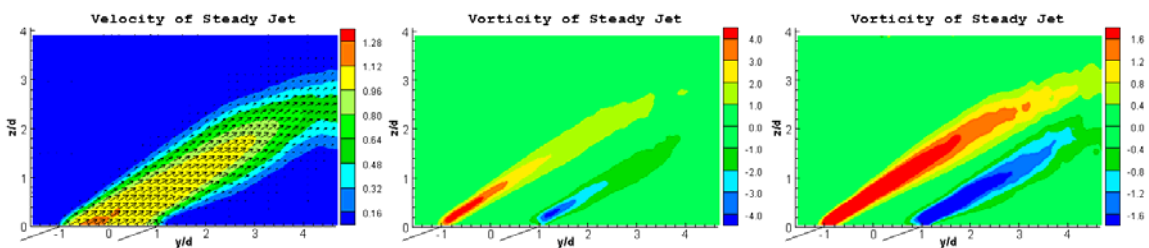


Figure 4-10. Velocity (left), vorticity on wider scale (middle), and vorticity on narrower scale (right) of steady jet.

4.2.3 Unsteady 10% Duty Cycle Case

Data for each unsteady case was sampled at $f_s = 50$ Hz, with the jets pulsing at $f = 0.5$ Hz, so there are 100 image pairs per cycle. Thirteen cycles of data were ensemble

averaged. Select frames from the ensemble are shown in the figures on the following pages. Note that for a frequency of $f = 0.5$ Hz, each cycle has a period of $T = 2$ seconds. Thus, for the $\Delta = 10\%$ case the valves open at $t = 0.00$ and close at $t = 0.10$ (200 ms). The results of the $\Delta = 10\%$ case are shown in Figures 4-11 and 4-12. There is an obvious delay from the time the valves open (or close) to the point where the effect is seen at the jet, due to the dynamics of the plenum and the smoke box. The beginning of the cycle is first evident at $t = 0.01$. The top of a vortex ring appears as the air first reaches the leading edge of the jet. This starting vortex is quite strong considering the small amount of jet flow at that point in the cycle ($t = 0.02$). At $t = 0.03$, the flow reaches the opposite side of the jet, and the lower part of the vortex ring appears there. At that point, the starting vortex, which developed as a separate entity, begins to be drawn into the main flow, and is no longer discernable by $t = 0.06$. Now the flow out of the jet is still increasing, and it reaches a maximum velocity at approximately $t = 0.10$, which is when the valves close. At $t = 0.11$, the effect of the valve closing is first seen near the jet. There is very little flow leaving the jet exit by $t = 0.12$, but the flow is still seen further from the jet exit. This is still the case at $t = 0.13$, but after that the air quickly dissipates until essentially disappearing by $t = 0.17$. After another 340 ms (at $t = 0.32$), residual air leaves the jet. This is caused by the closing of the valves having a kick-back effect, and is negligible compared to the other events in the cycle. There is nothing else happening from $t = 0.38$ to the start of the next cycle at $t = 1.00$. The maximum velocity was 5.0 m/s and occurred at $t = 0.09$ and $y = 1.97d$, $z = 0.39d$. The maximum positive (counterclockwise) vorticity was $\omega_i = 7.89$ and occurred at $t = 0.07$ and $y = 1.30d$, $z =$

0.51d. The maximum negative (clockwise) vorticity was $\omega_i = -6.93$ and occurred at $t = 0.08$ and $y = 2.76d$, $z = 0.24d$.

4.2.4 Unsteady 25% Duty Cycle Case

The results for the $\Delta = 25\%$ case are shown in Figures 4-13 and 4-14. In this case the valves close at $t = 0.50$ (250 ms). The first $t = 0.10$ of the cycle is the same as for the $\Delta = 10\%$ case, as seen when comparing the plots in Figures 4-13 and 4-14 to Figures 4-11 and 4-12 at $t = 0.10$. This is expected because there is no effect of the jet from one cycle to the next for any of the cases studied. Therefore, every cycle begins the same way. For the $\Delta = 25\%$ case, the velocity is a maximum at $t = 0.10$, and slowly decreases until $t = 0.18$. From $t = 0.18$ until the valves close at $t = 0.25$, the jet appears to have reached a steady state, but this does not actually happen until the jet is open longer (as will be shown for the $\Delta = 50\%$ case). This can also be seen in Figure 4-7 looking at the centerpoint velocity of the jet. Figure 4-7 also helps explain the peak velocity that occurs around $t = 0.10$ (200 ms). The large “hump” at the start of the cycle is actually a spike caused by the opening of the valves, and the spike gets damped out with the presence of the smoke box (adding a large volume to the plenum), as well as with the length the flow must travel before it reaches the jet exit. As in the $\Delta = 10\%$ case, there is still a large amount of jet flow still evident 60 ms after the valves close ($t = 0.28$), but as before the air quickly dissipates and is last seen at $t = 0.31$. At $t = 0.54$ (1080 ms), or 580 ms after the valves close, there is a vortex that has developed near the jet, but at a low enough velocity that it doesn't show up on the velocity plots. Again, this is due to the kick-back effect of the valves closing. This is also explained in Figure 4-7 with the much smaller “hump” that occurs 300 ms to 600 ms after the valves close. For the $\Delta = 25\%$ case, the

maximum velocity was also 5.0 m/s but this time it occurred at $t = 0.08$ and $y = 2.56d$, $z = 0.79d$. The maximum positive (counterclockwise) vorticity was $\omega_i = 7.52$ and occurred at $t = 0.06$ and $y = 1.06d$, $z = 0.43d$. The maximum negative (clockwise) vorticity was $\omega_i = -7.10$ and occurred at $t = 0.06$ and $y = 3.03d$, $z = 0.43d$.

4.2.5 Unsteady 50% Duty Cycle Case

The results for the $\Delta = 50\%$ case are shown in Figures 4-15 and 4-16. In this case the valves are turned off at $t = 0.50$ (1000 ms). The first $t = 0.25$ of the cycle is the same as for the $\Delta = 25\%$ case. The flow still appears to be steady at $t = 0.30$, but it starts to decrease at $t = 0.35$, then increase at $t = 0.40$, and finally decrease again between $t = 0.43$ and $t = 0.45$. At $t = 0.50$, the flow has not changed much, and this is actually close to what the steady jet looks like (see Figure 4-10). After that, the valves shut off and the flow diminishes as before within 120 ms (at $t = 0.56$). Between $t = 0.72$ and $t = 0.78$ there is again a small vortex that has developed near the jet due to the action of the valves closing. The maximum velocity for this case was 4.9 m/s and occurred at $t = t = 0.08$ and $y = 2.52d$, $z = 0.71d$. The maximum positive (counterclockwise) vorticity was $\omega_i = 7.93$ and occurred at $t = 0.06$ and $y = 1.22d$, $z = 0.51d$. The maximum negative (clockwise) vorticity was $\omega_i = -7.00$ and occurred at $t = 0.08$ and $y = 3.03d$, $z = 0.43d$.

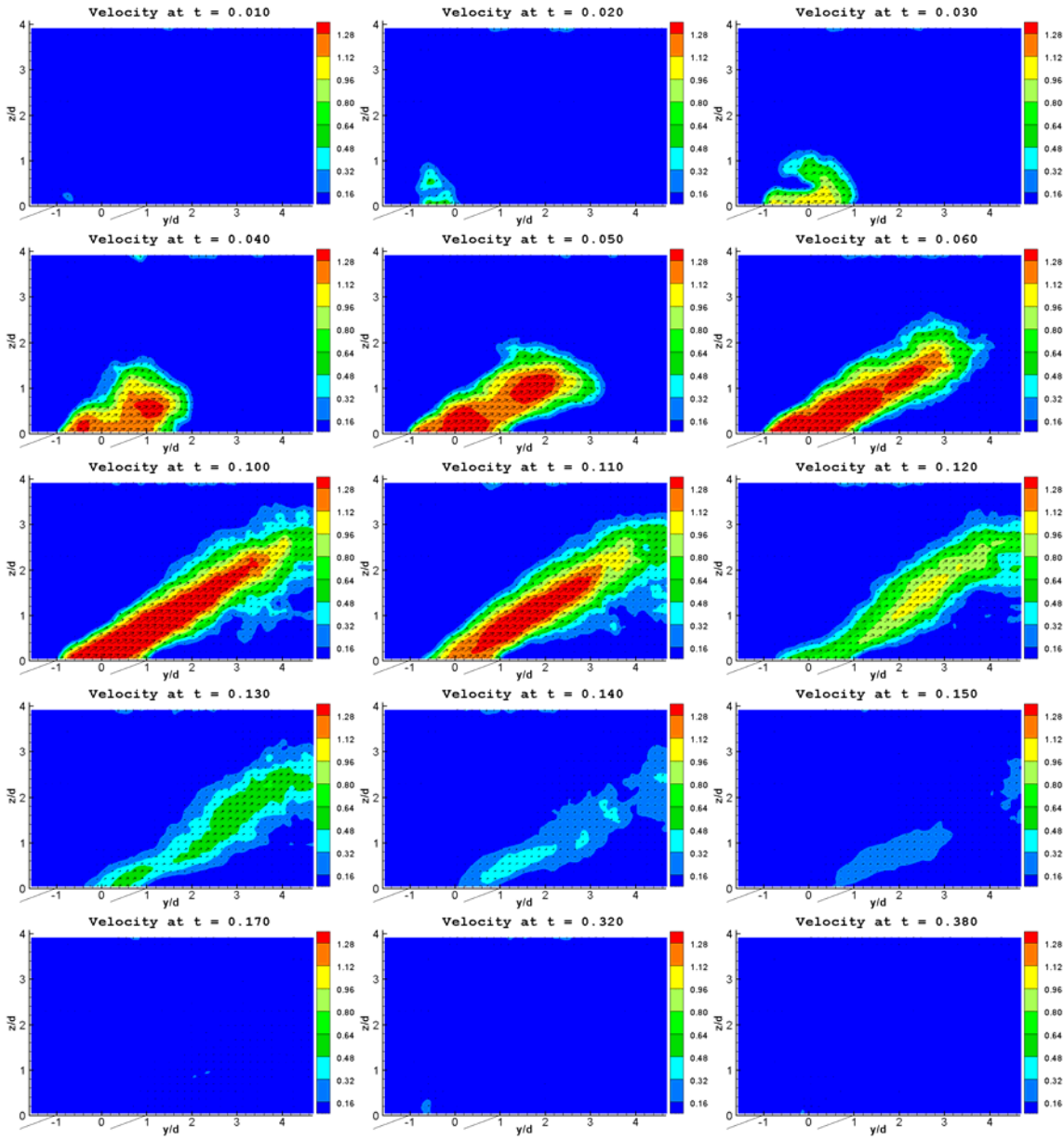


Figure 4-11. Normalized velocity plots (PIV measurement). $f = 0.5$ Hz, $\Delta = 10\%$.

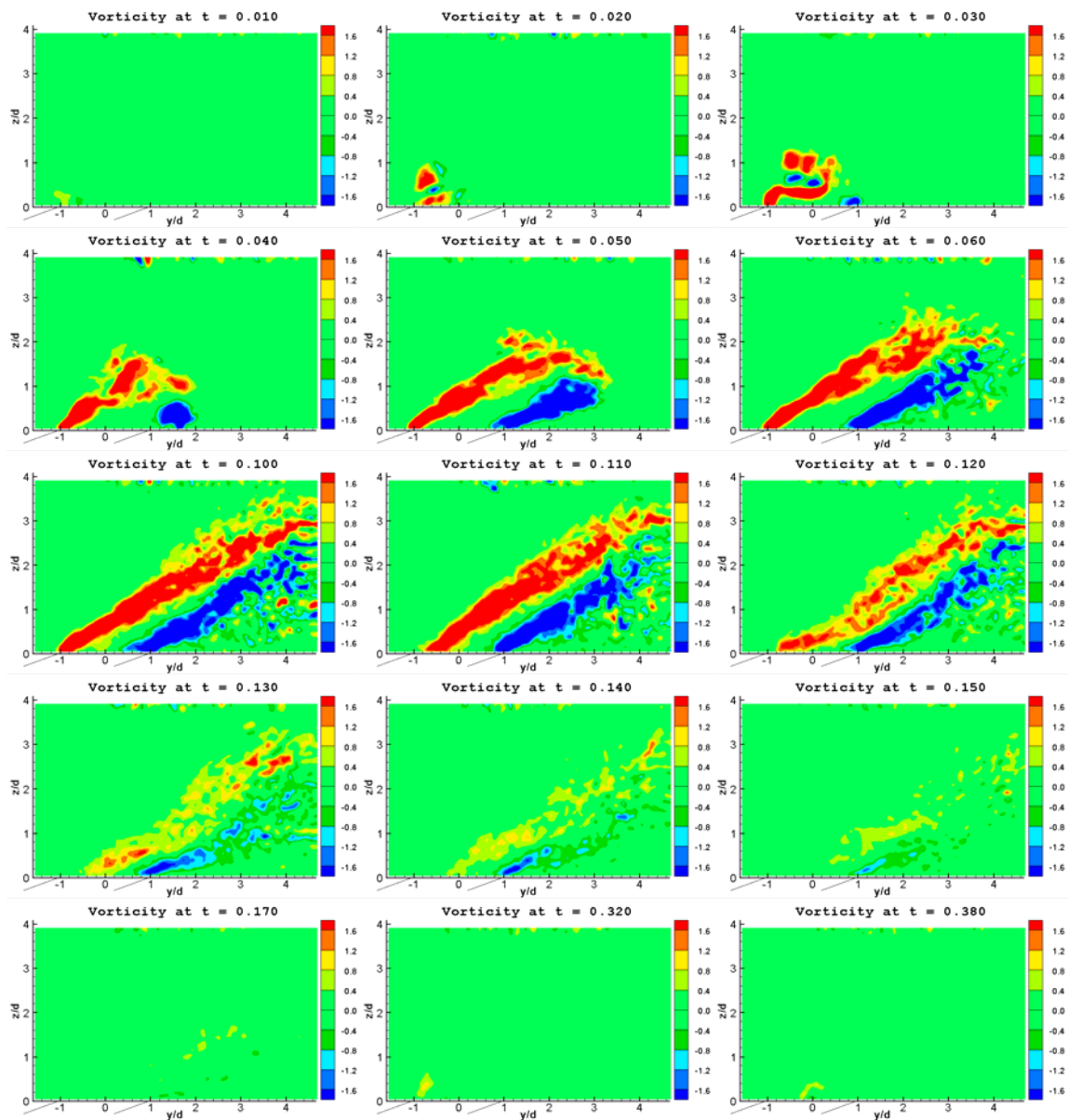


Figure 4-12. Normalized vorticity plots (PIV measurement). $f = 0.5$ Hz, $\Delta = 10\%$.

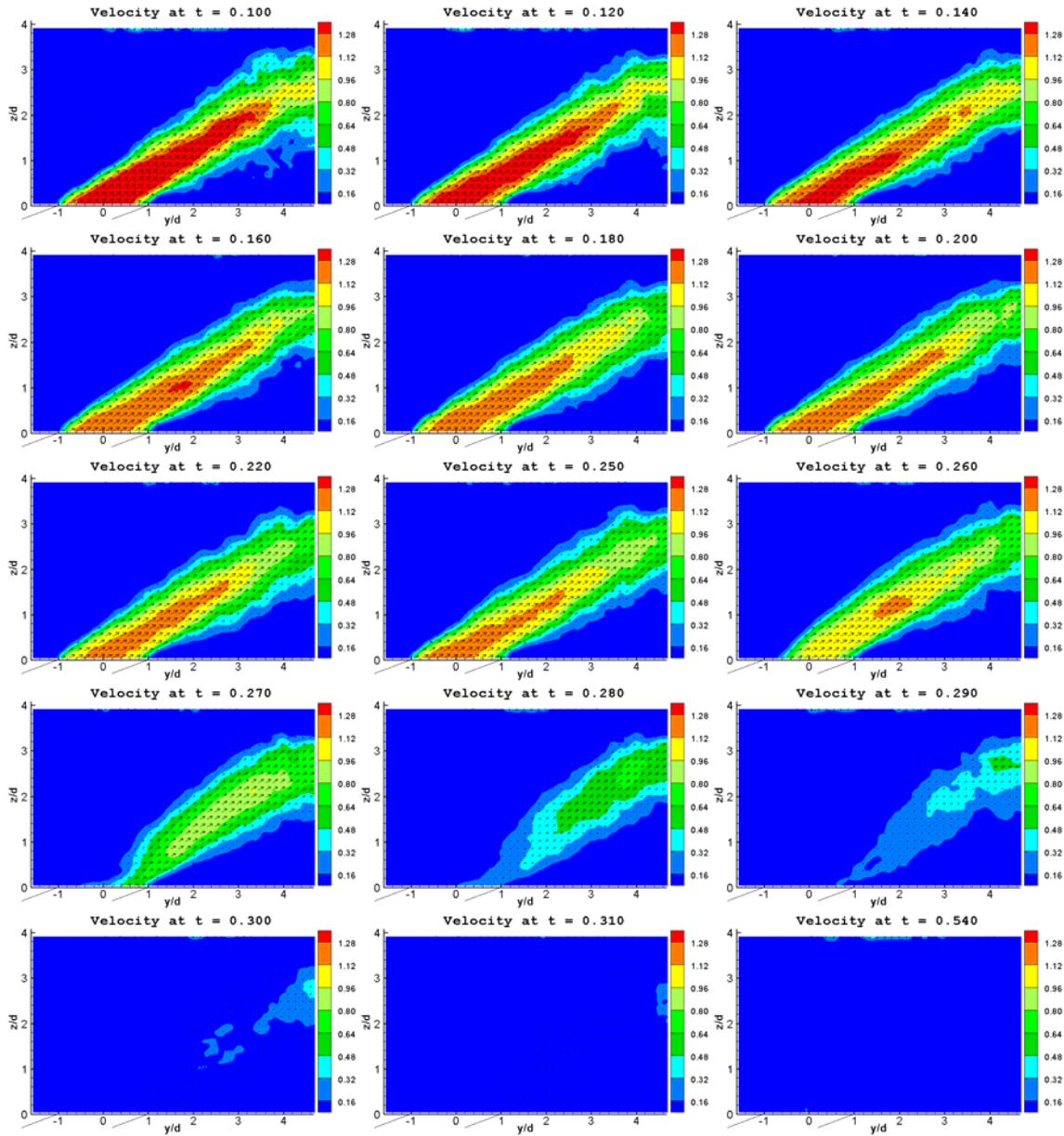


Figure 4-13. Normalized velocity plots (PIV measurement). $f = 0.5$ Hz, $\Delta = 25\%$.

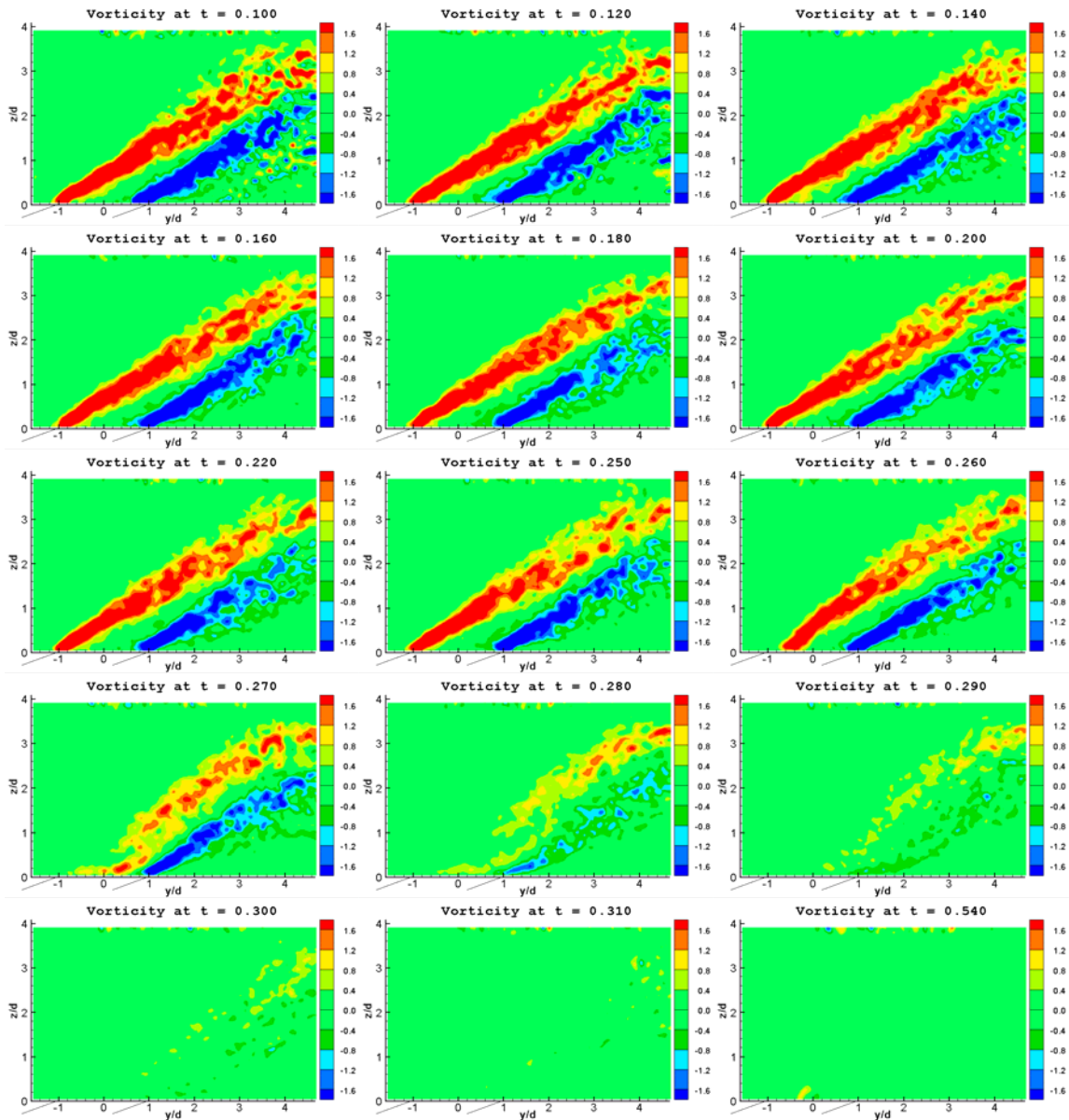


Figure 4-14. Normalized vorticity plots (PIV measurement). $f = 0.5$ Hz, $\Delta = 25\%$.

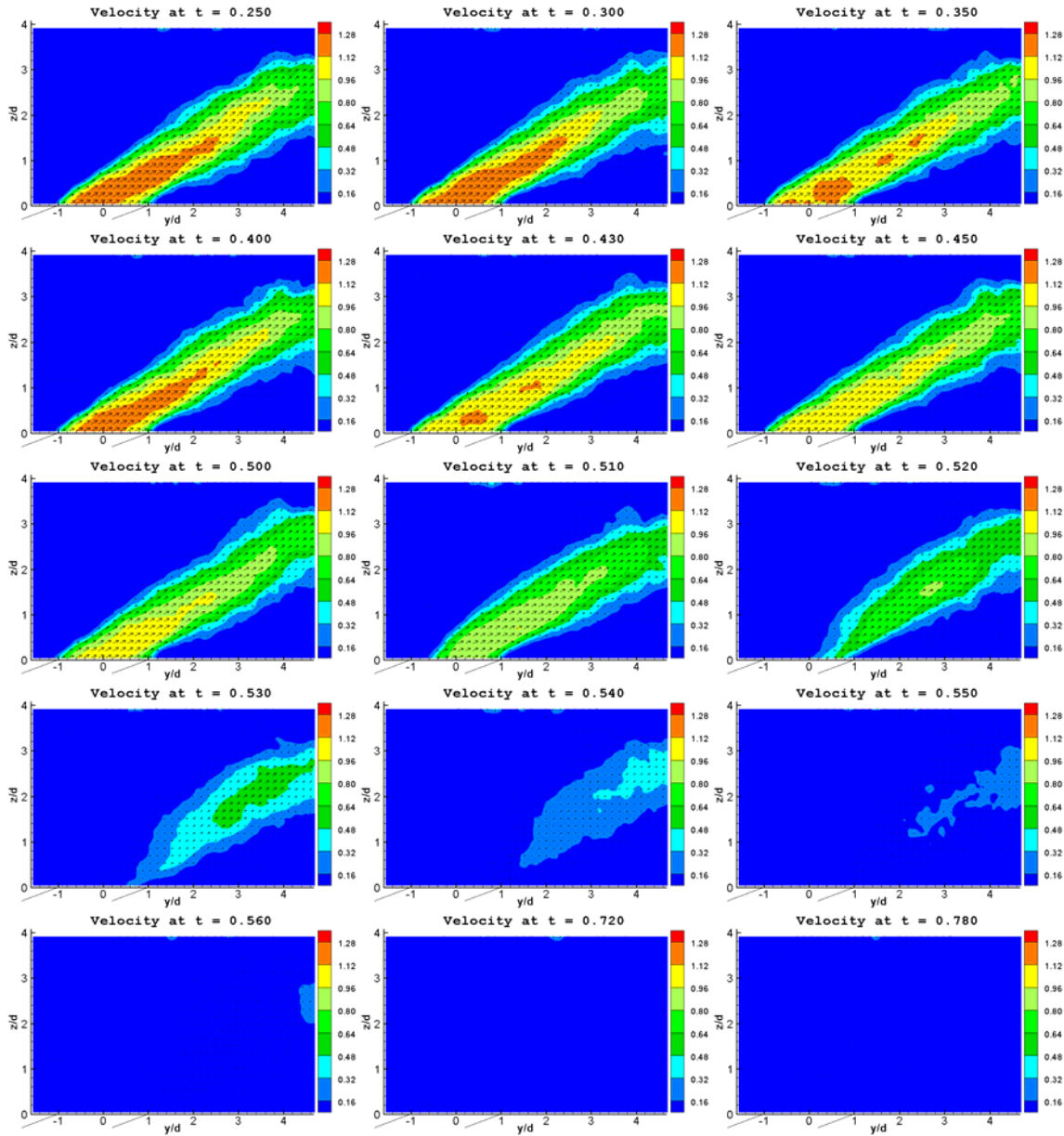


Figure 4-15. Normalized velocity plots (PIV measurement). $f = 0.5$ Hz, $\Delta = 25\%$.

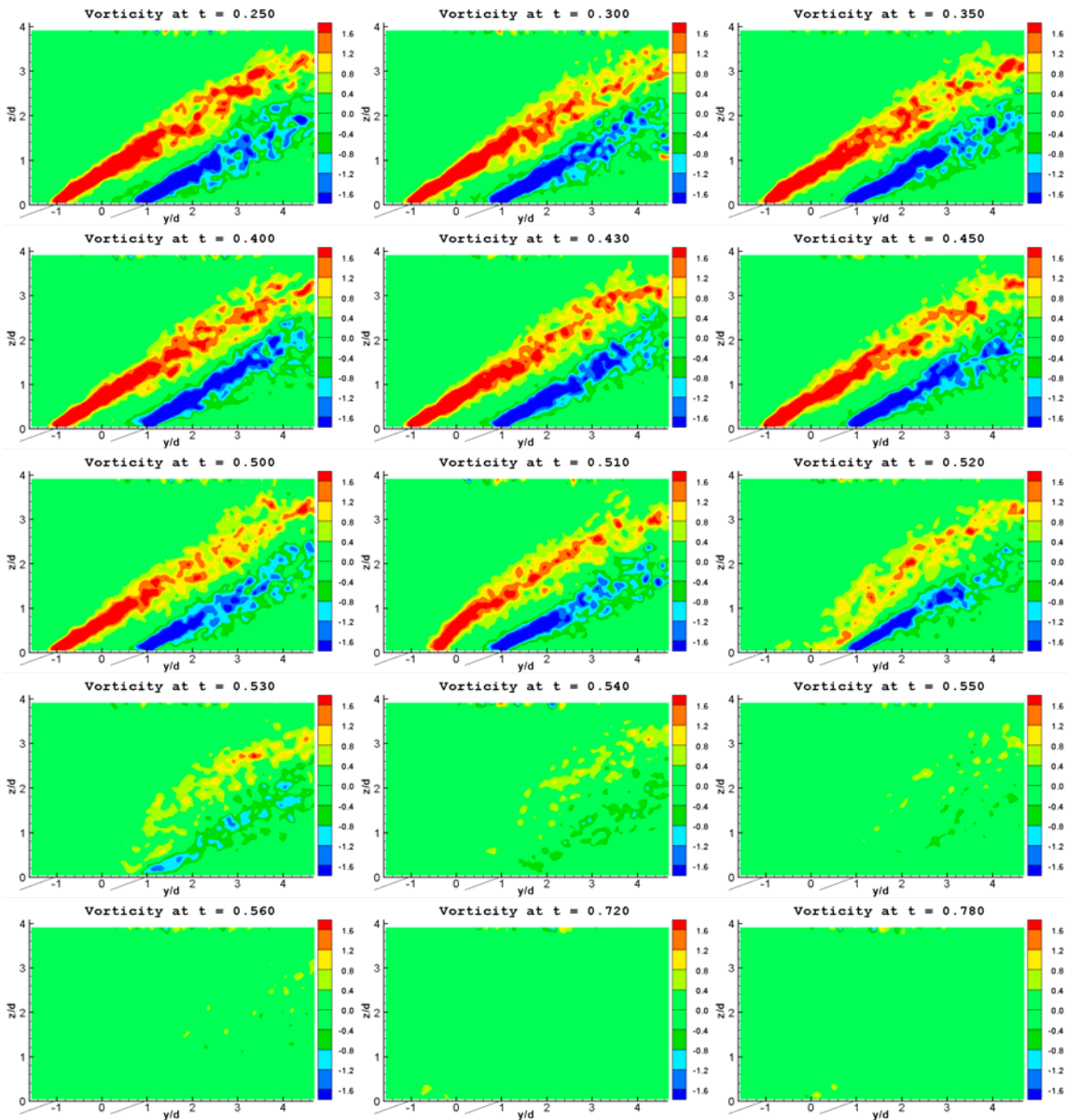


Figure 4-16. Normalized vorticity plots (PIV measurement). $f = 0.5$ Hz, $\Delta = 50\%$.

4.2.6 Conclusions for free jet PIV experiment

Each of the pulsed cases had a beginning event and an ending event due to the opening and closing of the valves. The action of the valve closing caused a small amount of residual air to be forced out of the jet. However, this event was negligible compared to the effect of the valve opening. The starting vortex developed even before an appreciable amount of mass flow had exited the jet. This occurs because of the impulse of the

pressure wave occurring when the valve opens. This impulse is somewhat damped out by the time it reaches the jet exit, due to the dynamics of the plenum and the smoke box, but still results in a strong starting vortex. In every case, the jet flow penetrated the quiescent air to just outside of the field of view, or about 5 jet diameters along the jet axis. The jet flow increased throughout the first 10% of the cycle, decreased slightly until 25% into the cycle, and decreased further to a steady value by 50% of the cycle. This is the effect of the starting impulse damping out, as was explained in Figure 4-7. The 10% duty cycle case has the most effect from the starting impulse, and could explain the results from the Bons studies, where the loss coefficient was reduced by over 50% for duty cycles as low as 10%. In those studies, the loss coefficient was reduced by 45% for a 1% duty cycle case. A 1% duty cycle case here would correspond to the valve being open for 20 ms. In the current study the starting vortex developed within 20 ms. Since there is very little mass flow at 40 ms into the cycle (keep in mind there is a 20 ms delay from the valves opening to the flow arriving at the jet exit), this would imply that this starting vortex may be the key to separation control for pulsed jets. Another key may be the maximum vorticity or velocity, since both of them also occur very early in the cycle (within the first 10%). Since there is no cross flow in this experiment, the next step is to add the crossflow and investigate the jet interaction with the boundary layer and which mechanisms are involved in controlling boundary layer separation.

5. JET IN CROSSFLOW RESULTS AND ANALYSIS

5.1 Separated Flow Case (No Jet Blowing)

In the final phase of the experiment, the jet is placed in a crossflow in order to study the interaction with the boundary layer. It is of particular interest to look at a separated boundary layer. For the current case, the boundary layer in the flow over the flat plate does not naturally separate. As discussed in Appendix D, the separated flow is caused by a ramp that is mounted across the span of the tunnel, just upstream of the jet. The tip of the ramp is 22 mm upstream of the center of the jet, and the trailing edge (back end) of the ramp is lined up with the outer diameter of the jet cylinder (which is 3 mm thick). The ramp creates a separation region that is approximately equal to the jet diameter at 25 mm. This separated flow can be seen in Figure 5-1. The figure represents the flow at center of the tunnel ($y = 2.25d$), without jet flow ($B = 0$). The shaded area in the bottom-left of the image is the ramp, and the low-velocity (blue) region downstream of that is the separation region. Notice the reverse flow that is present in the separated region. The vortex generator jet's effectiveness will be determined by how well it mitigates this reverse flow and separation. In this and subsequent figures, the velocity has been normalized by U_∞ and the vorticity by U_∞/d . The freestream velocity U_∞ was measured with a hotwire probe mounted at $x = 0$, $y = 5.25d$, $z = 3.15d$. The hot wire probe was removed before taking PIV measurements. The parameters obtained are maximum and minimum in-plane vorticity, how long (in time) the flow is attached (i.e. not separated), and how much attachment there is (i.e. at which point the attachment takes place) in the x-z plane. As discussed in Appendix D there are seven data planes,

and considering all seven planes for the $B = 0$ case the maximum and minimum vorticity is 4.83 and -1.53, respectively. The maximum vorticity occurred at $x = -0.6d$, $z = 1.0d$, in the $y = -1d$ plane, and the minimum vorticity occurred at $x = 4.1d$, $z = 0.07d$, in the $y = 5.25d$ plane. Negative vorticity is counterclockwise in the x - z plane, and positive vorticity is clockwise.

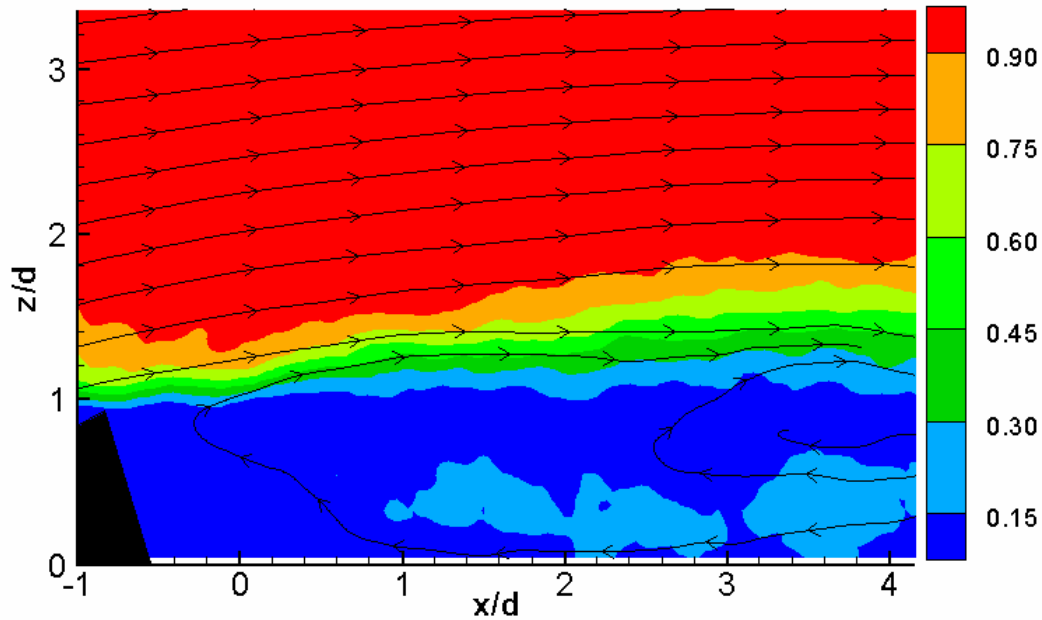


Figure 5-1. Separated Flow ($B = 0$, $y = 2.25d$)

5.2 Duty Cycle Comparison

With the free jet, the focus was the effect of duty cycle. There wasn't any difference between the starting and ending of the pulses between the different duty cycles. To see if the same were true for the jet in crossflow experiment, one case was run at 10% duty cycle and 50% duty cycle. The measurement plane was $y = 5.25d$, with the jet pulsing at 0.5 Hz ($F^+ = 0.004$) and a blowing ratio of $B = 2$. As a reminder of the location of the data planes Figure D-5 is repeated here as Figure 5-2, with the plane $y = 5d$ data plane highlighted in green.

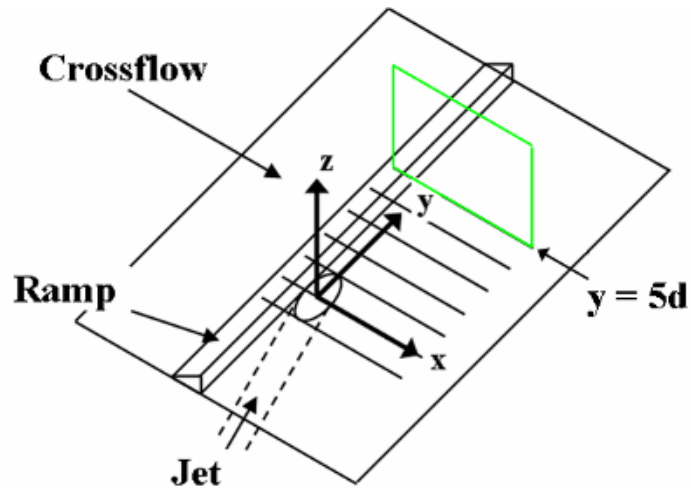
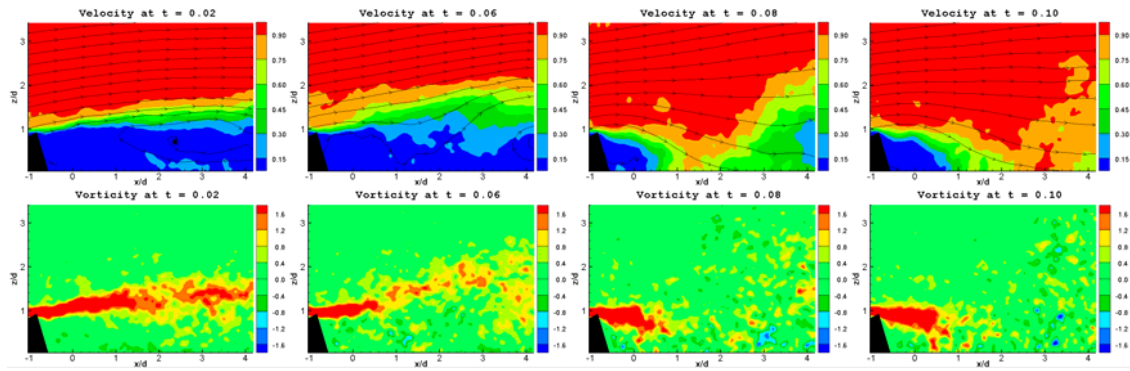
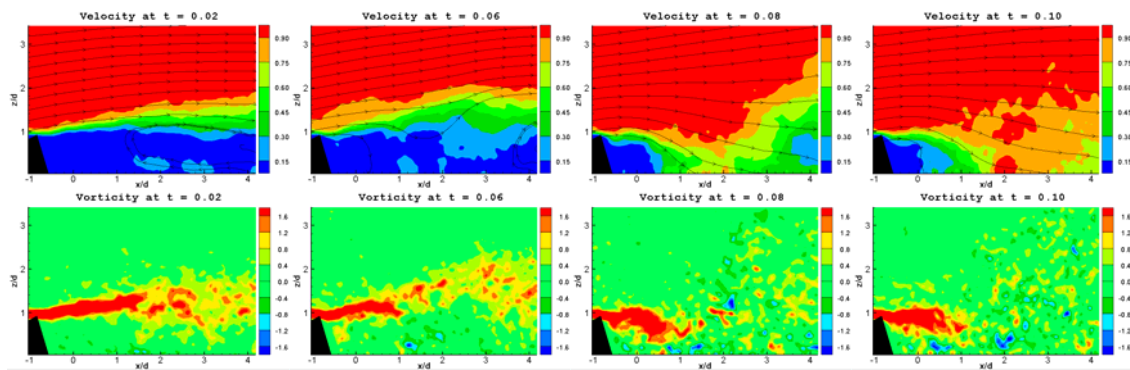


Figure 5-2. Ramp location, axis information, and data plane measurement locations

The jet is open for the first 10% of the 10% duty cycle case. This first part of the 10% duty cycle case is shown in the velocity and vorticity plots of Figure 5-3a ($t = 0.02, 0.06, 0.08, \text{ and } 0.10$). As a reminder, the parameter t is time normalized by the cycle period, which for these cases is $T = 2.0$ s. Likewise, the first 10% of the 50% duty cycle case is shown in Figure 5-3b. In comparing the plots in Figure 5-3, one can see that the first part of the cycle is the same for both cases. The 10% part of the cycle after the valve closes for both cases is shown in Figure 5-4. This time interval is $t = 0.10 - 0.20$ for the 10% duty cycle case (with $t = 0.12, 0.14, 0.16, \text{ and } 0.20$ shown in Figure 5-4a) and $t = 0.50 - 0.60$ for the 50% duty cycle case (with $t = 0.52, 0.54, 0.56, \text{ and } 0.60$ shown in Figure 5-4b). Again the data from these time intervals appear very similar for the two cases. Therefore, the effect of the jet on the crossflow is not strongly dependant on duty cycle. As long as the jet is on for a long enough time, the primary difference between duty cycles is that the effect of the higher duty cycles lasts longer, because the jet is on longer.

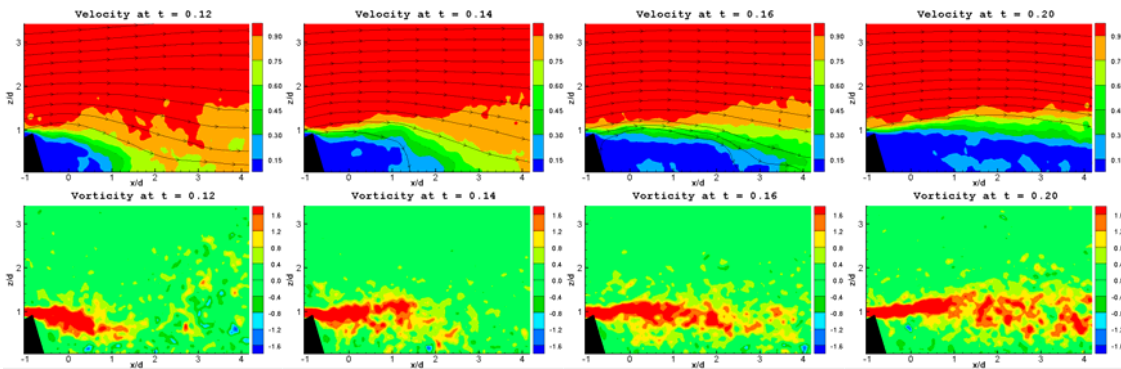


a) $\Delta = 10\%$, $t = 0.00 - 0.10$ (select instances at the beginning of the cycle)

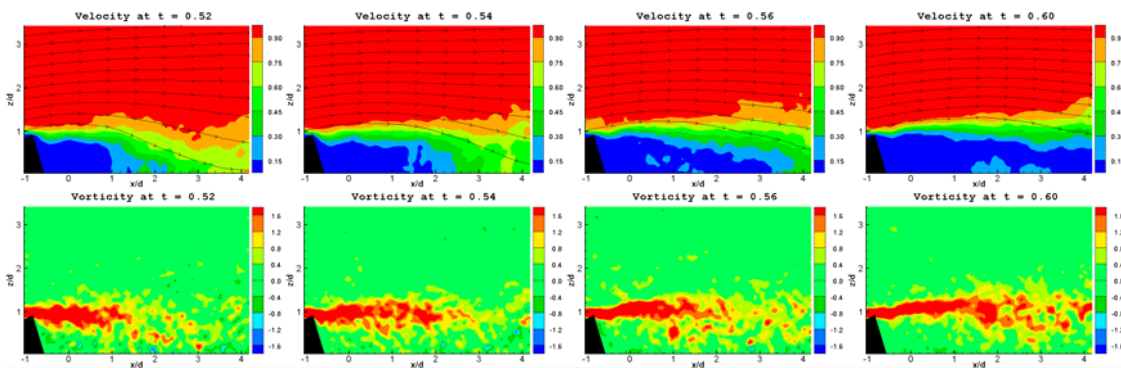


b) $\Delta = 50\%$, $t = 0.00 - 0.10$ (select instances at the beginning of the cycle)

Figure 5-3. First 10% of the $\Delta = 10\%$ case (a) and $\Delta = 50\%$ case (b), $F^+ = 0.004$, $B = 2$, $y = 5.25d$. The plots are velocity magnitude normalized by U_∞ (top), and in-plane vorticity normalized by U_∞/d (bottom).



a) $\Delta = 10\%$, $t = 0.10 - 0.20$ (select instances after valve closure)



b) $\Delta = 50\%$, $t = 0.50 - 0.60$ (select instances after valve closure)

Figure 5-4. First 10% after valve closure of the $\Delta = 10\%$ case (a) and $\Delta = 50\%$ case (b), $F^+ = 0.004$, $B = 2$, $y = 5.25d$. The plots are normalized as in Figure 5-3.

5.3 Effect of Blowing Ratio

Since changing the duty cycle doesn't strongly affect the crossflow response, a more interesting study is to look at the effects of blowing ratio. As discussed in Chapter 2, the plan was to study blowing ratios of $B = 1.0$, 2.0 , and 4.0 . After looking at the results of those blowing ratios, an additional blowing ratio of $B = 0.5$ was studied. Seven different planes of data were taken, at $y = -1.0$, 0 , 1.0 , 2.25 , 3.0 , 4.0 , and 5.25 jet diameters, as indicated in Figures 2-18 and 5-2. The plane $y = 5.25d$ was chosen because that is where attachment was most evident during the visualization with the tuft as described in section 2.3.2. The plane $y = 2.25d$ was chosen as a necessity to avoid a small hole in the tunnel roof used for a pitot tube mount at $y = 2d$ (which is the centerline

of the tunnel). The hole would cause the light sheet to break up and result in blank (dark) areas in the PIV images. Data for each plane was taken at blowing ratios of $B = 0.5, 1, 2,$ and $4,$ and at a frequency of $f = 0.5 \text{ Hz}$ ($F^+ = 0.004$) and a duty cycle of $\Delta = 50\%$. The two-dimensional planes of data for each case were combined to form a three-dimensional plot. Each data set is ensemble averaged just as the free jet data was, with 13 cycles phase locked and averaged resulting in 100 frames in 20 ms increments. Rather than showing 100 plots for each case, only select data subsets are shown in order to highlight certain parts of the cycle.

5.3.1 $B = 4$ Case ($f = 0.5 \text{ Hz}, \Delta = 50\%$)

Figure 5-5 shows the selected data subsets of the $B = 4$ case. The time of each frame is shown above each three-dimensional plot. The initial fully separated state of the flow is seen at time $t = 0.00$. The location of the jet is drawn onto the figure for reference. The ramp is not shown, but it is just upstream of the jet and extends across the entire span. Notice the reverse flow and circulation in the separated region. At this moment, the valves open and the air begins flowing to the jet. At $t = 0.01$ the jet flow has entered the $y = 0d$ plane. Behind the jet flow, in the $y = -1d$ plane, is a downward motion of air flow due to the entrainment caused by the starting vortex. This initial downward motion near the jet is maintained as the jet continues to entrain the air around it. As the jet flow penetrates deeper into the freestream, this entrainment causes the crossflow to swirl around the core of the jet flow. The jet flow does not mix well with the crossflow in this case because the jet flow momentum is so much higher and is not affected much by the crossflow. This can be seen at $t = 0.05$, as the jet has penetrated through the $y = 5.25d$ plane. The air downstream of the jet flow is drawn downward in the $y = -1d$ and

0d planes, but is then drawn upward in the $y = 2.25d$, $3d$, $4d$, and $5.25d$ planes. There is likely much out of plane motion (which is not measured) in the $y = 1d$ plane as the jet flow is drawing this downstream air towards itself. The flow has reached a “steady” state by $t = 0.20$, with the flow attached in the $y = -1d$, $0d$, and $1d$ planes, a large amount of reverse flow in the $y = 2.25d$ and $3d$ planes, and more attachment in the $y = 4d$ and $5.25d$ planes. In the $y \geq 2.25d$ planes, any flow downstream of the jet flow is drawn back upstream towards the jet. This is the freestream swirling around the jet flow. At $t = 0.5$, the valves close and stop the air flow to the jet. Without the momentum sustaining the jet flow, the crossflow begins to take over. This can be seen at $t = 0.55$, where the previously obstructed crossflow (in the planes $y \geq 2.25d$) is now able to flow in the downstream direction. In the $y = 2.25d$ plane, the drastic change in momentum causes a circulation region that draws freestream air downward as the shear layer reestablishes. By $t = 0.57$, the flow is attached across the entire measured span ($y = -1d$ to $y = 5.25d$). The shear layer stabilizes and the flow returns to its fully separated state by $t = 0.67$, with the last bit of attachment seen at $t = 0.66$.

There was at least some attachment for about 62% of the cycle. This occurred in the $y = 0d$ plane, and there was typically $4.53d$ of surface contact (attachment length) in that plane during that time period. This quantification was done for each plane, and the results are shown in Table 5.1.

Table 5.1. Summary of attachment characteristics for the $B = 4$ case.

y/d	-1.0	0.0	1.0	2.25	3.0	4.0	5.25	AVG
Attachment Start Time	0.05	0.05	0.07	0.56	0.56	0.55	0.54	0.34
Attachment End Time	0.65	0.67	0.66	0.61	0.61	0.61	0.61	0.63
Total Attachment Time	0.60	0.62	0.59	0.05	0.05	0.06	0.07	0.29
Typ. Attachment Length	4.13	4.53	0.79	2.17	2.17	1.97	2.56	2.62

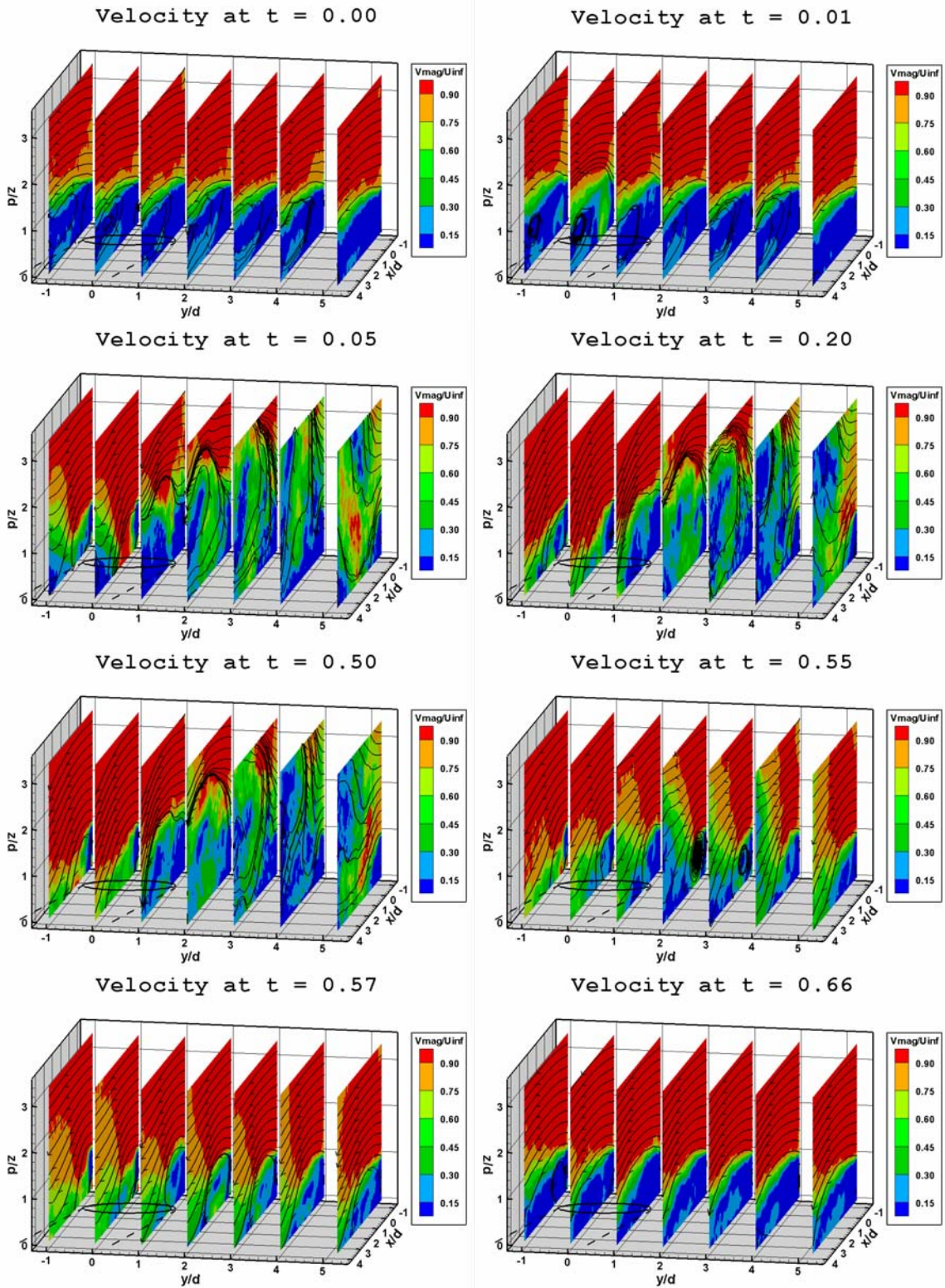


Figure 5-5. Normalized velocity plots (velocity magnitude divided by U_∞) for $B = 4$, $F^+ = 0.004$ Hz, $\Delta = 50\%$ case

Although not shown here, the vorticity plots indicate a maximum in-plane vorticity (normalized by U_∞/d) of $\omega_j = 8.05$ and a minimum of $\omega_j = -5.83$ for this case. Note that only the spanwise component of vorticity can only be calculated because velocity data is only available in the x-z plane. The maximum vorticity occurs at $x = -0.72d$, $z = 0.98d$ in the $y = 4d$ plane, and at $t = 0.34$. This point is very close to the ramp tip, which is located at $x = -0.87d$, $z = 0.87d$, indicating the large amount of vorticity is in the shear layer. The minimum vorticity occurs at $x = 4.03d$, $z = 0.31d$, in the $y = 3d$ plane, and at $t = 0.10$.

5.3.2 B = 2 Case (f = 0.5 Hz, Δ = 50%)

The $B = 2$ case is shown in Figure 5-6. This case starts out the same as the $B = 4$ case, with fully separated flow at $t = 0.00$. In this case the jet flow is just barely seen at $t = 0.01$, and more apparent at $t = 0.02$. A similar effect is seen at the start of the cycle with the initial downward movement of air just upstream of the jet (in the $y = -1d$ plane) as the starting vortex entrains the air around the jet flow. In this case the jet flow is not as strong and does not entrain the air around it as it did in the $B = 4$ case. This can be seen at $t = 0.09$, as the jet has penetrated through the $y = 3d$ plane, and is having an impact on the $y = 4d$ plane as it gets turned downstream. The jet flow in the $B = 2$ case has much lower momentum than the $B = 4$ case, and the jet flow does not maintain its form long as it penetrates into the crossflow. However, there is some entrainment in the $y = 1d$ and $2.25d$ planes as the jet flow draws downstream air towards itself. There is also attachment in the $y = 5.25d$ plane. As the flow reaches a steady state ($t = 0.20$), the flow in the $y = 4d$ plane becomes attached as well. The attachment in the $y = 4d$ and $5.25d$ planes is present in this case and not in the $B = 4$ case because the jet flow has turned downstream instead of acting as an obstruction to the crossflow. After the jet turns off

(i.e. the valves close), the flow behavior is similar to the $B = 4$ case. By $t = 0.55$, the crossflow has started to take over, most notably at $y = 2.25d$ as in the $B = 4$ case, where a circulation region has formed bringing freestream air down to the surface. As in the $B = 4$ case, there is spanwise attachment at $t = 0.57$, but here the last attachment comes at $t = 0.62$ before the flow returns to its fully separated state. As was done for the $B = 4$ case, a summary of the flow attachment is shown in Table 5.2. Also, the maximum vorticity in this case is $\omega_j = 7.89$, and occurs at $x = -0.76d$, $z = 1.02d$, in the $y = 4d$ plane, and at $t = 0.28$. Note that there is not much of a change from the previous case to this case in maximum vorticity. The minimum vorticity in this case is $\omega_j = -3.52$, and occurs at $x = 1.08d$, $z = 0.74d$, in the $y = 3d$ plane, and at $t = 0.06$.

Table 5.2. Summary of attachment characteristics for the $B = 2$ case.

y/d	-1.0	0.0	1.0	2.25	3.0	4.0	5.25	AVG
Attachment Start Time	0.06	0.56	0.57	0.57	0.55	0.12	0.07	0.36
Attachment End Time	0.63	0.61	0.60	0.60	0.59	0.59	0.58	0.60
Total Attachment Time	0.57	0.05	0.03	0.03	0.04	0.47	0.51	0.24
Typ. Attachment Length	0.59	1.18	0.98	1.18	2.36	2.95	3.35	1.80

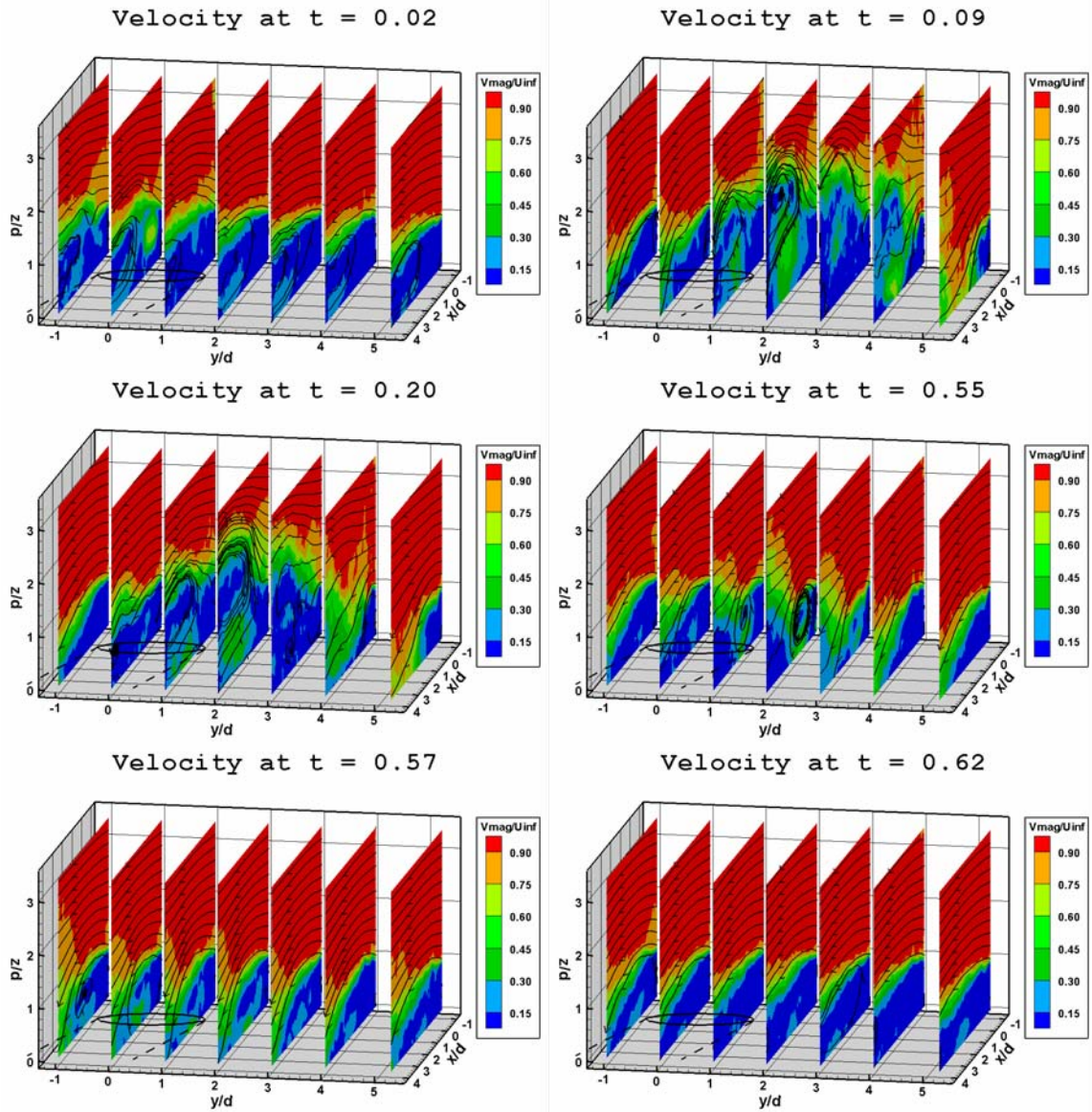


Figure 5-6. Normalized velocity plots (velocity magnitude divided by U_∞) for $B = 2$, $F^+ = 0.004$ Hz, $\Delta = 50\%$ case

5.3.3 $B = 1$ Case ($f = 0.5$ Hz, $\Delta = 50\%$)

The $B = 1$ case is shown in Figure 5-7. The $B = 1$ jet flow is apparent at $t = 0.02$, but is better seen at $t = 0.03$. In this case the downward motion in the $y = -1d$ plane is barely noticeable. The momentum of the jet flow is so much lower in this case that the jet flow gets turned downstream almost immediately upon penetrating the crossflow in the $y = 2.25d$ plane. Figure 5-7 shows the “steady” state flow at $t = 0.20$, with the trailing

edges of the $y = -1d$ and $y = 3d$ planes going in and out of attachment. The $y = 4d$ plane shows nearly full attachment. The $y = 5.25d$ plane is an indicator of how weak the $B = 1$ jet really is, as it has almost no effect that far away. The $y = 1d$ plane shows some entrainment of downstream air as the jet flow is still strong enough to draw that air towards itself. The $B = 2$ and $B = 4$ cases showed a circulation region form at $y = 2.25d$ after the jet turned off. In this $B = 1$ case, this same effect occurs but at $y = 1d$ and at $t = 0.53$. This brings near attachment in the $y = -1d$ through $y = 4d$ planes at $t = 0.55$. However, this weak attachment only persists until $t = 0.56$, except in the $y = 2.25d$ plane, where it lasts until $t = 0.59$. The flow then is fully separated. The summary of the flow attachment for this case is shown in Table 5.3. The maximum vorticity for the $B = 1$ case is $\omega_j = 5.79$, and occurs at $x = -0.94d$, $z = 0.96d$, in the $y = 3d$ plane, and at $t = 0.18$. The minimum vorticity is $\omega_j = -2.03$, at $x = -0.15d$, $z = 1.64d$, $y = 0d$, and $t = 0.71$.

Table 5.3. Summary of attachment characteristics for the $B = 1$ case.

y/d	-1.0	0.0	1.0	2.25	3.0	4.0	5.25	AVG
Attachment Start Time	0.00	0.00	0.00	0.54	0.11	0.09	0.12	0.12
Attachment End Time	0.00	0.00	0.00	0.59	0.57	0.58	0.18	0.27
Total Attachment Time	0.00	0.00	0.00	0.05	0.46	0.49	0.06	0.15
Typ. Attachment Length	0.00	0.00	0.00	0.20	0.98	3.15	0.98	0.76

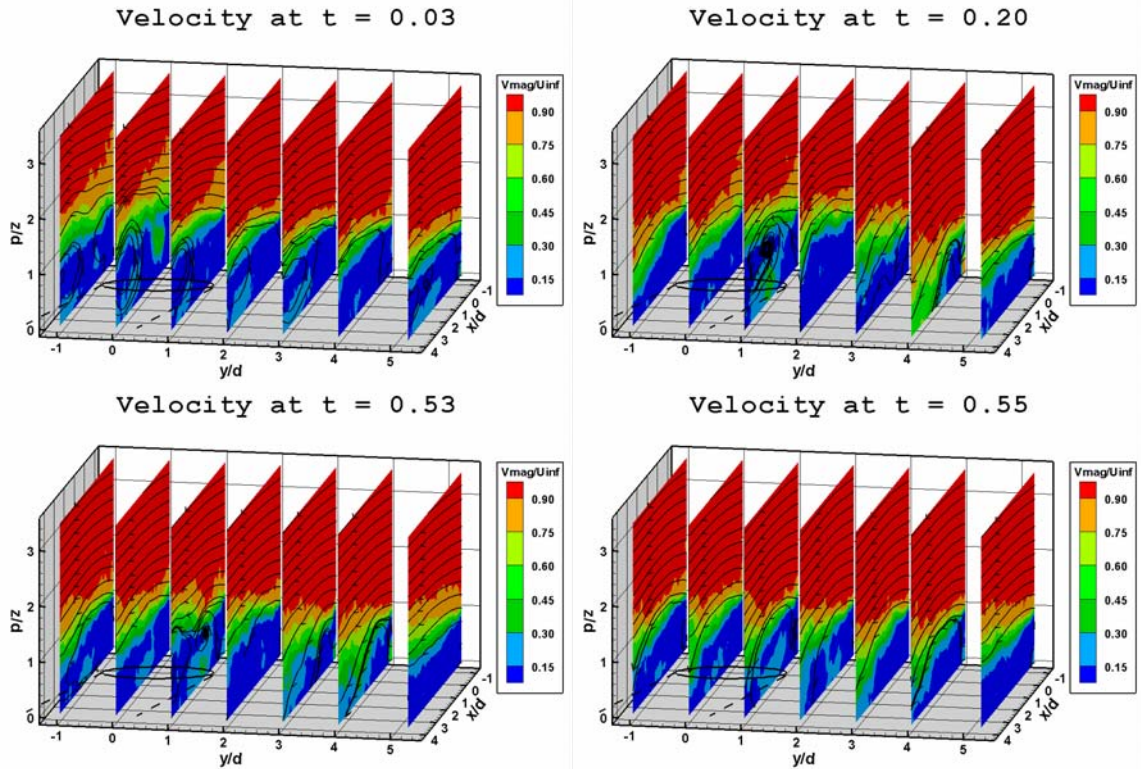


Figure 5-7. Normalized velocity plots (velocity magnitude divided by U_∞) for $B = 1$, $F^+ = 0.004$ Hz, $\Delta = 50\%$ case

5.3.4 $B = 0.5$ Case ($f = 0.5$ Hz, $\Delta = 50\%$)

Figure 5-8 shows the $B = 0.5$ case. In the $B = 0.5$ case, the jet flow is too weak to even penetrate into the crossflow. This is seen at $t = 0.06$ where the jet flow is evident, but the crossflow is undisturbed. By $t = 0.20$ there is a slight bending over of the flow in the $y = -1d$ plane, but other than that the flow still is fully separated. The flowfield remains much the same (with slight fluctuations on how much the crossflow is bent downward in the $y = -1d$ plane) until the valve shuts off at $t = 0.5$. There is still no noticeable effect on the remainder of the flow, and the entire three-dimensional field is back to its original state by $t = 0.57$. No summary table is shown in this case because there was no attachment whatsoever across the span, and the table would just be filled with zeros. The maximum vorticity in this case is $\omega_j = 4.96$, and occurs at $x = -1.10d$, $z =$

1.01d, in the $y = -1d$ plane, at $t = 0.33$. The minimum vorticity is $\omega_j = -1.88$, at $x = 3.12d$, $z = 0.29d$, $y = 5.25d$, and $t = 0.01$.

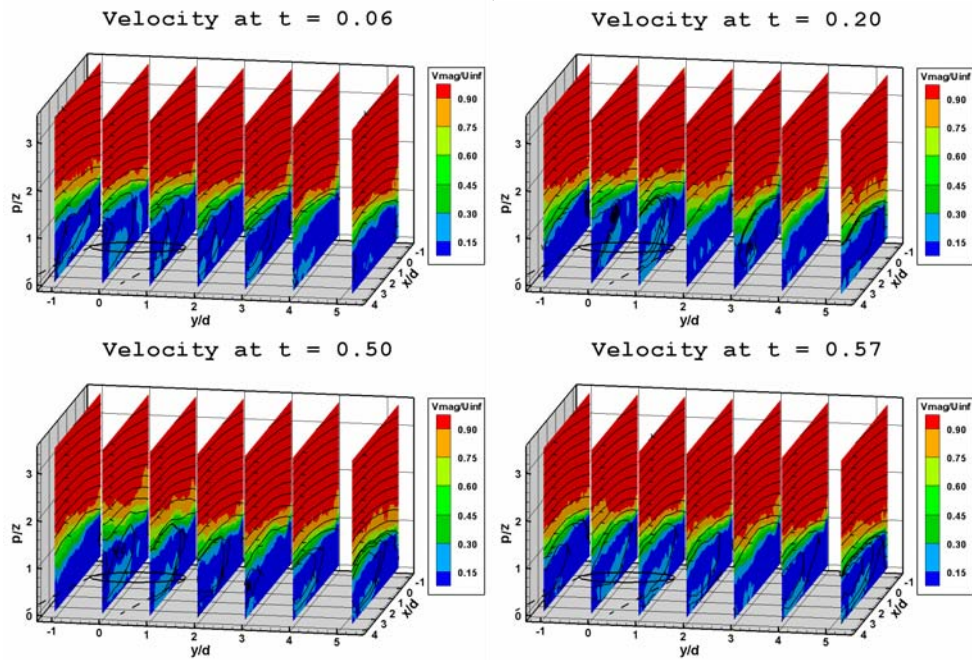


Figure 5-8. Normalized velocity plots (velocity magnitude divided by U_∞) for $B = 0.5$, $F^+ = 0.004$ Hz, $\Delta = 50\%$ case

5.4 Conclusions for jet in crossflow experiment

Table 5.4 shows a summary of Tables 5.1 through 5.3 describing the average attachment time and length for each case. Also included in Table 5.4 are the maximum and minimum vorticity values for each case. Figures 5-9 and 5-10 contain plots of the values in Table 5.4. Even though streamwise vorticity (the component of vorticity in the x-direction) was not measured (because no resolvable PIV data was taken in the y-z plane), there is a definite trend noted with the cross-stream vorticity. Both the counterclockwise and clockwise vorticity increased with blowing ratio. This is consistent with the results of Compton and Johnston [7], who concluded that maximum vorticity is strongly dependent on jet velocity. They were referring to streamwise vorticity, but an assumption can be made that it applies to cross-stream vorticity as well (assumption

explained in the next paragraph). This trend is shown in Figure 5-9. Clearly the vorticity is increasing for increasing jet velocity, although the clockwise vorticity didn't change much going from $B = 2$ to $B = 4$. This may indicate a limit of clockwise vorticity when increasing jet flow. If this is true, it would be because the maximum vorticity in this experiment is in the shear layer near the ramp tip, and is more influenced by the ramp than the jet flow at higher jet velocities. This would likely be different in a naturally separated environment where the shear layer would not be as strong. The counterclockwise vorticity does not show signs of leveling off, however. This may indicate that clockwise vorticity is responsible for the time of attachment, and the counterclockwise vorticity is responsible for the length of attachment. Clockwise motion would tend to bring the crossflow down to the surface, and counterclockwise motion would tend to draw the attached flow closer to the jet. This can be backed up by Figure 5-10. The $B = 2$ case included three planes that averaged over a second of attachment time. Likewise, the $B = 4$ case also included three planes with over a second of attachment time. However, the $B = 2$ case averaged much less attachment size than the $B = 4$ case. So there is a stronger increase in attachment size going from $B = 2$ to $B = 4$, which corresponds to a stronger increase in counterclockwise vorticity, but not much increase in attachment time, which corresponds to only a slight increase in clockwise vorticity. A similar phenomena occurs in comparing $B = 1$ and $B = 2$.

Table 5.6. Summary of averaged attachment from each case plus max and min vorticity.

B	Attached Time	Attached Length	ω_{\min}	x/d	z/d	t	ω_{\max}	x/d	z/d	t
4	0.29	2.62	-4.60	1.50	0.95	0.16	7.59	-0.63	1.08	0.34
2	0.25	1.80	-2.85	0.73	1.42	0.29	7.06	-0.85	0.97	0.35
1	0.15	0.76	-1.62	2.66	1.07	0.59	5.11	-0.73	0.99	0.51
0.5	0.00	0.00	-1.55	3.31	0.17	0.32	4.64	-0.48	1.03	0.58
0	0.00	0.00	-1.10	2.40	0.11	0.00	4.07	-0.33	1.06	0.00

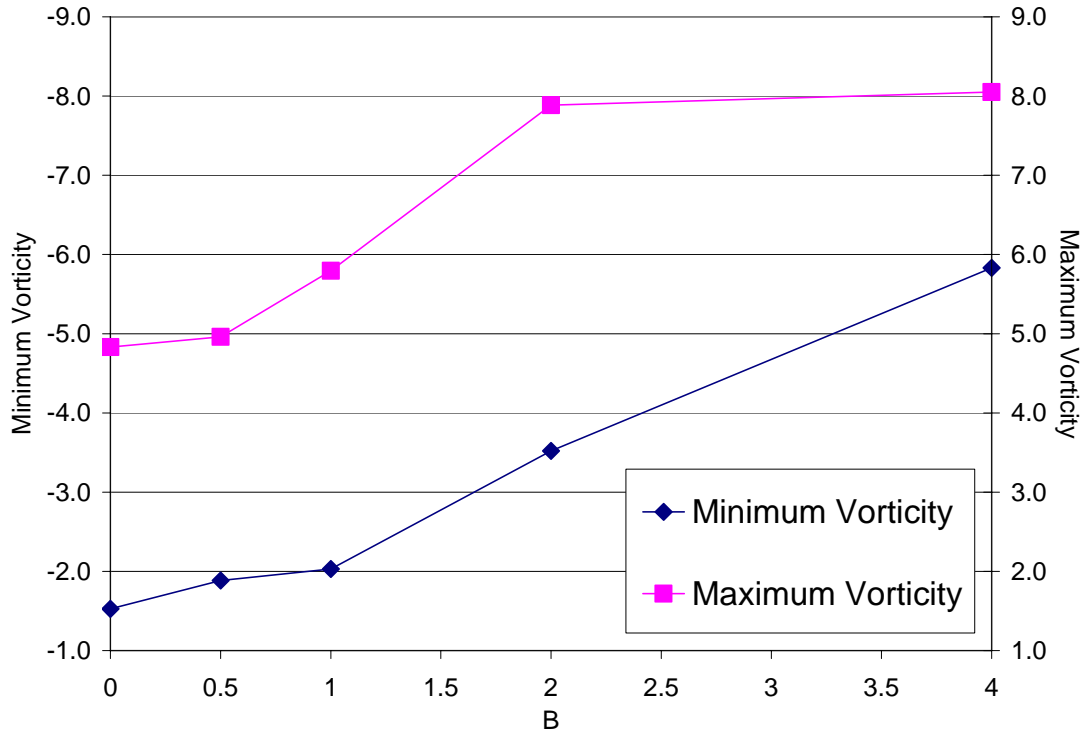


Figure 5-9. Maximum and minimum in-plane vorticity (averaged spanwise).

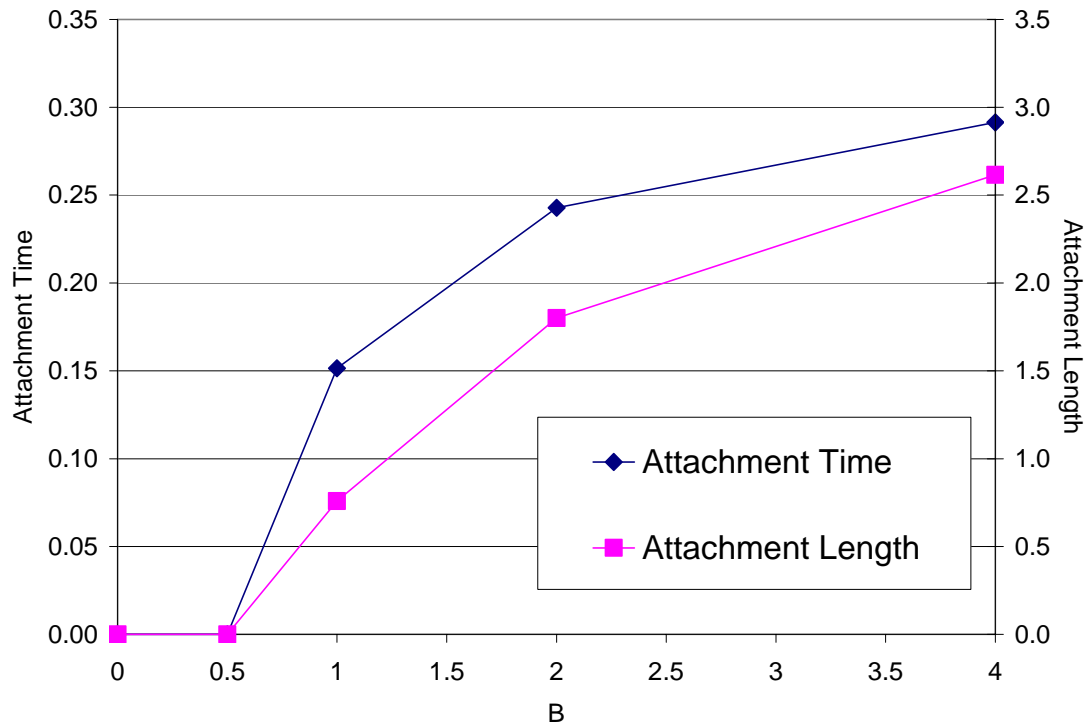


Figure 5-10. Attachment time and length (averaged spanwise).

It makes sense that cross-stream vorticity would relate to streamwise vorticity due to the nature of how the vortices are formed. It is impossible to see without overlapping the images since the particle displacement is so small, but in looking at the captured PIV images of the cross-stream planes, one can see a pair of counter-rotating vortices when the jet is on for the $B = 2$ case. There is a counterclockwise vortex on the side closest to the jet, and a clockwise vortex on the other side. So the crossflow is being pulled down near the jet, and being moved in the positive y -direction (the direction of the jet flow). Further away from the jet, the crossflow swirls underneath and around the jet. As the jet gets turned downstream by the crossflow, this swirling motion causes a clockwise circulation in the cross-stream plane. So the air moving one direction from the leading edge of the jet toward the positive y -direction meets the air moving in the opposite direction, and a counter-rotating vortex pair forms. This is why there was attachment near the jet and further from the jet, but not in between for the $B = 2$ and $B = 1$ cases. This also explains why there was no attachment away from the jet for the $B = 4$ case. Since the jet velocity was so high, and the jet did not get turned downstream in the planes that were studied, only one side of the counter-rotating vortex pair was seen. Had more planes further from the jet been studied, the jet flow would have moved downstream and there likely would have been attachment much further away from the jet. Also, the streamwise counter-rotating vortex pair explains much of the out-of-plane motion that was likely to occur in many of the cases. The counter-rotating vortex pair also shows how the vorticity in the x - z plane translates into vorticity in the y - z plane, thus confirming the results of Compton and Johnston referred to earlier.

A final key observation to note is the events of the beginning and ending of each cycle. Without having data in the cross-stream planes, it is difficult to trace out where the starting vortex is. However, at the beginning of each cycle near the jet (at $y = -1d$, for the $B = 1, 2$, and 4 cases), there was a downward motion that most certainly was the effect of the starting vortex. This brings the initial pull of the crossflow down towards the surface. The ending of each cycle was also important. When the valves providing the jet flow get cut off, the attachment (if present) would let up slightly as the flow from the jet loses momentum. When the jet flow is depleted soon after the valves close, the resulting pressure gradient causes the crossflow to flow down to the surface near the jet. This effect was strong enough in the $B = 2$ and $B = 4$ cases to provide attachment across the entire span, and in the $B = 1$ case for $y > 1d$, for about 10 ms. It does not last long because the jet air dissipates quickly away from the jet with no momentum behind it, and once the shear layer stabilizes again the flow is reverted back to its fully separated state. It is speculated that due to the damping effect of the feed plenum and smoke box, the starting and ending events are much less drastic than they would be in a less-damped system. If this were the case, we would see even more attachment (in length and time) at the beginning and ending of each cycle. The frequency and duty cycle could then be optimized to cause this beginning and ending event and not waste mass flow by letting the jet blow excessively. Johari and McManus [6] said that the jet injection time should be limited to that of the starting vortex formation. They also said that the starting vortex formation time could be estimated by $4d/V_j$, where V_j is the velocity of the jet. This is consistent with the findings in the free-jet case, when the jet velocity was 3.15 m/s and the starting vortex took 20 - 40 ms to form (would be estimated as 32 ms with the

equation). Bons, et al. [17], also concluded that the key mechanisms for controlling boundary layer separation with pulsed jets are the starting and stopping of the pulses rather than the injection itself.

Another optimization parameter to consider is the spacing of the jets. In the current study, there was only a single jet. In a more realistic study, there would be multiple jets across the span. The $B = 2$ case is the easiest to apply this concept to. In that case, there was attachment near the jet at $y = -1d$, and further from the jet at $y = 4$ and $5.25d$. In between those planes there were counter-rotating vortices that caused the attachment. In the planes outside of $y = -1d$ there would likely not be any attachment, since there is not very much attachment in the $y = -1d$ plane. The jets should therefore be spaced so the first jet causes attachment just behind the second jet. The center of the first jet to the rear of the second jet would be something greater than $5.25d$, so center-to-center spacing would be something greater than $6.25d$. It is not clear how much influence the $B = 2$ jet has past $5.25d$, so one cannot say for sure what the spacing should be without studying more planes. This would not necessarily attach the flow across the span, however, due to the planes in between $y = -1d$ and $4d$. These planes contain the counter-rotating vortex pair that helps maintain the attached flow. The spacing could be adjusted even narrower so that the flow may be attached across the span, but it is unclear how this would effect the overall attachment because the counter-rotating vortex pair would be affected.

The better way to optimize spacing would be to first make sure that the frequency is optimized. Remember, when the jet turns off for the $B = 2$ and $B = 4$ cases, there is temporary attachment across the entire measured span. If the frequency were optimized such that this happened often enough to keep the flow attached, then the spacing in these

cases would be something greater than seven diameters and the flow would be attached across the span. For the $B = 1$ case the flow was only attached in the $y = 2.25, 3,$ and $4d$ planes after the jet turned off. Therefore, a proper spacing would be 3 diameters to achieve attached flow across the span. Note that a blowing ratio of two would be preferred because one could get away with over twice the spacing even though the blowing ratio is twice as much. The overall mass flow from the jets would be less in the $B = 2$ case.

In summary, the parameters of blowing ratio, frequency, duty cycle, and jet spacing should all be considered in trying to control boundary layer separation and minimizing the required mass flow. In this experiment, an ideal frequency was unachievable, and therefore looking into duty cycle effects was not attempted. Also, jet spacing was limited to one jet. However, it was found that an increasing blowing ratio can cause an increase in attachment length, and that spanwise attachment can be obtained due to the effect of the jet shutting off at higher blowing ratios.

6. SUMMARY AND CONCLUSIONS

An experiment was set up to find the mechanisms involved in boundary layer separation control using Particle Image Velocimetry. This started with a rotating disk calibration experiment, which not only was an opportunity to get familiar with PIV, but also a chance to learn how to reduce errors in PIV data collection. The experiment was a success, with an average error of 1.56% in the final case studied. The main thing learned from that experiment was to make sure the particles have enough of a displacement, and that too short of a time between images can result in large errors.

The rotating disk experiment was followed by a free jet experiment using Hot Wire Anemometry. The jet was a large-scale model of the PakB blade design in the Low Speed Wind Tunnel Facility of the Air Force Research Laboratory, scaled at 25 times the jet diameter, with the same pitch and skew angles of 30° and 90° , respectively. The hot wire experiment provided a look at the behavior of the jet without the influence of crossflow, and used a familiar measurement technique. It would provide a baseline for the PIV results to be taken later. Duty cycles of 10%, 25%, and 50% were studied at a frequency of 4 Hz, and a jet velocity of 3.15 m/s. The conclusion drawn from the hot wire experiment was that the starting vortex is likely to be a key mechanism for controlling boundary layer separation.

The hot wire analysis of the free jet was followed up with a PIV analysis. Due to the requirement of having to seed the jet flow, a modification had to be made to the feed plenum. This changed the behavior of the jet, damping out what was already a damped flow of velocity from the valves, which output a square wave pulse of air. The pulsing

frequency had to be changed from 4 Hz to 0.5 Hz to accommodate this change. One test was run at 4 Hz using PIV, and then using the hot wire method. These tests compared very well, providing the bridge between the hot wire and the PIV experiment. The 4 Hz case was ran six times using the PIV method in order to estimate the variability of the results. Combining this variability with a standard measurement error of 0.1 pixel, the total uncertainty in the PIV results was estimated to be 5.3%. The free jet PIV experiment was then performed at 0.5 Hz, and a jet velocity of 3.15 m/s, looking at duty cycles of 10%, 25%, and 50%. There was basically the same behavior in the PIV case as the hot wire experiment, with the exception that the cycles lasted longer due to the lower frequency. The starting vortex formed in all cases, and it was still determined that it was a key mechanism in boundary layer separation control. The end of each cycle included a “kick-back” and a suction effect that could also have an influence on the boundary layer, but this effect appeared negligible compared to the starting vortex and the main jet flow. Both the starting vortex and “kick-back” effect were not as strong due to the added damping of the PIV setup.

The last phase of this project was the use of the PIV technique on the jet in a crossflow. It was determined that differences in duty cycles were not significant enough to perform a duty cycle study as before. Instead, with the crossflow experiment, the blowing ratio was varied from $B = 0$, $B = 0.5$, $B = 1$, $B = 2$, and finally $B = 4$. Seven spanwise planes were studied, spaced nominally in $1d$ increments and centered in the tunnel. The frequency was 0.5 Hz, and the duty cycle was 50% for all cases. Perpendicular (cross-stream) planes were attempted, but the out of plane motion was too great to obtain good PIV results. Due to the low-frequency limitations of the setup, the

jet could not be pulsed fast enough to maintain an attached flow for much longer than the duty cycle. Attachment was seen for blowing ratios as low as unity, although greater blowing ratios resulted in more attached area and longer attached times. It was determined that not only the starting event but also the ending event of the cycle were keys in eliminating separation. The starting event because it provided that first impulse that pulls the crossflow towards the surface, and the ending event because it provided a suction that brought spanwise attachment for the $B = 2$ and $B = 4$ cases. During the actual flow of the jet, attachment was not spanwise in these cases. In fact only three of the seven planes in the $B = 2$ and $B = 4$ cases showed any attachment during the duty cycle. The $B = 1$ case only showed attachment in two planes. This showed the need for optimizing spacing of the jets to provide spanwise attachment. Spanwise attachment was also speculated to be able to occur if the pulsing frequency was optimized so the effect of the beginning and ending events can be used to keep the flow attached for longer periods of time. The optimization of frequency, duty cycle, blowing ratio, and spanwise spacing of the jets will help to reduce the required mass flow for obtaining an attached boundary layer using pulsed vortex generator jets.

APPENDIX A. BACKGROUND TO PARTICLE IMAGE VELOCIMETRY

References from Raffel et al. [19], and Dantec Measurement Technology [20] were primarily used in the background study presented in this section. Particle Image Velocimetry (PIV) was developed to provide a two-dimensional velocity mapping of the flow. It is a non-intrusive measurement technique that can also be extended into three-dimensions. There are four major components to a PIV system, the laser, the camera, the optics, and the seeding. The formation of these components is shown in a basic PIV setup in Figure A-1. Not shown in Figure A-1 is the computer that is necessary to control the camera and can sometimes be used to control the laser.

The laser is typically dual-headed and outputs two separate beams. Each laser head is typically a high-powered laser (10 to 400 mJ) such as a Nd:YAG laser. The Nd:YAG consists of Neodymium ions that are seeded into a yttrium-aluminum-garnet crystal, which builds up energy and releases a beam with a 1064 nm wavelength when pumped by a flash lamp. There is usually a frequency doubler within the laser enclosure that halves the wavelength (i.e., 1064 nm to 532 nm). In order to achieve maximum energy from the laser, most PIV applications use a pulsed laser that outputs short bursts of high energy. Continuous wave lasers are also used with a shutter system to create the pulsing effect.

Upon leaving the enclosure, the laser beams are sent through a series of lenses or optics that expand the beam into a two-dimensional sheet. The light sheet optics are typically some combination of spherical and cylindrical lenses, with at least one cylindrical lens being necessary. The laser sheet illuminates the seeding particles that have been injected and mixed into the flow. The seeding particles should be something with a similar density as the fluid medium, so it mixes well with the flow, and should be

able to scatter light well. For air flows, the seeding should have a diameter on the order of the wavelength of the laser. For water flows, the seeding should be an order of magnitude greater to account for the higher refractive index of water over air. For air flows, a seeding consisting of some sort of oil is frequently used. Fog generators used for theatrical effect are also great for seeding air flow. A propylene glycol mixture is typically used in these generators.

The light reflected off of the particles is captured by the camera's CCD (charge-coupled device), which consists of an array of pixels that are charged by the light. The CCD is most sensitive to the blue/green range of the light spectrum; therefore the wavelength of the laser is typically in that range. The light reflected from the particles should cause a high charge on the CCD with a low level of background noise. Therefore, it is necessary to have the ambient lights off when doing a PIV experiment, or have a filter over the camera lens that only lets the wavelength of the laser through. The camera will capture two images separated by a short time delay, with the lasers timed such that one will illuminate the first frame and the other will illuminate the second frame. The laser heads are pulsed with short bursts (<10 ns) to create a stroboscopic effect, so that the particles appear "frozen" when the light hits them. The "frozen" images captured by the camera are transferred from the CCD array to memory that is either on-board the camera or is on a computer. The camera is then ready to capture more image pairs until the memory is full.

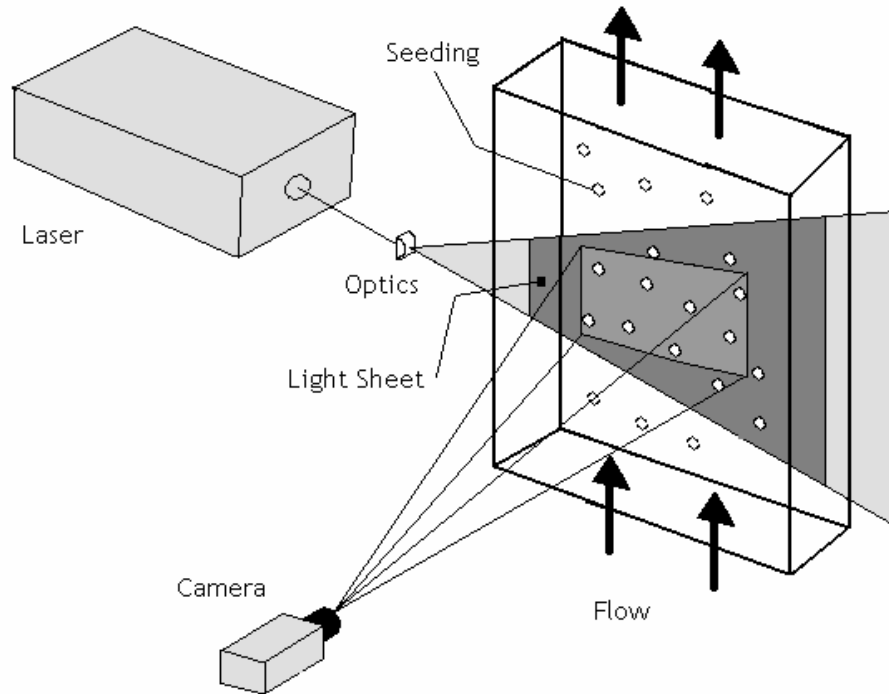


Figure A-1. Basic PIV setup showing the different components of a PIV system

The images stored in memory, either in the camera or the computer, are transferred to the computer's hard disk. Correlation software on the computer will break down the image pairs into small areas called interrogation regions. Each interrogation region is mapped from the first image to the second. The particles contained in the interrogation regions of the first image are compared to the particles in the interrogation regions of the second image. The time between image captures must be such that a sufficient number of particles are still in the interrogation region going from the first image to the second. Then, the displacement of the particles can be determined with the correlation software using FFT (Fast Fourier Transform) processing. After determining the displacement, the time between the images is factored in to calculate the velocity vector of that interrogation region. This process is summarized in Figure A-2. There will be one velocity vector for every interrogation region. Therefore, a higher spatial resolution can be obtained by having small interrogation regions. However, the interrogation region

must be large enough to contain a sufficient number of particles to determine a valid velocity vector. Factors such as particle displacement and displacement gradients can also effect the determination of the most appropriate interrogation region size. This is just a basic explanation of the cross-correlation process. Techniques such as overlapping, offsetting, filtering, and validating are also often used in the correlation process to help give better results.

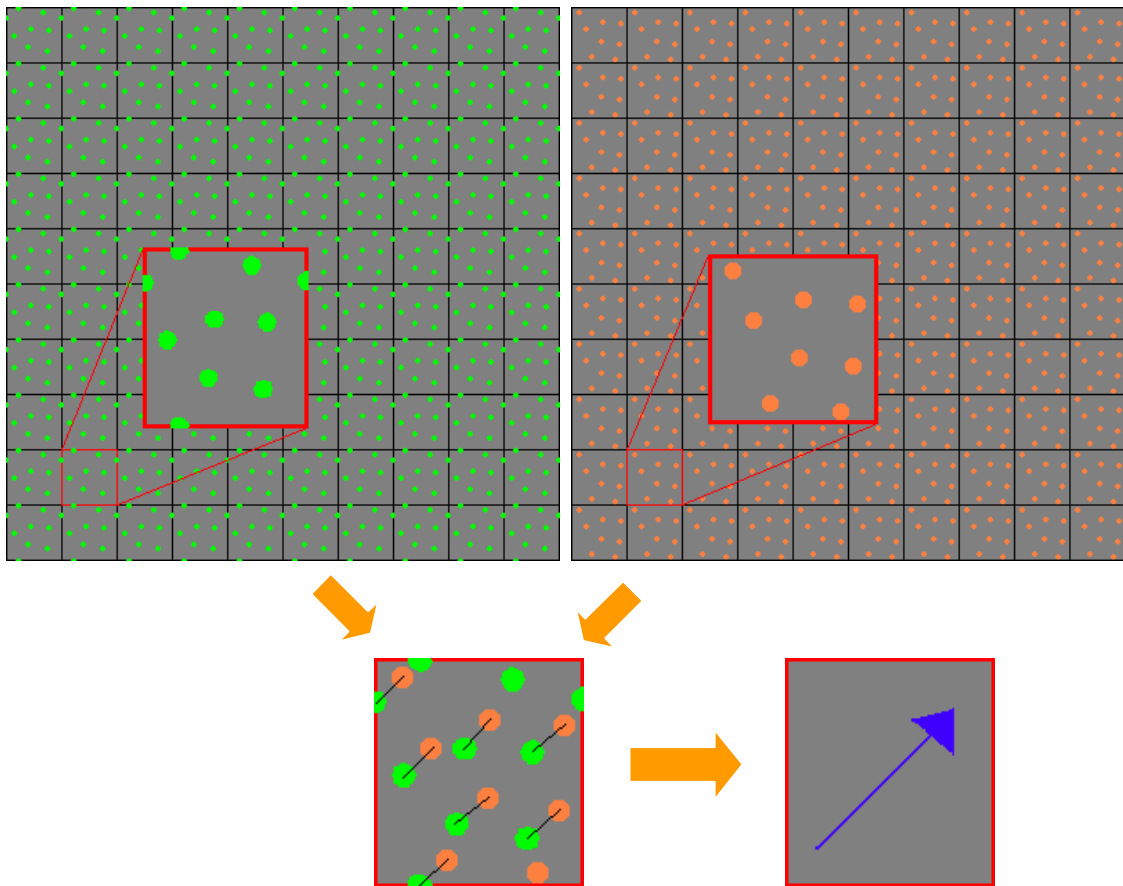


Figure A-2. Breakdown of images into interrogation regions that are correlated to give a velocity vector.

PIV Error Reduction

Certain measures can be taken to ensure that the errors in the PIV data obtained are as small as possible. These measures are covered in depth in the PIV installation guide from Dantec [20] and are briefly discussed here. One source of error is caused by the

particle size. On cameras used in cross-correlation PIV, the CCD array contains spaces between pixels. These spaces are used for quick storage of the first frame pixel information in order to free up the light-sensitive pixels for the second frame. If a particle is too small, the image of the particle on the CCD can fall between the light-sensitive pixels. Typically, there are micro lenses that focus the light that falls in these gaps onto the adjacent pixels. If the particle image fell in the gap in the center of four pixels, the light would be reflected equally to all four pixels. The FFT algorithm would interpolate the signal peak, but due to noise in the image the peak would be biased toward a single pixel which would be an incorrect indication of the particle position. To minimize the possibility of this happening, the diameter of the image particles should be greater than 3 pixels. One simple way to increase the particle image diameter, if necessary, is to adjust the focus of the camera so the particles are slightly out of focus. Also, increasing the f-number of the camera's aperture will increase the diameter of the particle image.

Another important factor to consider when trying to minimize PIV measurement error is the dynamic range of the particles. To assure a minimal signal drop-out, particles should be displaced less than 25% of the interrogation region size. For example, for an interrogation region size of 32 x 32 pixels, the displacement of the particles should be less than 8 pixels. If the displacement is much greater than that, there is too great a chance that either the initial or final particle position is outside the interrogation area. This requirement is somewhat relaxed when doing an adaptive correlation rather than just a simple cross-correlation. In an adaptive correlation, an initial correlation is done with larger interrogation regions before doing the correlation with successively smaller

interrogation regions. The initial larger interrogation regions allow fewer losses of pairs (signal drop-out) due to large displacements. The displacement of the particles is easily adjusted by changing the delay between the first and second image capture (the larger the delay, the larger the displacement, and vice versa).

In addition to particle displacement, particle displacement gradients are also very important to consider. If the velocity varies too much within an interrogation region, the vector determined from the correlation will not be a good representative of the flow within the interrogation region. Also, there will be a greater chance of loss of pairs at the higher velocity than the lower velocity, so with a larger velocity gradient there will be a bias toward the lower velocity. Therefore, the interrogation region size that is chosen should be small enough that the velocity distribution is fairly constant. Of course, the interrogation region should not be so small that there are many losses of pairs.

Out-of-plane motion is another cause of loss of pairs. A particle may be in the first image, but if the out of plane motion is too high it won't appear in the second image. This signal drop out can be prevented by making the light sheet thicker or by decreasing the time between images.

Out-of-plane movement by particles can also influence the accuracy of the in-plane particle measurements through an effect called parallax. If a particle is moving perpendicular to the plane at the center of the plane, the out-of-plane motion is correctly measured as zero. If the particle moves perpendicular to the plane at an off-center location, the out-of-plane motion is not measured as zero because the camera is able to detect the movement of the particle (the camera is no longer looking directly in-line to the movement of the out-of-plane particle). The error due to parallax is greatest at the

sides of the image, farthest away from the center. The error due to parallax can be minimized by having the camera as far away from the measurement plane as possible, limiting the spatial area recorded by the camera, and limiting the out-of-plane motion by decreasing the time delay between images.

The most important parameter in obtaining the most accurate PIV measurement is probably the signal-to-noise ratio. The number of particles in an interrogation region directly influences the signal. If there aren't enough particles then there is no way to obtain a good correlation. The greater number of particles in an interrogation region, the greater the signal. If a situation arises where seeding is limited, then the size of the interrogation region will also be limited to that which can sustain a sufficient concentration of particles. An image should have at least 5 particles per interrogation region.

The signal-to-noise ratio can also be helped by increasing the scatter of light off the particles. This is most easily accomplished by increasing the laser energy. Also, a thinner light sheet will concentrate the laser energy and reflect more light to the camera. The distance from the measurement plane to the camera may need to be shortened in order for the camera to detect a stronger signal. The signal can also be dimmed by too much seeding between the camera and light sheet, too much light attenuation through windows or optical access points, and too much ambient light interference.

APPENDIX B. ROTATING DISK SETUP AND PROCEDURE

The rotating disk experiment was performed on a tabletop in a small laboratory setting in Building 252 of Wright Patterson Air Force Base, near the Low Speed Wind Tunnel facility. The hardware available to set up this experiment was a Continuum SureLite SLI-10 PIV laser, Kodak (Redlake) ES4.0 MegaPlus camera with 105mm Nikon lens, EPIX PIXCI D2X frame grabbing board, Dell Precision 330 personal computer (1.4 GHz Pentium 4 with 2 GB memory), Quantum Composers 9318-032 pulse generator, Tetrax TDS 3054B oscilloscope, a 0.61 m x 1.83 m optical table, and various rails, mounts, and lenses.

A 0.30 m diameter aluminum disk was mounted on a rotating shaft and controlled from a box with a counter to set the speed. An array of small dots was created in AutoCAD and printed out. This piece of paper was taped on to the disk with black electrical tape to minimize reflections from the laser light. There was a 19 mm diameter extrusion (6 mm long) in the center of the disk, and a hole was made in the paper to accommodate it. A picture of the disk assembly and controller box is shown in Figure B-1. A small piece of reflective tape was placed on the outside of the disk to provide a marker to measure speed with an optical sensor (Spectral Dynamics Model 13135) connected to the oscilloscope. A calibration curve was created by setting the counter on the control box and observing the rotation speed of the disk on the oscilloscope. The calibration curve is shown in Figure B-2. There was no simple equation to fit the data to, but the graph was used as a reference to estimate the disk speed. The actual speed was always checked with the oscilloscope.

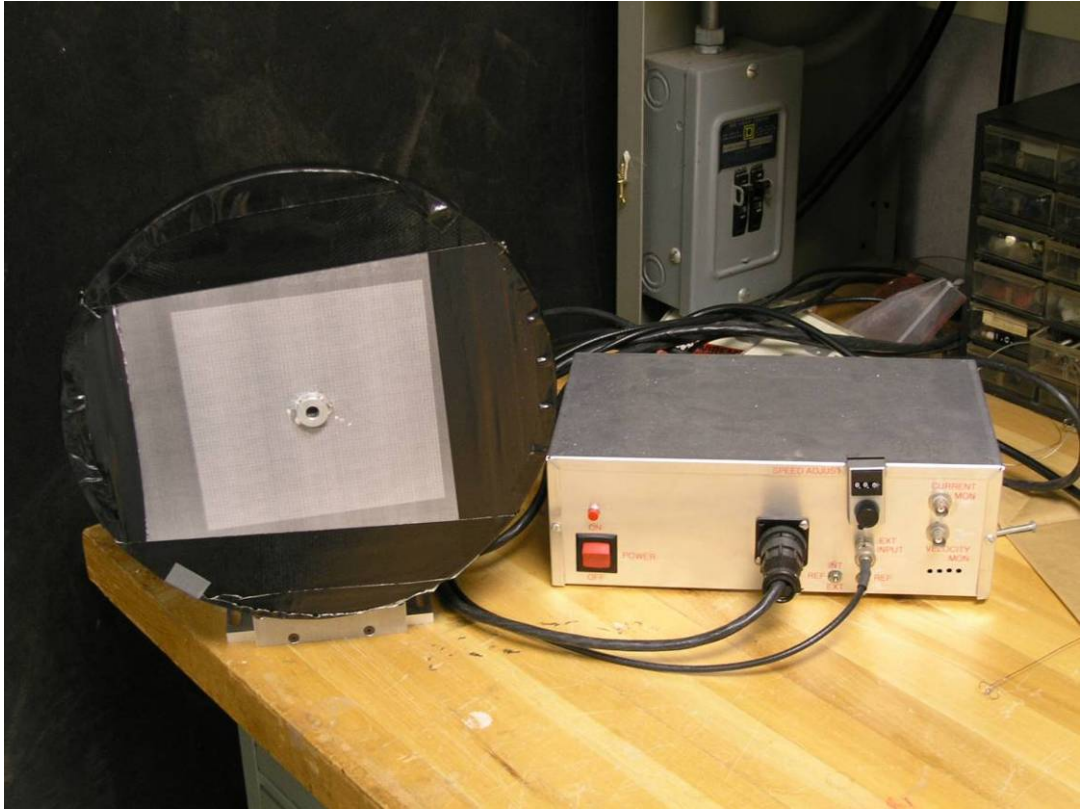


Figure B-1. Rotating disk with controller box.

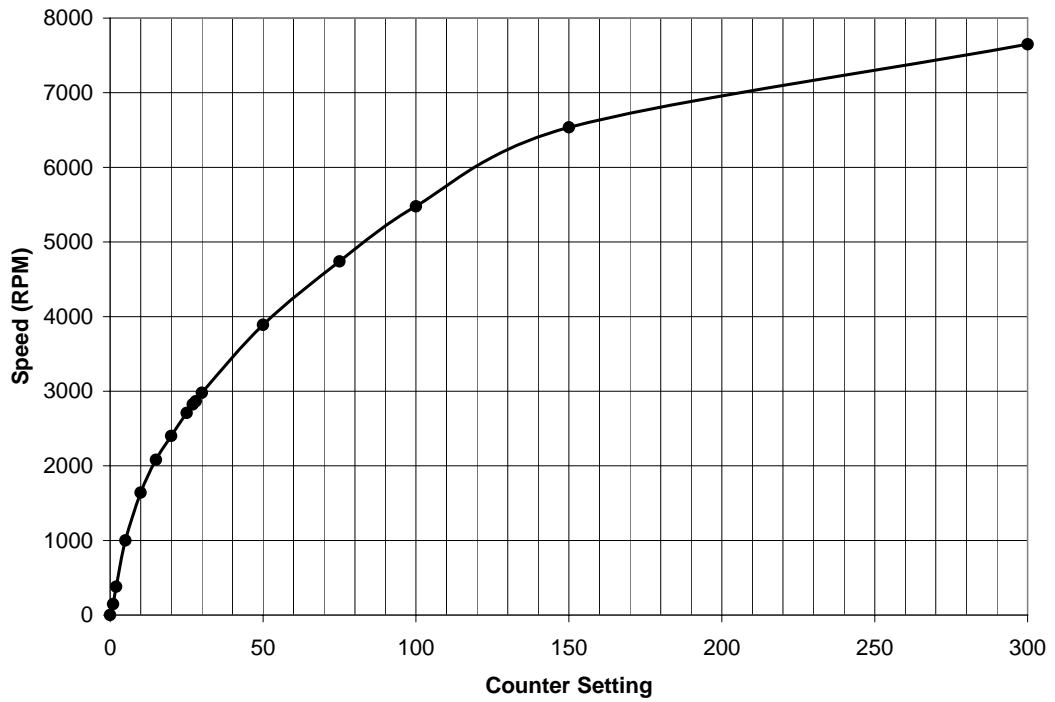


Figure B-2. Rotating disk calibration curve.

With the rotating disk calibrated, the PIV system needed to be set up so that the camera CCD was parallel to the plane of the disk, and the laser beams illuminated the plane of the disk. Since this is not a typical PIV experiment, the laser beams do not actually come into the test area in the form of a two-dimensional light sheet. Instead, a convex lens was used to spread the beam out into three dimensions in order to light up the face of the rotating disk. A right angle prism and a mirror were also used to route the beam to the test area. Before testing, the convex lens was removed to ensure the beam was centered on the center of the rotating disk. This also was an opportunity to ensure that the two beams landed on the same spot on the disk. If there was any misalignment, the optics inside the laser enclosure were adjusted according to the instructions in the user manual. After alignment was completed, the convex lens was put back in place. A picture of the layout of the rotating disk experiment is shown in Figure B-3, followed by a sketch in Figure B-4. The green lines indicate the path of the laser.

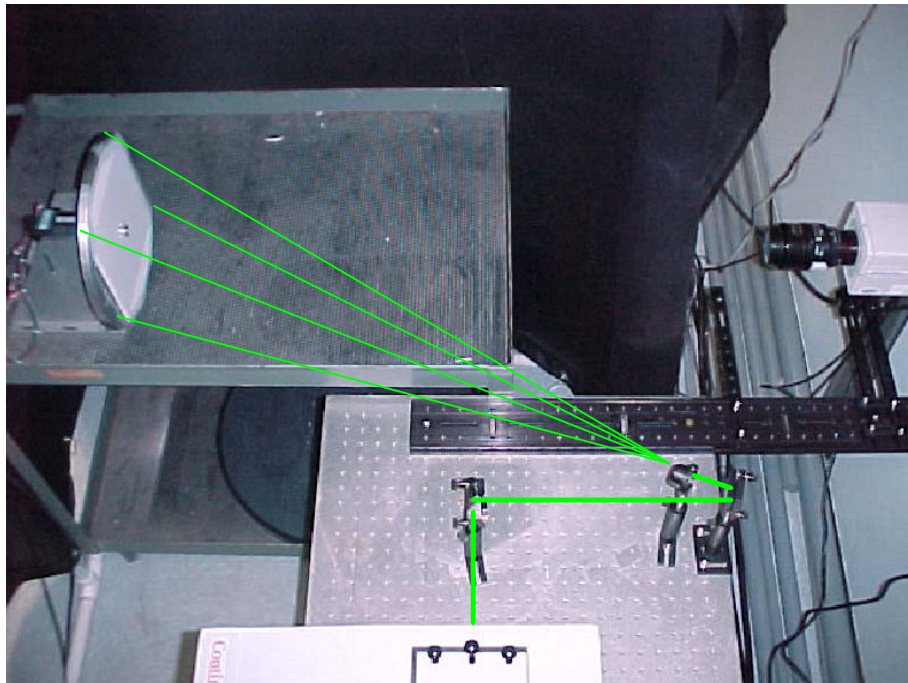


Figure B-3. Rotating disk experimental setup.

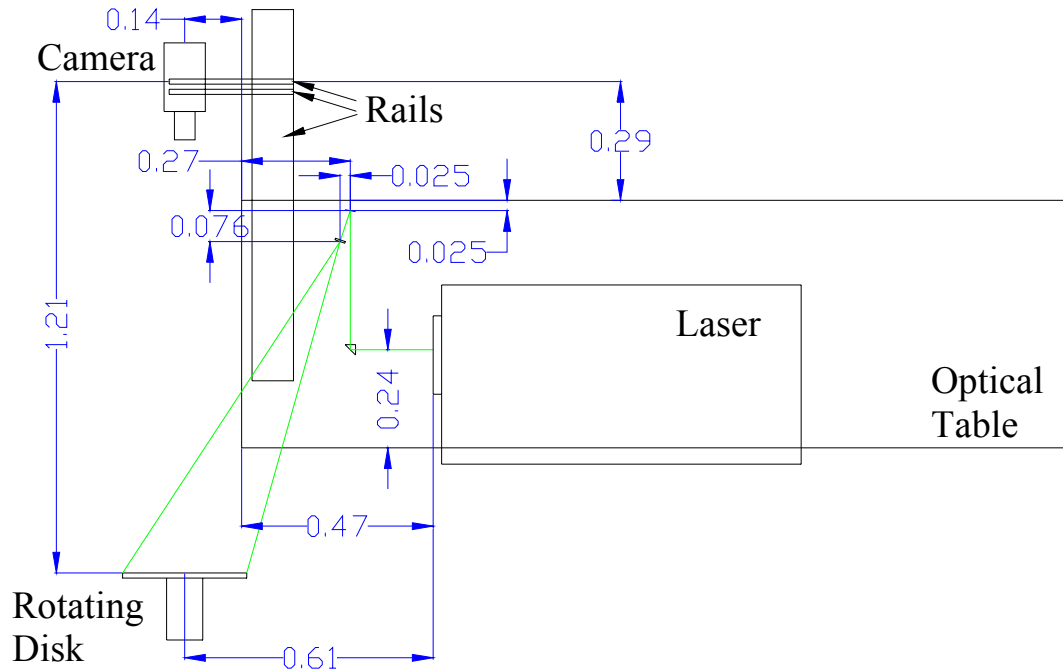


Figure B-4. Sketch of rotating disk setup. Dimensions are in meters.

Capturing PIV images with the Kodak camera, proved to be a difficult task. It was obvious that the camera needed to be run in double exposure mode in order to capture images in pairs, as the single frame rate of the camera is not fast enough for PIV. The problem came in how to trigger the camera and time it such that the each laser fires while the camera is actually exposing. Using the pulse generator, the behavior of the camera timing was deduced by varying the trigger and observing the two extremes of the first frame exposure (open and close). This was done with only one laser pulse firing. The delay of the camera trigger was shortened until no light in the image was observed, indicating the time just before the first frame exposes (opens). Likewise, the delay was extended until light was no longer observed in the image, indicating the time the first frame is closed. It was at this point that the light became visible in the second frame.

There is a setting in the EPIX software for TPD (transfer pulse delay) and TPW (transfer pulse width). The first frame begins to expose $5.8 \mu\text{s}$ after the trailing edge of

the camera trigger (which came from the pulse generator as a negative polarity 20 μs pulse). It continues to expose for 53.8 μs plus the sum of the TPD and TPW. The first frame exposure time is adjusted by changing TPD, as TPW cannot be set to higher than 10 μs . If TPW is too small then the charge transfer from the CCD of the camera will not complete and image quality will suffer, so TPW was kept at 10 μs . TPD was typically set to 5 μs . Therefore, the first frame exposure time was typically 68.8 μs . The second frame begins exposing immediately after the first frame closes, and for a fixed time period of 32.5 ms. There is also a strobe signal that is output by the camera to indicate the beginning of the transfer pulse delay. This was a 0.8 μs pulse that occurs 58.8 μs after the trailing edge of the camera trigger if $\text{TPD} \leq 40 \mu\text{s}$, and occurs 18.8 μs after the trailing edge of the camera trigger if $\text{TPD} > 40 \mu\text{s}$. The timing for the case of $\text{TPD} \leq 40 \mu\text{s}$ (which was always the case for this experiment) is summarized in Figure B-5.

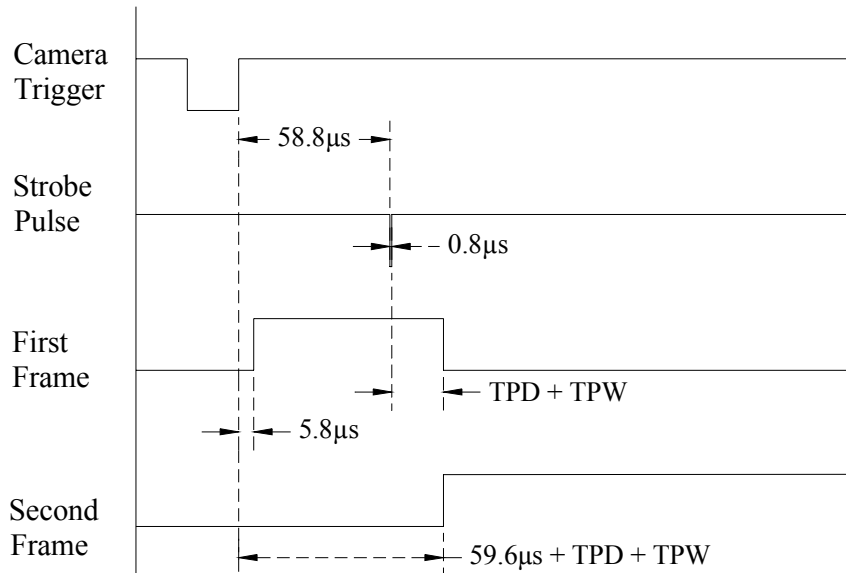


Figure B-5. Timing diagram for Kodak ES 4.0 camera.

With the timing of the camera frames determined, how the laser timing worked with the camera needed to be determined. The laser needs a “Fire” trigger, followed by a “Q-switch” trigger. Both of these could be triggered internally or externally, but in this experiment the triggering was done externally with the pulse generator. According to the specifications of the laser, a Q-switch delay of 186 μs is required for optimal laser operation. The Q-switch delay was kept at this value, except for when the laser beam needed to be observed (such as during an alignment), in which case the Q-switch delay was adjusted so the laser beam was barely visible. The “Fire” trigger for the first laser was set to coincide with the internal trigger of the pulse generator. The “Fire” trigger for the second laser varied depending on the speed of the disk, as the time between laser pulses factors in the displacement (and thus velocity) of the disk. For the case of the 1153 RPM disk, the time between laser pulses was 30 μs . Therefore, the “Fire” trigger for the second laser was set at a delay of 30 μs , since the “Q-switch” delay for both lasers was the same. The camera trigger delay then had to be adjusted so that the first laser illuminated the first frame of the camera, and the second laser illuminated the second frame.

For optimal image correlation, the two laser beams should be collinear so the two images are in the same plane. Even though the laser was spread out into a cone instead of a sheet, any misalignment was still very noticeable. While care was taken to make sure the two beams were aligned before testing, many times the beams would appear misaligned upon capturing images, with one image being noticeably brighter than the other. This caused problems in the correlation process, so it was imperative that the images be of equal brightness. It was discovered that the first laser beam had a secondary

(“satellite”) beam that was parallel to the main beam. This is shown in a burn of the laser beam on Kentek ZAP-IT burn paper in Figure B-6. Most of the time this satellite would show up, but a few times it didn’t. It was later determined that the beams were slightly misaligned, and that the alignment should be done at least 6 meters from the laser output. For this experiment, alignment was done at 1 meter as instructed by the user manual for the laser, which said to do the alignment somewhere between 0.5 and 2 meters from the laser output. While the beams were likely slightly out of alignment, it did not affect the data in the final experiment as images were obtained that had equal lighting. A sample pair of these images from the final set of data is shown in Figure B-7. The disk speed in this case is 1153 RPM ($\omega = 120.7$ rad/s). Here the paper on the disk is black with a pattern of white dots, and although the white dots did not extend to the full image, good results were still obtained.

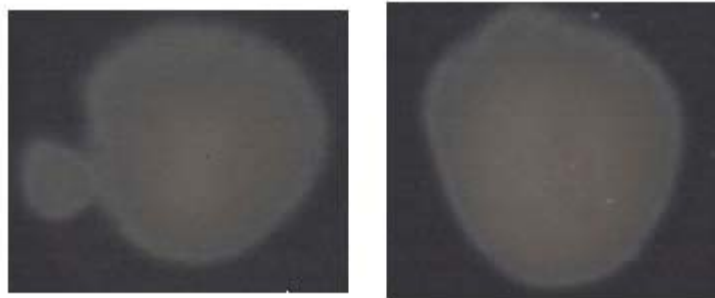


Figure B-6. Burn of Laser A (left) and Laser B (right).

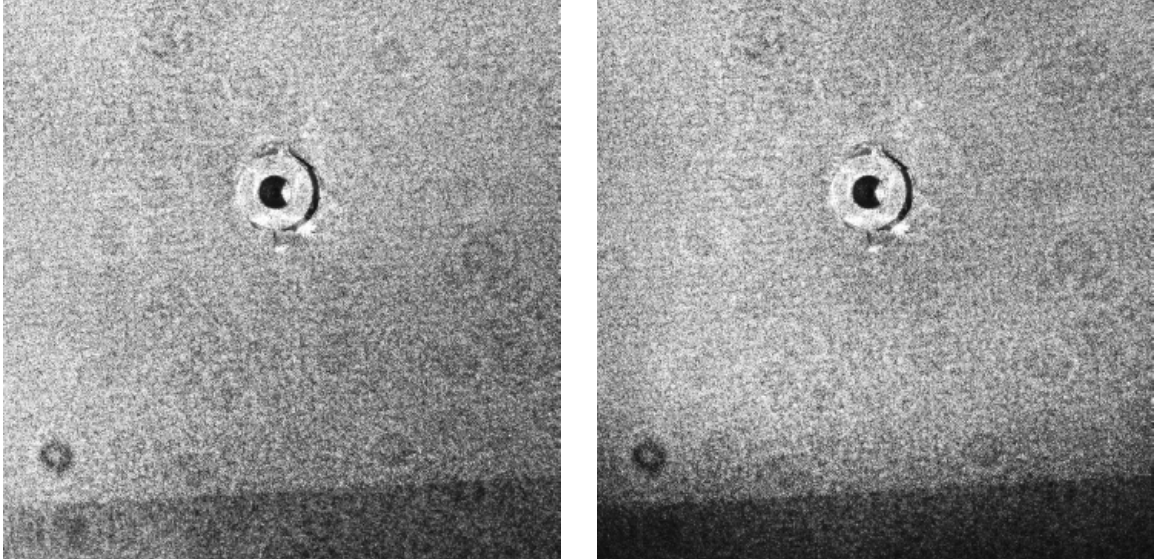


Figure B-7. Sample PIV images of rotating disk (Image A left, Image B right).

The images saved to disk were loaded into FlowManager, where they were correlated and averaged. The correlation technique used was an adaptive correlation starting with 512×512 pixel interrogation regions and incrementing to 64×64 pixel interrogation regions (512×512 , 256×256 , 128×128 , 64×64). The resulting vector maps from these images (a total of 49 image pairs) were averaged to obtain the vector map and corresponding contour plot shown in Figure B-8. The origin is defined as the center of the disk and is not necessarily the center of the image.

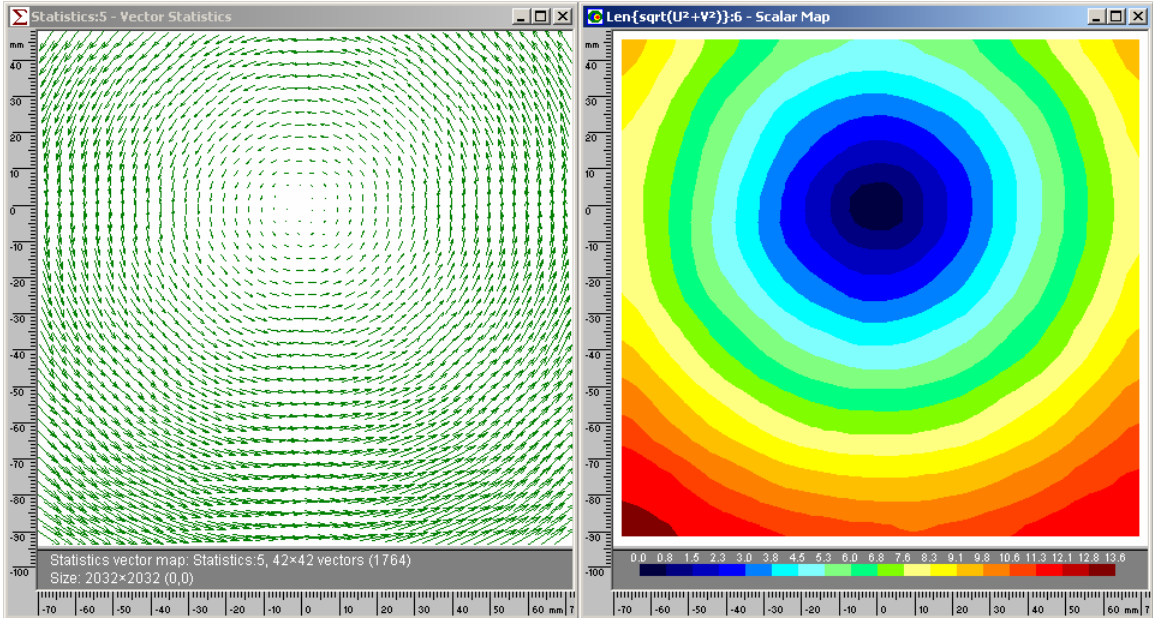


Figure B-8. Vector map (left) and contour plot (right) for 1153 RPM disk.

To be able to make a comparison to the known velocity of the disk, the vectors from the plot in Figure B-8 were exported to a text file and then imported into MatLab. The known velocity of the disk was determined by first observing the oscilloscope which displayed the period of each revolution in milliseconds. Then the rotational speed was derived from the recorded period. For the case shown here, the period was 52.05 ms and the resulting disk speed was 1153 RPM ($\omega = 120.7$ rad/s). Then the velocity was calculated using the relationship

$$V = \omega r \tag{B.1}$$

where V is the magnitude of the velocity vector, ω is the rotational speed in radians per second, and r is the radial distance of the velocity vector from the origin, which is defined as the center of the disk.

Equation B.1 was used to obtain a velocity magnitude for every point in the vector map of Figure B-8. With the exact values from Equation 2.1 and the experimental values from Figure B-8, a contour plot was created in MatLab comparing the two. This

comparison is shown in Figure B-9. The percent error was also calculated for each point, and a contour plot of this was also made in MatLab. This plot is shown in Figure B-10.

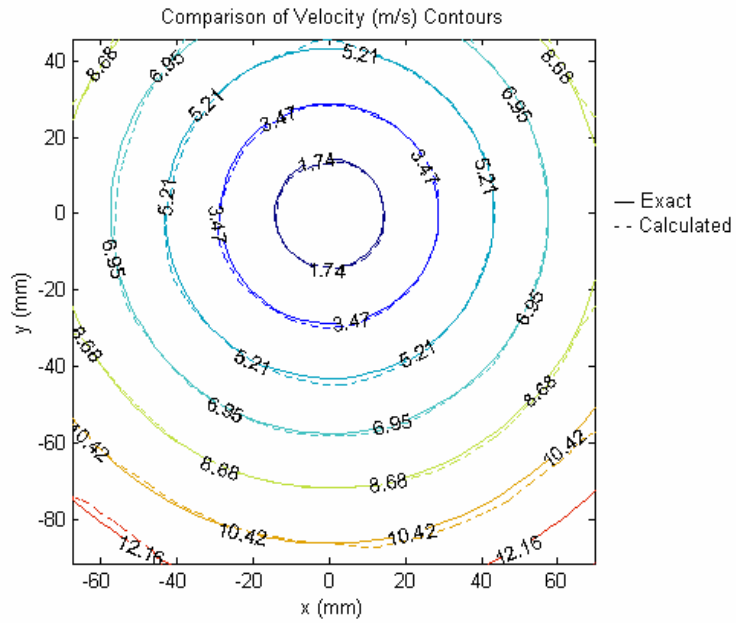


Figure B-9. Comparison of PIV “calculated” velocity values to expected “exact” values.

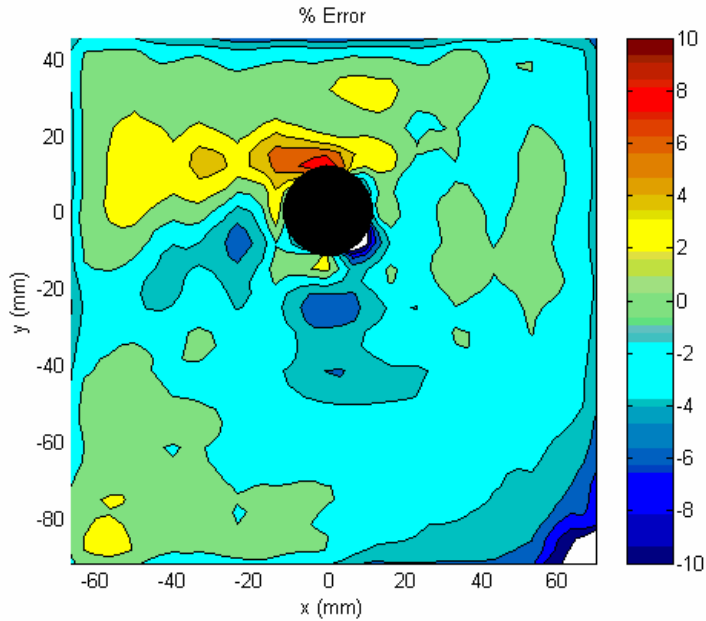


Figure B-10. Contours showing percent error between experimental and known velocities.

As Figure B-9 shows, the calculated values from the PIV experiment compare very nicely to the known velocities based on the speed of the disk. This is also shown in Figure B-10, where the average error is only 1.56%, and the standard deviation of that error is 1.62%. This ignores the region shown by the black circle in Figure B-10. The circle corresponds to the extruded part of the rotating disk that is not in plane with the rest of the disk and was not covered with the printed paper. It is expected that these errors would be high due to the low velocity of the disk as well as the lack of “particles” to correlate.

The procedure for obtaining and analyzing rotating disk PIV data is summarized:

1. Turn on laser power supplies first in order to give them enough time to warm up (approximately 20 min).
2. Tape a ruler on the disk to measure the field of view and to make sure the camera is focused on the disk.
3. Make sure the laser is aligned properly by observing the location of the laser light at low power. Leave the room lights on and make sure the windows are covered and the laser warning light is on before firing the laser. The Q-switch delay should be adjusted so that the laser light is barely visible. The two lasers should also be aligned to each other, and this can be verified by removing the convex lens and observing the beam location on the disk. If the two beams hit at different locations, then one of the laser beams needs to be aligned.
4. Turn on the rotating disk by adjusting the counter control to the appropriate number (see calibration curve), and allow a few minutes for the speed to stabilize. Use a

piece of reflective tape and the optical sensor to determine the actual disk speed on the oscilloscope.

5. Adjust the delay generator to give the desired time between laser pulses. Observe the actual delay from the photo diode signal on the o-scope. For a set delay of 10 μs , the actual delay will typically be 10.2 μs .
6. Set camera to operate in triggered double exposure mode, with a transfer pulse width of 10 μs and a transfer pulse delay of 5 μs . The camera frame rate should be set to 4 Hz, with a resolution of 2048 x 2048 pixels and 1 x 1 binning with a bit depth of 8.
7. Turn off the room lights and make sure the curtains surrounding the laser are closed. Return the laser to full power by adjusting the Q-switch delay back to the optimal value of 186 μs .
8. Begin acquiring images in XCAP. If the brightness of one image is drastically different from another, or if the images are blurry, the correlations will most likely come out bad. If inconsistent brightness is the problem, verify the alignment of the laser. A more precise alignment may need to be performed by observing the lasers at a larger distance (greater than 6 meters). If the images are blurry, verify the focus of the camera.
9. When satisfactory images are obtained, save them to disk.
10. Import images into FlowManager.

11. Experiment with various correlation techniques on various images to determine the best one to apply to all images.
12. Correlate all images.
13. Average the vector maps and compare results to the known velocity of the disk.

APPENDIX C. HOT WIRE EXPERIMENTAL SETUP AND PROCEDURE

After verifying the ability to use PIV to gather accurate velocity measurements with the rotating disk experiment, the PIV method could be used on the vortex generator jet. But before making PIV measurements, a more familiar technique was used to measure the VGJ. This hot wire anemometry experiment would also provide a mode of comparison to the later PIV measurements. The hot wire experiment was set up on a bench top next to the Low Speed Wind Tunnel. The vortex generator jet is a 25.4 mm inner-diameter copper tube (outer diameter is 28.6 mm) that is 203 mm long between the centers of both ends. One end is square cut, while the other was cut to a 30° angle so it would be flush with the surface of the plate. The jet was slipped into a 28.6 mm hole drilled at 30° into a 12.7 mm thick Lexan plate. The jet was sealed to the plate with grey silicone RTV. A 102 mm diameter PVC pipe (406 mm long) was attached to the jet through a 102 mm to 102 mm coupling, a 102 mm to 51 mm bushing, and a 51 mm to 38 mm bushing with a force-fit 38 mm tube that had a slight taper to just over 38 mm. Hose clamps and a 31.8 mm to 31.8 mm rubber coupling were used to secure the plenum to the jet. A 102 mm cap at the bottom of the plenum had a 6.3 mm swage fitting tapped into it to allow feed air to enter. The inside of the plenum contained two layers of filter matting to help spread the flow out before entering the jet. Near the top of the plenum, just under the lip of the coupling, were 54 1.8 mm diameter holes. These holes were necessary to correct a resonance problem that occurred with a sealed plenum. Whenever the air was pulsed into the plenum without these vent holes, the plenum would resonate at about 40 Hz. This resonance would dominate the jet flow and needed to be eliminated. The vent holes were successful in meeting this need.

The feed pressure of the air was set to 40 psi. Before that air reaches the plenum, it passes through a high speed Parker Instrumentation general valve (Parker Instrumentation VAC-100 psig), that has an opening time less than 1 ms and is controlled by a Parker Instrumentation Iota One pulse driver. The valve controller allows for up to 50% duty cycles. Therefore, for a frequency of 4 Hz (250 ms period), the valve could be open for up to 125 ms.

The hot wire used to collect data was a TSI 1241-T1.5 Standard “X” Probe, shown in Figure C-1. It is an end-flow x-wire probe that allows the measurement of both the magnitude and angle of the two-dimensional velocity vector by incorporating two hot wires in an “x” formation on the probe.

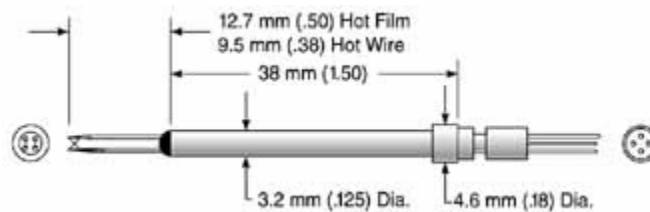


Figure C-1. TSI Model 1241 Standard "X" Probe (source: www.tsi.com).

Calibration of the hot wires was completed using a TSI Model 1127 calibrator and a Druck LPM5481 low differential pressure sensor. The hot wire probe was mounted above a jet in the calibrator, and the transducer measured the pressure in the calibrator plenum. LabView software calculated a velocity from the measured pressure and mapped it to voltage data from the hot wire. The pressure was varied enough to cover the range of anticipated velocity and provide a good data fit for the calibration. After calibrating the probe for the velocity magnitude, the angle of the probe with respect to the calibrator jet was varied at three fixed velocities. These known angles were then used to provide a calibration for the calculated angles from the hot wire probe voltage.

The hot wire probe was traversed using two micro-controlled traverses (National Aperture MM-4M-EX-200 mounted vertically and MM-4M-EX-260 mounted horizontally). The traverses were stepped a total of 16 cm in the direction parallel to the plate, and 10 cm in the perpendicular direction, using 2 mm increments in each direction. The hot wires were powered by a TSI IFA100 constant temperature anemometer. Voltage data was collected on a desktop computer using the National Instruments (NI) BNC-2110 connector block as an I/O device. The BNC-2110 was connected to a NI PCI-6052E data acquisition card in the computer. Temperature measurements were made using J-type thermocouples connected to the SXCI subsystem of a NI PXI-1010 Chassis. The PXI-1010 was connected to the computer through a MXI-3 fiberoptic link (NI PXI-8335 connected to NI PCI-8335). The micro traverses were driven by a National Aperture MC-3SA servo amplifier system, and controlled through a NI PCI-7344 motion control card in the computer. Atmospheric pressure was measured with a Wallace and Tiernan FA-129 pressure gauge. Dew point temperature was obtained from the Air Force base weather observation center, either by calling them or checking their website. LabView software was used to assimilate all the collected data and output respective velocity and running conditions. Data collection was phase locked with the pulsing of the jet. A TTL signal from the valve controller triggered each data collection cycle at the start of the valve opening. A schematic of the setup is shown in Figure C-2, and a picture showing the two-dimensional traverse and the region of data collection is shown in Figure C-3.

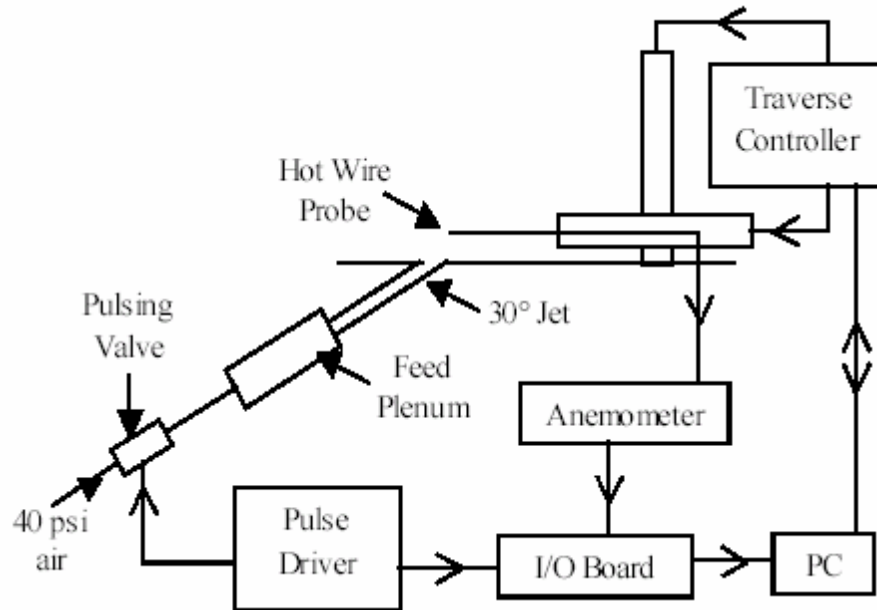


Figure C-2. Schematic of hot wire experimental setup.

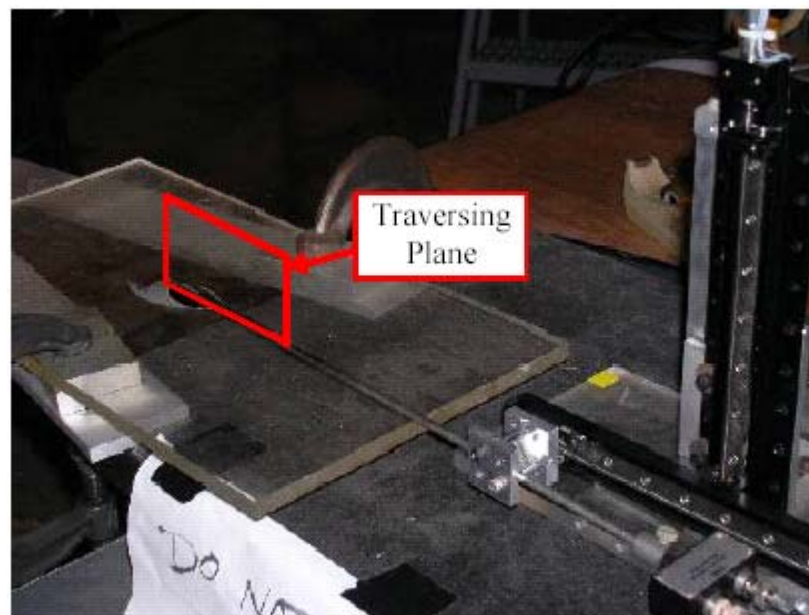


Figure C-3. Picture of flat plate and hot wire traverse showing measurement plane.

The procedure for obtaining and analyzing free jet HW data is summarized on the following page. Any MatLab or TecPlot files referenced in this procedure can be found in Appendix F. The LabVIEW files referenced here were not created by the author and will not be shown. Credit goes to Dr. Rolf Sondergaard for making these LabVIEW files.

1. Set inlet pressure to 40 psi.
2. Start pulsing valve at the desired duty cycle and frequency.
3. Make sure hot wire probe is at the desired starting location (10 mm behind leading edge of jet, and 4 mm above the surface of the plate). Be VERY careful using a ruler around the hot wire probe; even slight contact with the wire will most likely break it.
4. Make sure the PXCI chassis is turned on, and then turn on the computer, traverse controller, and anemometer.
5. Move the hot wire probe to the desired starting location, if necessary, by running 'microtrav2D.vi' in LabVIEW. Again, be careful to make sure the probe will not make contact with anything before moving it.
6. Open 'Phs Lckd Grid Data Auto X-wire.vi' and enter the desired acquisition rate, samples per channel, current dewpoint temperature, and current atmospheric pressure. Then run the program to collect the data.
7. When data is done collecting, click on "Done with Traverse" (do not click "Stop" or data will be lost).
8. Run MatLab code 'hwplot.m' to read in data file and output a TecPlot readable file.
9. Run TecPlot macro 'velvort.mcr' to plot and format data.
10. Make sure plot(s) are in the desired format and then run TecPlot macro 'aviexport.mcr' to export the plots to a movie file.

APPENDIX D. PIV EXPERIMENTAL SETUP AND PROCEDURE

Free Jet

A 1.5" diameter hole was drilled at about a 30° angle in the table below the tunnel, to allow the jet to pass underneath the table. A 102 mm extension had to be made for the jet, making it 305 mm long, for the jet to reach through the bottom of the table on which it was mounted. The plenum was the same as the one used for taking the hot wire data, with some modifications. In order to seed the jet flow, an 87 liter plastic storage bin was used as a smoke box. Two 25.4 mm diameter tubes connected the smoke box to the feed plenum. One of these tubes allowed smoke into the plenum, and the other acted as a return so there would be no net mass flow into the plenum. The nozzle of the fog generator was inserted into the smoke box to deliver the smoke. All connections to the smoke box were sealed with silicone RTV to ensure no losses in mass flow. Adding the smoke box changed the dynamics of the plenum enough that the holes in the plenum could be taped over without causing any resonance problems.

The Boundary Layer Tunnel (BLT) would not give a good velocity profile at velocities under about 3 m/s. Additionally, a freestream velocity of 3.15 m/s was desired because it matches the reduced frequency to that of the LSWT if the frequency was made to be 0.5 Hz and the characteristic length is considered to scale with the jet. A blowing ratio of at least 2 was desired, with a blowing ratio of 4 being even more desirable. Since the freestream velocity could not be decreased, the velocity of the jet had to be increased in order to obtain higher blowing ratios. Using the single valve would not allow velocities over 2.45 m/s at 40 psi. To circumvent this problem, three additional valves (four valves total) were connected in parallel. This would ideally give four times the mass flow and thus four times the velocity in the jet. However, this was not the case as

each valve gave a smaller flow rate than the one that was used for the hot wire measurements. The four valves together gave a jet velocity of 3.75 m/s at 40 psi. Increasing the feed pressure to 80 psi (approximately the maximum pressure available) brought the jet output from these four valves to 5.9 m/s. Therefore, a blowing ratio of nearly 2 could be achieved. This was deemed acceptable and the free jet was studied at a jet velocity of 3.15 m/s.

A 100 psi differential pressure transducer (Druck model PDCR 22) and a J-type thermocouple were added upstream of the valves. This allowed a calculation of the mass flux through the feed line using Equation D.1 (taken from [21]):

$$G^* = \frac{\dot{m}}{A^*} = \frac{P_0}{\sqrt{T_0}} \sqrt{\frac{\gamma}{R} \left(\frac{2}{\gamma+1} \right)^{\frac{\gamma+1}{\gamma-1}}} = 0.04042 \frac{P_0}{\sqrt{T_0}} \quad (\text{D.1})$$

where $\gamma = 1.4$ and $R = 287.04 \text{ J/kg K}$ were used as constants. Equation D.1 assumes isentropic flow. P_0 and T_0 are stagnation pressure and temperature, respectively. The A^* refers to the choked area of the feed line. Thus, flow is assumed sonic in this equation. This is a reasonable assumption because there is a 4:1 area reduction in the feed line upstream of the pressure transducer and the thermocouple. The mass flux was used to calculate the blowing ratio by knowing the mass flux at $B = 1$. The velocity of the jet was measured to be 3.15 m/s when the mass flux was 345 kg/s-m^2 , so $B = 2$ would be achieved at $G^* = 690 \text{ kg/s-m}^2$.

The pressure transducer was calibrated using a Druck DPI510 pressure calibrator to regulate the pressure and a Tektronix TDS 3054B oscilloscope to indicate the voltage. The DPI510 was about 3 years past its last calibration, so it was checked against a Ruska Series 7000, which had a recent calibration. The DPI510 was determined to have a

calibration uncertainty of ± 0.003 psi. Due to fluctuations in the pressure readings, the DPI510 had an additional uncertainty of ± 0.05 psi. The oscilloscope had an uncertainty of ± 0.05 mV. When multiplied by the slope of the calibration curve, an uncertainty of ± 0.07 psi results. Taking twice the standard deviation of the calibration curve, there was an additional ± 0.25 psi uncertainty. Using the RSS (root sum of squares) value of the uncertainties, the overall uncertainty of the pressure transducer was ± 0.26 psi. The maximum absolute pressure of the DPI510 was 75 psi. The atmospheric pressure indicated by the DPI510 at the start of the calibration was 14.310 psi, and at the end of the calibration was 14.317 psi. The average of these two values was subtracted from the indicated pressure to give differential pressure. The calibration was carried out by starting at atmospheric pressure, going to 15 psia, then up to 75 psia in increments of 5 psi. The pressure was then varied back down to atmospheric pressure in the same 5 psi increments. The calibration curve is shown in Figure D-1.

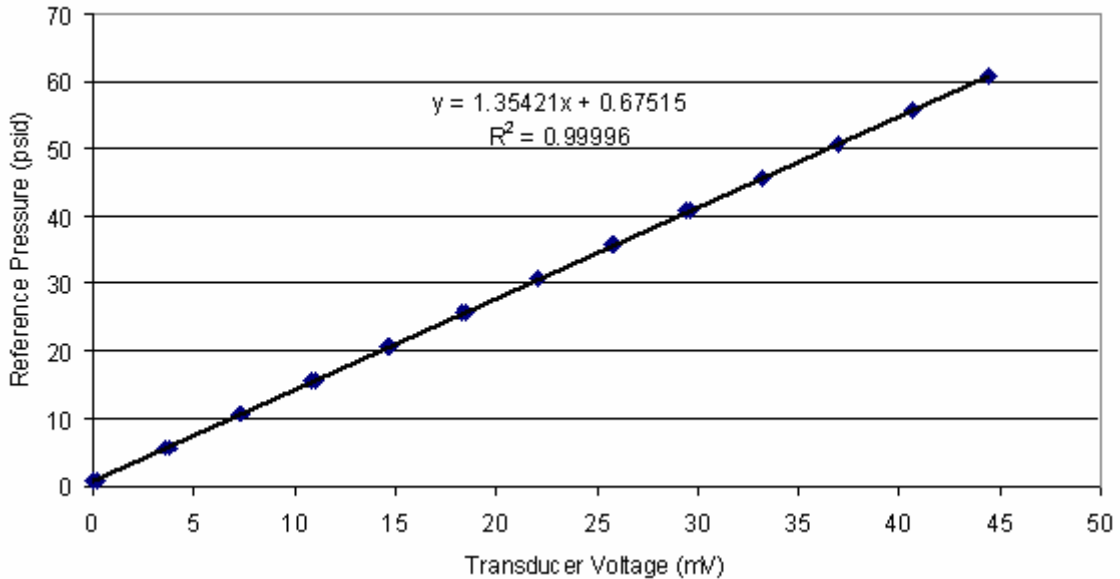


Figure D-1. Calibration curve for pressure transducer (Druck PDCR 22).

Because the setup of the feed plenum had changed since the hot wire measurements, the hot wire results, while still informative, could not be directly compared to the PIV results. Therefore, one case was repeated for the new setup with the hot wire to directly compare to the PIV results. The components of the hot wire setup had also changed due to transportation issues. The valve (Parker Instrumentation VAC-100 psig) was the only component that was the same. The other three valves were installed (two Parker Instrumentation VAC-250 psig and one other VAC-100 psig), but they remained closed for the hot wire test. The pulse driver that controlled the valve (Parker Instrumentation Iota One) also sent its TTL signal to the I/O board (National Instruments BNC-2120) to trigger the beginning of each cycle. A TSI 1241-20 hot film probe was connected to a TSI IFA-100 constant temperature anemometer, which output the probe voltage to the I/O board. The position of the hot wire probe was controlled by a National Aperture MC-3SA Servo Amplifier System. The traverse controller and the I/O board were connected to a National Instruments PXI-1002 chassis, which communicated with the PC (Dell Dimension 8250), through a fiber optic link. A LabView program on the PC was used to read in the TTL signal, hot wire voltages, and traverse position. This setup is summarized in Figure D-2. While not explicitly shown, the smoke box is attached to the feed plenum, although the smoke was not turned on for the hot wire experiment so as not to contaminate the hot wire.

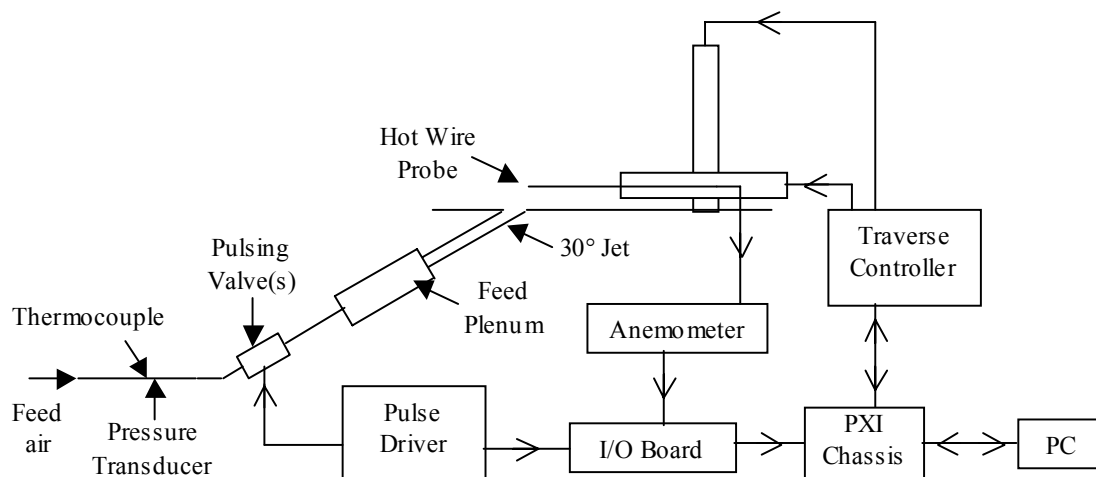


Figure D-2. Schematic of new hot wire traverse setup.

The PIV setup for the free jet is shown in Figure D-3. The smoke machine used to fill the smoke box and seed the jet flow was a Safex F2010. The pulse driver is used to drive the valves as well as trigger the camera. The camera (IDT X-Stream Vision XS-3 with Nikon 60 mm lens) was set to begin exposing the first frame upon receiving the trigger from the pulse driver, which signifies the start of the cycle (valve opening) of the pulsed jet. The camera outputs a positive TTL signal that corresponds to the camera exposing. The delay generator (Quantum Composers 9318-032) used the rising edge of this signal to begin triggering the laser (New Wave Pegasus PIV). The first laser was triggered without any delay. The second laser trigger was delayed by a certain time interval, depending on the expected velocity of the jet. The first frame exposure time of the camera was set to equal the delay between laser pulses, so that the second frame began exposing just before the second laser fires. The laser beams were guided to the measurement area with a Dantec light arm, and Dantec light sheet optics were used to spread the beam into a two dimensional sheet. The images captured by the camera are

stored in on-board memory (4Gb), until they are ready to be saved to disk. A high-speed USB cable sends the images from the camera's memory to the computer's hard disk. The computer used in this setup is the same as the previous rotating disk experiment, the Dell Precision 330. A picture of the setup is shown in Figure D-4. Note that the cardboard box under the table was later replaced with the plastic storage bin for the smoke box. Also, the camera in the picture is the Kodak ES4.0, which was later changed to the IDT camera. Finally, the laser itself is not visible; it is the laser power supply that is indicated in the picture.

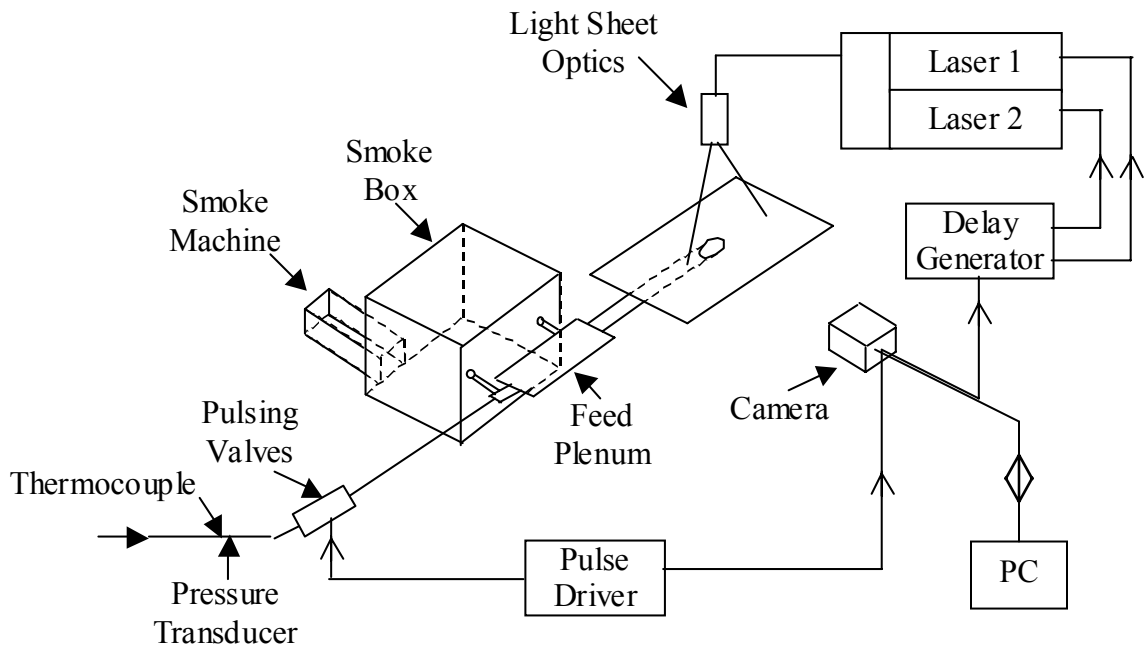


Figure D-3. Schematic of free jet PIV setup.

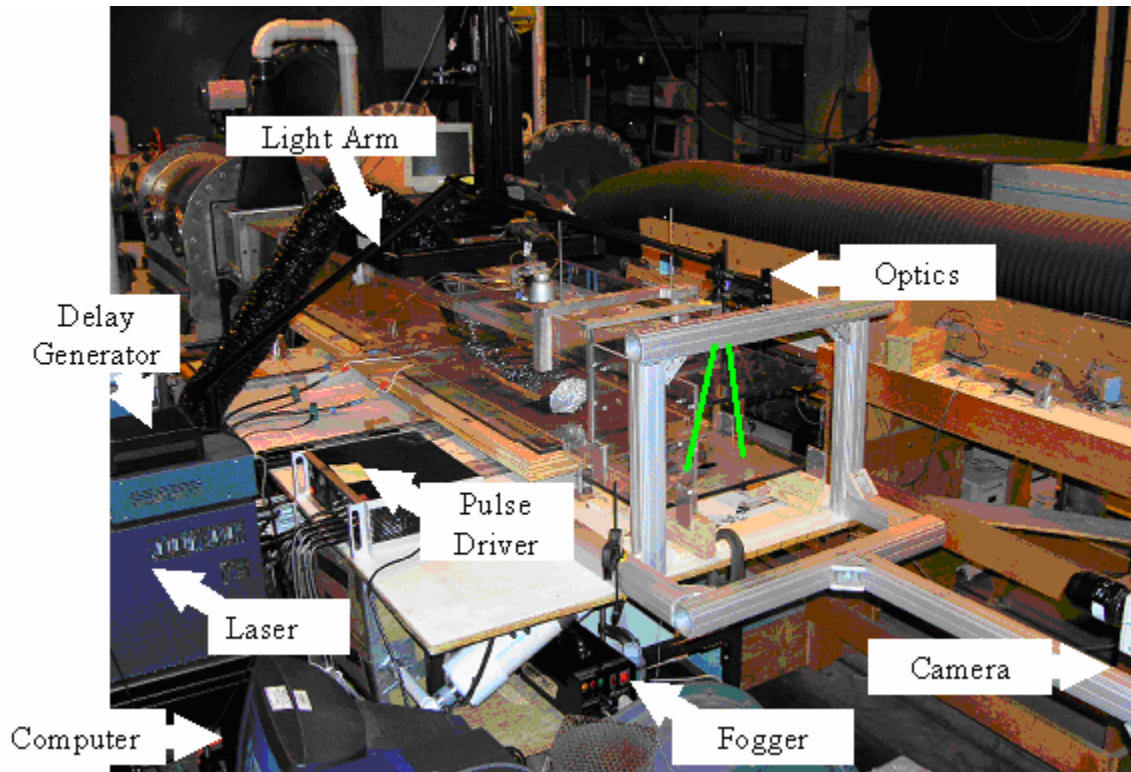


Figure D-4. Picture of free jet PIV setup.

The procedure for obtaining and analyzing free jet PIV data is summarized below.

Any Matlab or Tecplot files referenced here can be found in Appendix G.

1. Give laser, chiller, and fogger enough time to warm up (20 min for laser and chiller, 10 min for fogger).
2. Make sure the inlet pressure is at the desired state by observing the transducer voltage on the oscilloscope.
3. Make sure valve(s) are set to operate at the desired duty cycle and frequency.
4. Make sure the first laser pulse is triggered off the camera and the second laser is set to the desired delay.

5. Make sure camera is focused on the desired measurement plane and adjust focus and/or field of view if necessary.
6. Set camera to operate in double frame mode, externally triggered on a single pulse, with a frame rate according to the desired rate of data collection, and set the number of frames to record according to the desired number of images. For maximum lighting in the second frame, set the first frame exposure time equal to the delay between laser pulses.
7. When the laser is ready to operate, make sure the laser sheet is as thin as possible and will cover the desired measurement plane, without extending much outside that plane. This will ensure maximum intensity of the laser light. Do this at the lowest possible energy setting to reduce laser hazards.
8. Fill the smoke box and plenum by switching the fogger on for about 10 seconds on its lowest setting.
9. Turn lights out and make sure any ambient light is minimized.
10. Turn on laser, making sure it is triggered externally, on high power, with each laser energy turned to its maximum. Make sure proper eye protection is worn, and then open the laser shutter.
11. Begin pulsing the jet. The camera's first frame exposure time, sensor gain, and pixel gain should then be adjusted to optimize the quality of the acquired images.
12. Stop pulsing the jet, and refill the smoke box.

13. Start pulsing the jet, and set the camera to live mode.
14. When the images appear to have an optimal seeding density (not so much seed that it saturates the image, and not too little that valid vectors can't be obtained), begin recording images.
15. Save the acquired images to the hard drive in 8-bit Bitmap format.
16. Run Matlab code `imagesort.m` (or `imagesortsteady.m` if it is not necessary to sort the images by time such as for steady flow) to rename acquired images.
17. Transfer images to WSU computer (Wright State owned computer with newer version of FlowManager and faster processor).
18. Import images into FlowManager.
19. Experiment with various correlation techniques on various images to determine the best one to apply to all images.
20. Correlate all images.
21. Export resulting velocity fields to text file.
22. Transfer exported file to PR computer (owned by the Propulsion Directorate of AFRL and has Matlab and TecPlot installed on it).
23. Run Matlab code that reads in exported file, calculates ensemble average velocities and vorticities, and outputs a TecPlot readable file (`PIVplot.m` or `PIVplotsteady.m`).

24. Run TecPlot macro that reads in data file and creates velocity and vorticity plots (velvort.mcr).
25. Make sure the plots have the desired scales and labels, and then run the TecPlot macro that exports the velocity and vorticity plots to an AVI file (aviexport2.mcr).

Jet in Crossflow

The setup for the jet in crossflow experiment is basically the same as the free jet experiment. Of course the major difference is the added crossflow from the Boundary Layer Tunnel. The crossflow was seeded with a second smoke machine (Rosco Model 4500) inserted upstream of the tunnel in the settling chamber. Another change is the camera becomes mounted on the side of the tunnel instead of at the end, in order to take boundary layer measurements. The laser sheet is also rotated 90 degrees for the same reason. The hot wire probe was used to measure the freestream velocity, and the pressure transducer and thermocouple were used as before to calculate the jet velocity and thus the blowing ratio. One thing to note is that after using the valves for several weeks at low pressure (only about 20 psi was required for $B = 1$ using all four valves in the free jet experiment), and then increasing the pressure to obtain higher blowing ratios for the jet in crossflow experiment, the valves loosened up and allowed a jet velocity of 13 m/s at 90 psi of feed pressure. That meant blowing ratios of up to $B = 4$ could be obtained.

Since the behavior of the valves had changed, the velocity of the jet could no longer be determined based on the previous assumption of a mass flux of $G^* = 345 \text{ kg/s-m}^2$ corresponding to $B = 1$. A new mass flux had to be determined. Also, the assumption wasn't made this time of mass flux increasing proportionally with blowing ratio. Instead, the mass flux was determined at all blowing ratios ($B = 1$, $B = 2$, and $B = 4$), which were

measured with the hot wire probe. A summary of the findings is shown in Table D-1. The jet velocity, V_j , is of course the blowing ratio, B , multiplied by 3.15 m/s. The voltage, V , is the voltage read on the oscilloscope off the pressure transducer. The line pressure, P , is determined from the transducer calibration in Figure D-1, and G^* is the mass flux determined from Equation D.1. Although not initially planned, a blowing ratio of 0.5 was also studied. The mass flux value in that case was extrapolated by a linear curve fit of the values in Table 2-1. This resulted in a mass flux of 89.25 kg/s/m².

Table D-1. Mass flux for each blowing ratio studied.

B	V_j (m/s)	V (mV)	P (psi)	G^* (kg/s/m ²)
1	3.15	13.1	18.4	299
2	6.3	28.5	39.3	639
3	9.45	47.6	65.1	1059
4	12.6	65.1	88.8	1444

Another main difference between the free jet setup and the jet in crossflow is the added need for a separated flow. Separated flow over a turbine blade is caused by a pressure gradient due to the curvature of the blade. Since this is a flat plate model in a constant area tunnel, there is no pressure gradient to drive separation. Several attempts were made to create a profile for the top wall that would accomplish this. The profiles were made from foam and taped to the top wall. The profiles were made to create a converging-diverging section just upstream of the jet. The idea was that if the flow could stay attached to the top wall, the pressure gradient would force a separation at the bottom wall. In order for the flow to stay attached to the top wall, the foam profile was cut open to allow a channel from the peak of the profile (where the area was the smallest in the tunnel) to an opening in the top of the tunnel. A blower was used to draw air into the channel and turn it toward the top of the tunnel, keeping it attached to the top wall. This did not force any separation at the bottom wall until the entire top wall was angled

outward as much as possible. With the top wall angled at a divergent 20° , flow separation was finally achieved along the bottom wall. Unfortunately, by the time the separated flow reached the jet, the separated region was so large that the jet would not have been able to control it. Moving the separation point downstream and moving the jet upstream were not possible without making major modifications to the tunnel. Therefore, the idea of a pressure gradient driven separation was scrapped in favor of a simple ramp placed on the bottom wall, just upstream of the jet.

Three ramp sizes were attempted. The larger one (31 mm tall, angled at about 40°) created so large of a separation region that the jet could not control it. The smaller one (10 mm tall, angled about 30°) was so small that the flow quickly reattached even if the jet wasn't being used. The final ramp that was used was 22 mm tall, angled at about 30° . The jet was seen to control the separation with this ramp because it created a separation region that was approximately equal to the diameter of the jet. The separation "visualization" was done with a small rod with a thin piece of ribbon tape taped to the end. This tuft indicated the direction of flow, and thus whether or not the flow was separated. The orientation of the ramp with respect to the jet is shown in Figure D-5. Figure D-5 also shows the measurement planes that were taken for this experiment. Notice that all the planes are parallel with the main flow. Perpendicular planes were attempted, however there was too much out-of-plane motion to obtain good results with the PIV method. Also note that the jet is not centered on the tunnel to avoid the jet flow impinging on the side wall. The tunnel centerline is along $y = 2d$ ($y = 2$ ”).

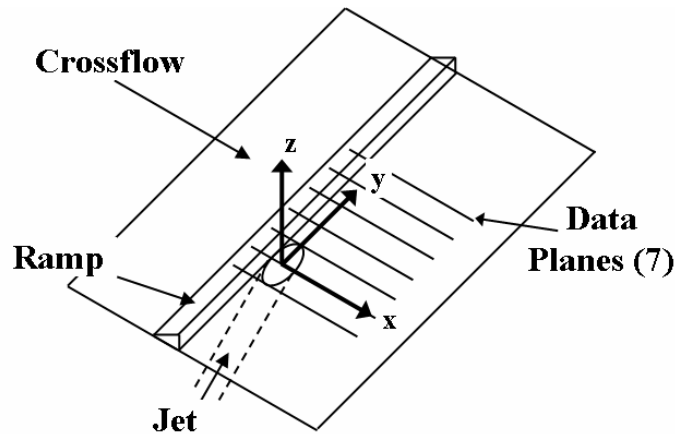


Figure D-5. Ramp location, axis information, and data plane measurement locations.

The procedure for obtaining and analyzing crossflow PIV data is given below. The Matlab and TecPlot files referenced can be found in Appendix H, except the ones already shown in Appendix G.

1. Turn on laser, laser chiller, and foggers first in order to give them enough time to warm up (approximately 20 min for laser, chiller, and Rosco fogger, and 10 min for Safex fogger). Also make sure that the power supply to the pressure transducer is on.
2. Turn on crossflow by switching the blower control to 'Hand', checking first that the valve to the other tunnel is closed (there are two tunnels that use the same air blower), that the bypass valve is open, and the bypass duct is positioned to blow away from the experimental area or any other object that could be affected by the high-velocity exhaust.
3. Turn on freestream chiller by opening the chiller valve a small amount (about a 15 degree turn). Observe the temperature of the freestream and adjust the chiller valve

accordingly. The temperature should not be much different than that which the hot wire probe was calibrated at.

4. Note the atmospheric pressure from the barometer in the control room. Get the dewpoint temperature by calling the base weather center or looking it up on their website.
5. Make sure all panels on top wall of the tunnel are in place and that the tunnel is in running condition (nothing upstream of the test area to interfere with the experiment).
6. Close the bypass valve so the blower is feeding air to the tunnel.
7. Position the hot wire in the freestream and measure the velocity at that point. Adjust the flow rate until the desired velocity is obtained (typically 3.15 m/s).
8. When the laser is ready to operate, make sure the laser sheet is as thin as possible and will cover the desired measurement plane, without extending much outside that plane. This will ensure maximum intensity of the laser light. Do this at the lowest possible energy setting to reduce laser hazards. Adjust the light arm mirrors so that the sheet has uniform intensity and is as intense as possible (looking at the laser only at low power).
9. Make sure the plane of the light sheet will be parallel to the plane captured by the camera.

10. Make sure camera is focused on the measurement plane formed by the light sheet and adjust focus and/or field of view if necessary. The aperture should be fully open in the case of looking at a large field of view with a relatively low laser energy (nominally 10 mJ/pulse).
11. Set camera to operate in double frame mode, externally triggered on a single pulse, with a frame rate according to the desired rate of data collection (typically 50 Hz for a jet frequency of 0.5 Hz), and set the number of frames to record according to the desired number of images (typically 2600 in order to capture 13 cycles of data). For cases where the jet is steady blowing or not blowing at all, set the trigger source to internal.
12. Make sure the inlet pressure to the feed air is at the desired state (based on feed temperature and desired blowing ratio, see Figure D-14, Equation 2.2, and Table 2-1) by observing the transducer voltage on the oscilloscope. Bleed any excess pressure out of the line before making this measurement.
13. Make sure the valves are set to operate at the desired duty cycle and frequency. The valves should be pulsed a few times prior to testing to make sure they open all the way without sticking. A quick check of the jet velocity with a pitot tube is recommended before testing.
14. Make sure laser pulse delays are set correctly.
15. Turn lights out and make sure any ambient light is minimized.

16. Turn on laser, making sure it is triggered externally, on high power, with each laser energy turned to its maximum. Make sure proper eye protection is worn, and then open the laser shutter.
17. Begin seeding the crossflow. The camera's first frame exposure time, sensor gain, and pixel gain should then be adjusted to optimize the quality of the acquired images. The first frame exposure time should typically be set equal to the laser pulse delay, and the sensor gain and pixel gain are typically set to 4.
18. Stop seeding the crossflow.
19. Fill the smoke box and plenum with smoke. The amount of smoke necessary will vary depending on freestream and jet flow rates.
20. Start pulsing the jet, and set the camera to live mode.
21. When the images of the jet smoke appear to have an optimal seeding density (not so much seed that it saturates the image, and not too little that valid vectors can't be obtained), turn on the smoke machine to seed the crossflow. The crossflow seeding should be adjusted for optimal image quality. When the images look ready for capture, begin recording images.
22. Save the acquired images to the hard drive in 8-bit Bitmap format.
23. Run Matlab code `imagesort.m` (or `imagesortsteady.m` if it is not necessary to sort the images by time such as for steady flow) to rename acquired images.
24. Transfer images to WSU computer.

25. Import images into FlowManager.
26. Experiment with various correlation techniques on various images to determine the best one to apply to all images.
27. Correlate all images.
28. Export resulting velocity fields to text file.
29. Transfer exported file to PR computer (owned by the Propulsion Directorate of AFRL and has Matlab and TecPlot installed on it).
30. Run Matlab code that reads in exported file, calculates ensemble average velocities and vorticities, and outputs a TecPlot readable file (PIVplot.m or PIVplotsteady.m).
31. Run TecPlot macro that reads in data file and creates velocity and vorticity plots (velvort2.mcr).
32. Make sure the plots have the desired scales and labels, and then run the TecPlot macro that exports the velocity and vorticity plots to an AVI file (aviexport2.mcr).

APPENDIX E. MATLAB CODE FOR PLOTTING ROTATING DISK DATA

Cont.m

```
clear all
close all
%final interrogation region size
ir=128;
%read in active open spreadsheet
channel_in=ddeinit('excel','Sheet1');
%read in number of data points
m=ddereq(channel_in,'r2c6');
%read in speed of disk
r=ddereq(channel_in,'r4c6');
%read in x-dimension values
x1=ddereq(channel_in,'c7');
%read in y-dimension values
y1=ddereq(channel_in,'c2');
%read in scalar values from PIV calculation
z1=ddereq(channel_in,'c3');
%read in exact velocity
v1=ddereq(channel_in,['r1c4:r' num2str(m) 'c4']);
%read in percent error
e1=ddereq(channel_in,['r1c5:r' num2str(m) 'c5']);
%eliminate the extra values in the x and y arrays
i=1;
j=1;
for k=2:m
    if y1(k) == y1(k-1)
        i=i+1;
    end
    if y1(k) ~= y1(k-1)
        break
    end
end
for k=2:m
    if x1(k) == x1(k-1)
        j=j+1;
    end
    if x1(k) ~= x1(k-1)
        break
    end
end
x=ddereq(channel_in,['r1c1:r' num2str(i) 'c1']);
y=ddereq(channel_in,['r1c8:r' num2str(j) 'c8']);

for k=1:j
```

```

for l=1:i
    z(k,l) = z1(1+(k-1)*i);
    v(k,l) = v1(1+(k-1)*i);
    e(k,l) = e1(1+(k-1)*i);
end
end

%divide contour levels for velocity plots
sn=max(v1)/8;
s=str2num(sprintf('%6.2f',[0 sn 2*sn 3*sn 4*sn 5*sn 6*sn 7*sn 8*sn]));
%divide contour levels for error plot
d=[-10 -8 -6 -4 -2 0 2 4 6 8 10];
%open figure
figure;
%create contour plot of exact velocity
[cv1,hv1]=contour(x,y,v,s);
set(hv1,'LineStyle','-','edgecolor','black','linewidth',1);
%label contours
clabel(cv1,hv1);
%title and label plot
title(['Exact Velocity (m/s) at a Disk Speed of ' num2str(round(r)) ' RPM']);
xlabel('x (mm)');
ylabel('y (mm)');
%set white background and position of grid
set(gcf,'color',[1 1 1],'position',[232 258 516 420]);
%set aspect ratio to 1:1
set(gca,'DataAspectRatio',[1 1 1]);
%export plot to bitmap file
saveas(gcf,[num2str(round(r)) '(' num2str(ir) ')exact'],'bmp');
%open new figure, plot calculated velocity with dashed lines and label contours
figure;
[cz1,hz1]=contour(x,y,z,s);
set(hz1,'LineStyle','-','edgecolor','black','linewidth',1);
clabel(cz1,hz1);
%title and label plot, set white background, position, and aspect ratio
title('Calculated Velocity (m/s)');
xlabel('x (mm)');
ylabel('y (mm)');
set(gcf,'color',[1 1 1],'position',[232 258 516 420]);
set(gca,'DataAspectRatio',[1 1 1]);
%export to file
saveas(gcf,[num2str(round(r)) '(' num2str(ir) ')calc'],'bmp');
%open new figure, plot percent error with a colorbar legend
figure;
[ce,he]=contourf(x,y,e,d);
colorbar;

```



```

%title and label plot, set white background, position, and aspect ratio
title('% Error');
xlabel('x (mm)');
ylabel('y (mm)');
set(gcf,'color',[1 1 1],'position',[232 258 516 420]);
set(gca,'DataAspectRatio',[1 1 1]);
%export to file
saveas(gcf,[num2str(round(r)) '(' num2str(ir) ')error'],'bmp');
%create new figure and plot calculated velocity contours in dashed lines
figure;
[cz hz]=contour(x,y,z,s);
set(hz,'LineStyle','-','edgecolor','black','linewidth',1);
%turn hold on to plot multiple plots on same figure
hold on
%plot exact velocity contours in solid lines and label contours
[cv hv]=contour(x,y,v,s);
set(hv,'LineStyle','-','edgecolor','black','linewidth',1);
clabel(cv,hv);
%title and label plot
title('Comparison of Velocity (m/s) Contours');
xlabel('x (mm)');
ylabel('y (mm)');
%create white area for text (legend) placement
fill([73 107 107 73],[-8 -8 8 8],'w')
t=sprintf('— Exact\n- - Calculated');
text(75,0,t,'FontWeight','Normal','FontSize',10);
%set background color to white and position figure and axis with aspect ratio of 1:1
set(gcf,'color',[1 1 1],'position',[232 258 516 420]);
set(gca,'DataAspectRatio',[1 1 1],'position',[0.13 0.11 0.662625 0.815]);
%save to file
saveas(gcf,[num2str(round(r)) '(' num2str(ir) ')comp'],'bmp');

```

APPENDIX F. MATLAB AND TECPLOT CODES USED FOR HOT WIRE
EXPERIMENT

Hwplot.m

% Give name of data file to read (fname1) without the '.dat' extension. Give name of data
file to write
% (fname2) without the extension. Then press F5 to save and run. Program will read in
the data and save
% it in vector plotting format.

clear all

fname1='G:\Moore\HotWir~1\Rm21Se~1\041102\041102f05dc1b2x0y5';
fname2='G:\Moore\HotWir~1\Rm21Se~1\041102\f05dc1b2x0y5';
%the last line before data header (the last line of text)
jmax=36;
%number of lines in the data header
h=8;

tic

clc

fname = ([fname1 '.dat']);
n1=dlmread(fname,'t',[jmax-8) 0 (jmax-8) 0]);
m1=dlmread(fname,'t',[jmax-6) 0 (jmax-6) 0]);
trav=dlmread(fname,'t',[jmax-3) 0 (jmax-3) 0]);
m=(m1-h)/4;
n=((n1-1)/trav)+1;
for t=1:trav
clc
disp(['Reading input data for traverse #' num2str(t) ' of ' num2str(trav) '...']);
if t == 1
dat=dlmread(fname,'t',[jmax 0 (jmax-1+m+h) (n-1)]);
time=dat((h+1):(m+h),1);
x1=dlmread(fname,'t',[jmax+h-1) 1 (jmax+h-1) (n1-1)]);
y1=dlmread(fname,'t',[jmax+h-2) 1 (jmax+h-2) (n1-1)]);
k=0;
for i=1:2:(n1-2)
k=k+1;
x(k)=x1(i);
y(k)=y1(i);
xmm(k)=x(k)*10;
ymm(k)=y(k)*10;
end
else
dat=dlmread(fname,'t',[jmax ((t-1)*(n-1)+1) (jmax-1+m+h) (t*(n-1))]);
end

```

for i=1:m
if t == 1
vel(i,(1:((n-1)/2))) = dat((i+h),(2:2:(n-1)));
a(i,(1:((n-1)/2))) = (pi/180)*dat((i+h),(3:2:n));
else
vel(i,(((t-1)*((n-1)/2)+1):(t*((n-1)/2)))) = dat((i+h),(1:2:(n-2)));
a(i,(((t-1)*((n-1)/2)+1):(t*((n-1)/2)))) = (pi/180)*dat((i+h),(2:2:(n-1)));
end
end
end
vel=vel';
a=a';
for i=1:m
clc
disp(['Creating u- and v-component vectors (' num2str(i) '/' num2str(m) ')...']);
for j=1:(((n-1)/2)*trav)
u(j,i) = vel(j,i)*cos(a(j,i));
v(j,i) = vel(j,i)*sin(a(j,i));
end
end
n2=((n-1)/2);
jmax=((n-1)/2)*trav;
for i=1:m
if ((trav == 1) | (n == 3))
break
end
clc
disp(['Calculating vorticity (' num2str(i) '/' num2str(m) ')...']);
for j=1:jmax
if (j == 1)
jp2=j+2*n2;
jp=j+n2;
ip2=j+2;
ip=j+1;
vort(j,i)=(-v(ip2,i)+4*v(ip,i)-3*v(j,i))/(-x(ip2)+4*x(ip)-3*x(j))-(-u(jp2,i)+4*u(jp,i)-
3*u(j,i))/(-y(jp2)+4*y(jp)-3*y(j)));
elseif (j == n2)
jp2=j+2*n2;
jp=j+n2;
ip2=j-2;
ip=j-1;
vort(j,i)=(-v(ip2,i)+4*v(ip,i)-3*v(j,i))/(-x(ip2)+4*x(ip)-3*x(j))-(-u(jp2,i)+4*u(jp,i)-
3*u(j,i))/(-y(jp2)+4*y(jp)-3*y(j)));
elseif (j == (jmax-n2+1))
jp2=j-2*n2;
jp=j-n2;

```

```

ip2=j+2;
ip=j+1;
vort(j,i)=(-v(ip2,i)+4*v(ip,i)-3*v(j,i))/(-x(ip2)+4*x(ip)-3*x(j))-(-u(jp2,i)+4*u(jp,i)-
3*u(j,i))/(-y(jp2)+4*y(jp)-3*y(j));
elseif (j == jmax)
jp2=j-2*n2;
jp=j-n2;
ip2=j-2;
ip=j-1;
vort(j,i)=(-v(ip2,i)+4*v(ip,i)-3*v(j,i))/(-x(ip2)+4*x(ip)-3*x(j))-(-u(jp2,i)+4*u(jp,i)-
3*u(j,i))/(-y(jp2)+4*y(jp)-3*y(j));
elseif (j > 1) & (j < n2)
jp2=j+2*n2;
jp=j+n2;
ip=j+1;
im=j-1;
vort(j,i)=(v(ip,i)-v(im,i))/(x(ip)-x(im))-(-u(jp2,i)+4*u(jp,i)-3*u(j,i))/(-y(jp2)+4*y(jp)-
3*y(j));
elseif (j > n2) & ((rem((j-1),n2))==0) & (j < (jmax-n2))
jp=j+n2;
jm=j-n2;
ip2=j+2;
ip=j+1;
vort(j,i)=(-v(ip2,i)+4*v(ip,i)-3*v(j,i))/(-x(ip2)+4*x(ip)-3*x(j))-(u(jp,i)-u(jm,i))/(y(jp)-
y(jm));
elseif (j > n2) & (rem(j,n2)==0) & (j <= (jmax-n2))
jp=j+n2;
jm=j-n2;
ip2=j-2;
ip=j-1;
vort(j,i)=(-v(ip2,i)+4*v(ip,i)-3*v(j,i))/(-x(ip2)+4*x(ip)-3*x(j))-(u(jp,i)-u(jm,i))/(y(jp)-
y(jm));
elseif (j > (jmax-n2+1)) & (j < jmax)
jp2=j-2*n2;
jp=j-n2;
ip=j+1;
im=j-1;
vort(j,i)=(v(ip,i)-v(im,i))/(x(ip)-x(im))-(-u(jp2,i)+4*u(jp,i)-3*u(j,i))/(-y(jp2)+4*y(jp)-
3*y(j));
else
jp=j+n2;
jm=j-n2;
ip=j+1;
im=j-1;
vort(j,i)=(v(ip,i)-v(im,i))/(x(ip)-x(im))-(u(jp,i)-u(jm,i))/(y(jp)-y(jm));
end

```

```

end
end
b=1;
while b ~= 0
    fname = ([fname2 '.dat']);
    fid=fopen(fname,'a');
    fseek(fid,0,1);
    b=ftell(fid);
    if b == 0
        break
    end
    fclose(fid);
    beep;
    fname2 = inputdlg(['Error creating ' fname2 '.dat. File already exists. Please input
another file name. (.dat" will be automatically be appended to file name)'],'Enter File
Name',[1 120],[fname2],'on');
    fname2 = char(fname2);
end
if ((trav == 1) | (n == 3))
    vars = ' VARIABLES = "X (mm)", "Z (mm)", "U (m/s)", "V (m/s)", "Mag (m/s)", "Ang
(rad)";
else
    vars = ' VARIABLES = "X (mm)", "Z (mm)", "U (m/s)", "V (m/s)", "Mag (m/s)", "Ang
(rad)", "Vort (s^-1)";
end
fprintf(fid,'%s\r\n',vars);
for i=1:m
    clc
    disp(['Creating Output File (Zone ' num2str(i) ' of ' num2str(m) ')...']);
    zone=([' zone t="Time = ' num2str(time(i),'%5.3f) 's", i=' num2str((n-1)/2) ' j='
num2str(trav) ]]);
    fprintf(fid,'%s\r\n',zone);
    if ((trav == 1) | (n == 3))
        array=[xmm' ymm' u(:,i) v(:,i) vel(:,i) a(:,i)];
        fprintf(fid,'%8.3ft %8.3ft %8.3ft %8.3ft %8.3ft %8.3fr\n',array');
        text=([' text x=50, y=93.5, t="Velocity (m/s) at &(ZONENAME:' num2str(i) ')",
AN=CENTER, F=COURIER-BOLD, CS=FRAME, H=4, ZN=' num2str(i) ]]);
    else
        array=[xmm' ymm' u(:,i) v(:,i) vel(:,i) a(:,i) 100*vort(:,i)];
        fprintf(fid,'%8.3ft %8.3ft %8.3ft %8.3ft %8.3ft %8.3ft %8.3fr\n',array');
        text=([' text x=50, y=93.5, t="&(VARNAME:8) at &(ZONENAME:' num2str(i) ')",
AN=CENTER, F=COURIER-BOLD, CS=FRAME, H=4, ZN=' num2str(i) ]]);
    end
    fprintf(fid,'%s\r\n\r\n',text);
end
fclose(fid);

```

```

button = questdlg('Convert output file to Tecplot binary file?','ASCII to Binary','No');
if button == 'Yes'
    dos(['preplot ' fname]);
end
e=toc;
hour1=e/3600;
hour=floor(hour1);
e1=e-(3600*hour);
min1=e1/60;
min=floor(min1);
sec=round(e1-(60*min));
clc
disp(['Time Elapsed (h:m:s) - ' num2str(hour) ':' num2str(min) ':' num2str(sec)]);

```

velvort.mcr

```

#!MC 900
$!VarSet |MFBD| = 'C:\Program Files\TEC90'

$!LOOP 1
$!PROMPTFORYESNO |fclear|
    INSTRUCTIONS = "All frames will be deleted. Continue?"
$!IF "|fclear|" == "No"
$!Continue
$!ENDIF
$!PICK ADDALL
    SELECTFRAMES = YES
$!PICK CLEAR

$!INTERFACE
    AUTOREDRAWISACTIVE = FALSE
$!VarSet |H| = 7
$!VarSet |W| = 11
$!VarSet |ATH| = 4
$!VarSet |ALH| = 4
$!VarSet |YO| = 5
$!VarSet |TH| = 6
$!VarSet |GX1| = 7.5
$!VarSet |GX2| = 87.5
$!VarSet |GY1| = 8.237
$!VarSet |GY2| = 89.995
$!VarSet |XPOS1| = 14.2
$!VarSet |XPOS2| = 40
$!VarSet |times| = 1
$!VarSet |skip| = 4
$!PROMPTFORTEXTSTRING |plot|

```

INSTRUCTIONS = "Enter 1 to plot velocity, 2 for vorticity, or 3 to plot both."

```

$!IF |plot| == 1
  $!VarSet |times| = 1
$!ENDIF
$!IF |plot| == 2
  $!VarSet |times| = 2
$!ENDIF
$!IF |plot| == 3
  $!VarSet |times| = 2
  $!VarSet |H| = 4
  $!VarSet |W| = 6.286
  $!VarSet |ATH| = 4
  $!VarSet |ALH| = 4
  $!VarSet |YO| = 5
  $!VarSet |TH| = 6
  $!VarSet |GX1| = 7.5
  $!VarSet |GX2| = 87.5
  $!VarSet |GY1| = 8.237
  $!VarSet |GY2| = 89.995
  $!VarSet |XPOS1| = 14.2
  $!VarSet |XPOS2| = 40
  $!VarSet |skip| = 4
$!PICK ADDALL
  SELECTFRAMES = YES
$!PICK COPY
$!PICK PASTE
$!ENDIF

$!PROMPTFORTEXTSTRING |R|
  INSTRUCTIONS = "Enter number of data regions to add."

$!LOOP |times|
$!FRAMECONTROL PUSHTOP
$!IF |LOOP| == 1
$!LOOP |R|
  $!IF |LOOP| == 1
    $!VarSet |data| = "|macrofilepath|\ "
  $!ENDIF
  $!PROMPTFORFILENAME |data|
    DIALOGTITLE = "Load Data File |LOOP|"
    DEFAULTFNAME = "|data|"
    FILEFILTER = "*.dat;*.plt"
  $!IF |LOOP| == 1
    $!VarSet |DN| = ""|data|""
  $!ENDIF

```

```

$!IF |LOOP| > 1
$!VarSet |DN| = '|DN| "|data|"'
$!ENDIF
$!ENDLOOP

$!READDATASET "|DN|"

$!IF |plot| == 2
$!Continue
$!ENDIF
$!VarSet |CONTVAR| = 5
$!VarSet |CONTMIN| = 0.5
$!VarSet |CONTMAX| = 4.0
$!VarSet |NUMLEVELS| = 8
$!VarSet |RS| = 2.5
$!VarSet |RH| = 4
$!VarSet |LX| = 92.3
$!VarSet |LY| = 88.8
$!VarSet |CVARNAME| = "Velocity (m/s)"
$!FRAMENAME = "Velocity"
$!VarSet |CFORMAT| = "FIXEDFLOAT"
$!VarSet |VECTORS| = "YES"
$!VarSet |OVERRIDE| = "NO"
$!VarSet |YPOS| = 0.5
$!ENDIF
$!IF |LOOP| == 2
$!VarSet |CONTVAR| = 7
$!VarSet |CONTMIN| = -200
$!VarSet |CONTMAX| = 200
$!VarSet |NUMLEVELS| = 9
$!VarSet |RS| = 2.2
$!VarSet |RH| = 4
$!VarSet |LX| = 92.5
$!VarSet |LY| = 88.8
$!VarSet |CVARNAME| = "Vorticity (s^-1)"
$!FRAMENAME = "Vorticity"
$!VarSet |CFORMAT| = "INTEGER"
$!VarSet |VECTORS| = "NO"
$!VarSet |OVERRIDE| = "YES"
$!VarSet |YPOS| = 0.5
$!IF |plot| == 3
$!VarSet |YPOS| = 4.5
$!READDATASET "|DN|"
$!ENDIF
$!ENDIF

```



```

$!FRAME LAYOUT SHOWHEADER = NO
$!FRAME LAYOUT SHOWBORDER = NO
$!FRAME LAYOUT XYPOS {X = 0}
$!FRAME LAYOUT XYPOS {Y = |YPOS|}
$!FRAME LAYOUT HEIGHT = |H|
$!FRAME LAYOUT WIDTH = |W|
$!FIELDLAYERS SHOWMESH = NO
$!FIELDLAYERS SHOWBOUNDARY = NO
$!GLOBALCONTOUR VAR = |CONTVAR|
$!FIELDLAYERS SHOWCONTOUR = YES
$!CONTOURLEVELS DELETERANGE
  RANGEMIN = |MINC|
  RANGEMAX = |MAXC|
$!VarSet |D| = ((|CONTMAX| - |CONTMIN|) / (|NUMLEVELS| - 1))
$!LOOP |NUMLEVELS|
$!VarSet |CONT| = (|CONTMIN| + (|LOOP| - 1) * |D|)
$!CONTOURLEVELS ADD
  RAWDATA
  1
  |CONT|
$!ENDLOOP
$!GLOBALCONTOUR LEGEND {SHOW = YES}
$!GLOBALCONTOUR LEGEND {SHOWHEADER = NO}
$!GLOBALCONTOUR LEGEND {ROWSPACING = |RS|}
$!GLOBALCONTOUR LEGEND {TEXTSHAPE {HEIGHT = |RH|}}
$!GLOBALCONTOUR LEGEND {XYPOS {X = |LX|}}
$!GLOBALCONTOUR LEGEND {XYPOS {Y = |LY|}}
$!GLOBALCONTOUR LEGEND {NUMFORMAT {FORMATTING = |CFORMAT|}}
$!GLOBALCONTOUR LEGEND {NUMFORMAT {PRECISION = 2}}
$!GLOBALCONTOUR LEGEND {BOX {BOXTYPE = NONE}}
$!GLOBALTWO DVECTOR UVAR = 3
$!GLOBALTWO DVECTOR VVAR = 4
$!RESETVECTORLENGTH
$!FIELDLAYERS SHOWVECTOR = YES
$!FIELD [1-|NUMZONES|] VECTOR {IJKSKIP {I = |skip|}}
$!FIELD [1-|NUMZONES|] VECTOR {IJKSKIP {J = |skip|}}
$!FIELD [1-|NUMZONES|] VECTOR {ISTANGENT = YES}
$!FIELD [1-|NUMZONES|] VECTOR {COLOR = BLACK}
$!FIELD [1-|NUMZONES|] VECTOR {PATTERNLENGTH = 5}
$!GLOBALTWO DVECTOR RELATIVELENGTH = 1
$!GLOBALTWO DVECTOR HEADSIZEASFRACTION = 0.3
$!GLOBALFRAME PRESERVEAXISSCALE = NO
$!TWO DAXIS YDETAIL {RANGEMIN = 0}
$!TWO DAXIS YDETAIL {RANGEMAX = 104}
$!TWO DAXIS XDETAIL {RANGEMIN = 0}

```

```

$!TWO DAXIS XDETAIL {RANGEMAX = 160}
$!GLOBALFRAME PRESERVEAXISSCALE = YES
$!TWO DAXIS YDETAIL {AUTOGRID = NO}
$!TWO DAXIS YDETAIL {GRSPACING = 10}
$!TWO DAXIS YDETAIL {AXISPOSITION = |GX1|}
$!TWO DAXIS GRIDAREA {EXTENTS {X1 = |GX1|}}
$!TWO DAXIS GRIDAREA {EXTENTS {X2 = |GX2|}}
$!TWO DAXIS XDETAIL {AXISPOSITION = |GY1|}
$!TWO DAXIS GRIDAREA {EXTENTS {Y1 = |GY1|}}
$!TWO DAXIS GRIDAREA {EXTENTS {Y2 = |GY2|}}
$!TWO DAXIS YDETAIL {TITLE {OFFSET = |YO|}}
$!TWO DAXIS YDETAIL {TITLE {TEXTSHAPE {HEIGHT = |ATH|}}}
$!TWO DAXIS YDETAIL {TICKLABEL {TEXTSHAPE {HEIGHT = |ALH|}}}
$!TWO DAXIS XDETAIL {TITLE {TEXTSHAPE {HEIGHT = |ATH|}}}
$!TWO DAXIS XDETAIL {TICKLABEL {TEXTSHAPE {HEIGHT = |ALH|}}}
$!ALTERDATA
  EQUATION = 'V8 = C'
$!RENAMEDATASETVAR
  VAR = 8
  NAME = "|CVARNAME|"

#dummy geometry to make sure all are clear
$!ATTACHGEOM
  RAWDATA
  1
  1
  1 1
$!PICK ADDALL
  SELECTGEOMS = YES
$!PICK CLEAR

$!PICK ADDALL
  SELECTTEXT = YES
$!PICK EDIT
  TEXTHEIGHTBYPERCENT = |TH|

$!LOOP 2
$!VarSet |XPOS| = |XPOS1|
$!IF |LOOP| == 2
$!VarSet |XPOS| = |XPOS2|
$!ENDIF
$!ATTACHGEOM
  POSITIONCOORDSYS = FRAME
  XYZPOS
  {
  X = |XPOS|

```

```

    Y = |GY1|
  }
  RAWDATA
  1
  2
  0 0
  -7.5 -6.81
  $!ENDLOOP

```

```

$!FIELDLAYERS SHOWVECTOR = |VECTORS|
$!GLOBALCONTOUR COLORMAPFILTER{COLORMAPOVERRIDEACTIVE =
|OVERRIDE|}
$!GLOBALCONTOUR COLORMAPFILTER{COLORMAPOVERRIDE 1 {INCLUDE
= YES}}
$!GLOBALCONTOUR COLORMAPFILTER{COLORMAPOVERRIDE 1
{STARTLEVEL = 4}}
$!GLOBALCONTOUR COLORMAPFILTER{COLORMAPOVERRIDE 1
{ENDLEVEL = 6}}
$!GLOBALCONTOUR COLORMAPFILTER{COLORMAPOVERRIDE 1 {COLOR =
CUSTOM20}}

```

```

$!ENDLOOP
$!ENDLOOP
$!RemoveVar |MFBD|

```

Aviexport.mcr

```

#!MC 900
$!VarSet |MFBD| = 'C:\Program Files\TEC90'
$!VarSet |S| = ((3/25)*|NUMZONES|)
$!ACTIVEFIELDZONES += [1-|NUMZONES|]
$!ACTIVEFIELDZONES -= [2-|NUMZONES|]
$!FRAMECONTROL POP
  FRAME = 1
$!ACTIVEFIELDZONES += [1-|NUMZONES|]
$!ACTIVEFIELDZONES -= [2-|NUMZONES|]
$!EXPORTSETUP BITDUMPREGION = ALLFRAMES
$!EXPORTSETUP IMAGEWIDTH = 751
$!EXPORTSETUP EXPORTFORMAT = AVI
$!EXPORTSETUP ANIMATIONSPEED = |S|
$!PROMPTFORTEXTSTRING |fname|
  INSTRUCTIONS = "Enter file name (avi will be put in the directory of this macro).
Warning! If file already exists, it will be overwritten."
$!EXPORTSETUP EXPORTFNAME = "|MACROFILEPATH|\|fname|.avi"
$!EXPORTSTART
$!VarSet |N| = (|NUMZONES|-1)

```

```
$!LOOP |N|
$!VarSet |F|=(|LOOP|+1)
$!ACTIVEFIELDZONES += [|F|]
$!ACTIVEFIELDZONES -= [|LOOP|]
$!FRAMECONTROL POP
  FRAME = 1
$!ACTIVEFIELDZONES += [|F|]
$!ACTIVEFIELDZONES -= [|LOOP|]
$!EXPORTNEXTFRAME
$!ENDLOOP
```

```
$!EXPORTFINISH
$!RemoveVar |MFBD|
```

APPENDIX G. MATLAB AND TECPLOT CODES USED FOR FREE JET PIV
EXPERIMENT

imagesort.m

```

clear all
tic
%%%%%%%%%%%%%%%%%%%%%%%%%%%%%%%%%%%%%%%%%%%%%%%%%%%%%%%%%%%%%%%%%%%%%%%%
%%%%%%%%%%%%%%%%%%%%%%%%%%%%%%%%%%%%%%%%%%%%%%%%%%%%%%%%%%%%%%%%%%%%%%%%
%% TO UNDO
RENAME%%%%%%%%%%%%%%%%%%%%%%%%%%%%%%%%%%%%%%%%%%%%%%%%%%%%%%%%%%%%%%%%%%%%%%%%
%%%%%%%%%%%%%%%%%%%%%%%%%%%%%%%%%%%%%%%%%%%%%%%%%%%%%%%%%%%%%%%%%%%%%%%%
%% CUT RENAMED IMAGES AND PASTE THEM INTO THE ORIGINAL
FOLDER (PARENTDIR)
%% THEN SWITCH 'A' AND 'B' IN LINES 59 AND 60 AND COMMENT OUT
LINES 66-74
%%%%%%%%%%%%%%%%%%%%%%%%%%%%%%%%%%%%%%%%%%%%%%%%%%%%%%%%%%%%%%%%%%%%%%%%
%%%%%%%%%%%%%%%%%%%%%%%%%%%%%%%%%%%%%%%%%%%%%%%%%%%%%%%%%%%%%%%%%%%%%%%%

%directory of images to be renamed and sorted
PARENTDIR = ['G:\Moore\PIV\FreeJe~1\Crossflow\041221\f05dc50B1CL\'];
%time between image pairs (in ms)
period=20;
%number of images
images=2600;
%number of cycles
cycles=13;
%desired file name beginning (will be appended with time and index values)
%(total file name cannot exceed 27 characters)
name=['f05dc50B1CL'];
%multiply period by 10 if necessary to get rid of decimal point
%period=period*10;
%Copy image files or move them?
com='move';
%%%%%%%%%%%%%%%%%%%%%%%%%%%%%%%%%%%%%%%%%%%%%%%%%%%%%%%%%%%%%%%%%%%%%%%%
%%%%%%%%%%%%%%%%%%%%%%%%%%%%%%%%%%%%%%%%%%%%%%%%%%%%%%%%%%%%%%%%%%%%%%%%
clc
f=['%0' num2str(length(num2str(images/2))) 'd'];
f1=['%0' num2str(length(num2str(images))) 'd'];
disp('Creating Folders...');
%number of timesteps
ts=(images/cycles)/2;
g=['%0' num2str(length(num2str(period*(ts-1)))) 'd'];
%number of timesteps per folder
tspf=0;
while (cycles*(tspf+1)*2) <= 642
tspf=tspf+1;

```

```

end
folders=ceil(ts/tspf);
for t=1:folders
tmin(t)=(t-1)*tspf*period;
if (t == folders)
    tmax(t) = period*(ts-1);
else
    tmax(t)=tmin(t)+((tspf-1)*period);
end
NEWDIR = [num2str(tmin(t),g) '-' num2str(tmax(t),g)];
STATUS=MKDIR(PARENTDIR,NEWDIR);
end
imax=cycles-1;
jmax=(images/cycles)-1;
c=0;
for i = 0:imax
for j = 0:2:jmax
for m = 0:1
c=c+1;
clc
disp(['Renaming and sorting images (' num2str(c,f1) '/' num2str(images) ')']);
k=(j*period)/2;
if m == 0
    d = 'A';
else
    d = 'B';
end
A=['ImgA' num2str((c-1),'%06d') '.bmp'];
B=[name 't' num2str(k,g) 'n' num2str(i,'%03d') d '.bmp'];
s1=['rename ' PARENTDIR A ' ' B];
[a,b]=dos(s1);
if a==1
    error(b);
end
for t = 1:folders
if (k >= tmin(t)) & (k <= tmax(t))
    s2=[com ' ' PARENTDIR B ' ' PARENTDIR num2str(tmin(t),g) '-' num2str(tmax(t),g)
    '\'];
[a,b]=dos(s2);
if a==1
    error(b);
end
end
end
end
end
end
end

```

```

end
end
e=toc;
hour1=e/3600;
hour=floor(hour1);
e1=e-(3600*hour);
min1=e1/60;
min=floor(min1);
sec=round(e1-(60*min));
disp(['Time Elapsed (h:m:s) - ' num2str(hour) ':' num2str(min,'%02d') ':'
num2str(sec,'%02d')])

```

imagesortsteady.m

```

clear all
tic
%%%%%%%%%%%%%%%%%%%%%%%%%%%%%%%%%%%%%%%%%%%%%%%%%%%%%%%%%%%%%%%%%%%%%%%%
%%%%%%%%%%%%%%%%%%%%%%%%%%%%%%%%%%%%%%%%%%%%%%%%%%%%%%%%%%%%%%%%%%%%%%%%
%directory of images to be renamed and sorted
PARENTDIR = ['G:\Moore\PIV\FreeJe~1\Crossflow\041105\dc100b1CL\'];
%number of images
images=1000;
%desired file name beginning (will be appended with index values)
name=['dc100b1CL'];
%%%%%%%%%%%%%%%%%%%%%%%%%%%%%%%%%%%%%%%%%%%%%%%%%%%%%%%%%%%%%%%%%%%%%%%%
%%%%%%%%%%%%%%%%%%%%%%%%%%%%%%%%%%%%%%%%%%%%%%%%%%%%%%%%%%%%%%%%%%%%%%%%
clc
f=['%0' num2str(length(num2str(images/2))) 'd'];
f1=['%0' num2str(length(num2str(images))) 'd'];
disp('Creating Folders...');
folders=ceil(images/642);
for t=1:folders
tmin(t)=(t-1)*321;
if (t == folders)
tmax(t) = (images/2)-1;
else
tmax(t)=tmin(t)+320;
end
NEWDIR = [num2str(tmin(t),f) '-' num2str(tmax(t),f)];
STATUS=MKDIR(PARENTDIR,NEWDIR);
end
imax=(images/2)-1;
c=0;
for i = 0:imax
for m = 0:1
c=c+1;
clc

```

```

disp(['Renaming and sorting images (' num2str(c,f1) '/' num2str(images) ')']);
if m == 0
    d = 'A';
else
    d = 'B';
end
A=['ImgA' num2str((c-1),'%06d') '.bmp'];
B=[name 'n' num2str(i,f) d '.bmp'];
s1=['rename ' PARENTDIR A ' ' B];
[a,b]=dos(s1);
if a==1
    error(b);
end
for t = 1:folders
    if (i >= tmin(t)) & (i <= tmax(t))
        s2=['move ' PARENTDIR B ' ' PARENTDIR num2str(tmin(t),f) '-' num2str(tmax(t),f) '\
'];
        [a,b]=dos(s2);
        if a==1
            error(b);
        end
    end
end
end
end
end
e=toc;
hour1=e/3600;
hour=floor(hour1);
e1=e-(3600*hour);
min1=e1/60;
min=floor(min1);
sec=round(e1-(60*min));
disp(['Time Elapsed (h:m:s) - ' num2str(hour) ':' num2str(min,'%02d') ':'
num2str(sec,'%02d')]);

```

PIVplot.m

```

clear all
%file names to read in (.log file and .txt file) without extension
fname1=['G:\Moore\PIV\FreeJe~1\Crossflow\041221\f05dc50B1CL];
%file name to output (.dat file) without extension
fname2=['G:\Moore\PIV\FreeJe~1\Crossflow\041221\f05dc50B1CL];
%Divide data file into 'div' parts to reduce variable size (to solve "Out of Memory"
errors)
div=2;
%number of datasets contained in the file

```



```

datasets=1;
%which dataset to start with
dmin=1;
%which dataset to finish with
dmax=1;
%number of cycles each data set contains
cycles=13;
%number of cycles to average
cycles1=13;
%first time value per cycle (ms)
to=0;
%final time value per cycle (ms)
tf=1980;
%time step (ms)
dt=20;
%horizontal axis ('X' or 'Y')
horiz='X';

tic
clc
if dt==0
    dt1=1;
else
    dt1=dt;
end
m1=1+((tf-to)/dt1);
m=round(m1);
if rem(m1,m) ~= 0
    disp('Invalid time step. Program Terminated. ');
    break
end
b=1;
while b ~= 0
    if rem(m,div) ~= 0
        beep;
        div=input(['Data divided into unwhole parts. Choose a divisor that divides evenly into '
num2str(m) '\n>>']);
    else
        b=0;
    end
end
fname = ([fname1 '.log']);
fid=fopen(fname);
if fid == -1
    error(['Cannot locate file ' fname])
end

```

```

zones=0;
while 1
    tline = fgetl(fid);
    if isempty(tline) == 1
        zones=zones+1;
        continue
    end
    if tline == -1
        break
    end
end
fclose(fid);
zones=zones/datasets;
if (cycles*m) ~= zones
    disp('Amount of data not consistent with given timestep and number of cycles. Program
Terminated. ');
    disp(['Number of Timesteps = ' num2str(m) ', Number of Cycles = ' num2str(cycles) ',
Number of Data Zones = ' num2str(zones)]);
    break
end

n=0;
n1=1;
n2=1;
flag1=0;
flag2=0;
fname=([fname1 '.txt']);
disp('Reading input data...')
fid=fopen(fname);
nline = str2num(fgetl(fid));
xline1 = nline(1);
yline1 = nline(2);
while flag2 == 0
    n=n+1;
    nline = str2num(fgetl(fid));
    xline = nline(1);
    yline = nline(2);
    if ((xline == xline1) & (flag1 ~= 1))
        flag1=1;
    end
    if ((xline ~= xline1) & (flag1 ~= 1))
        n1=n1+1;
    end
    if ((yline == yline1) & (flag1 == 1))
        flag2=1;
        n2=n/n1;
    end
end

```

```

end
end
fclose(fid);
clc
x=dlmread(fname,'\t',[0 0 (n-1) 0]);
y=dlmread(fname,'\t',[0 1 (n-1) 1]);
for p=dmin:dmax
o=0;
for l=1:div
disp(['Data Set ' num2str(p) ' of ' num2str(datasets)]);
disp(['Reading input data (' num2str(l) '/' num2str(div) ')...'])
dat=dlmread(fname,'\t',[(((l-1)*((n*zones)/div))+((p-1)*(n*zones))) 2 (l*((n*zones)/div)-
1+((p-1)*(n*zones))) 3]);
j=0;
for i=1:(m/div)
o=o+1;
clc
disp(['Data Set ' num2str(p) ' of ' num2str(datasets)]);
disp(['Reading input data (' num2str(l) '/' num2str(div) ')...'])
disp(['Calculating average velocities (' num2str(o) '/' num2str(m) ')...'])
u1(1:n,1)=0;
v1(1:n,1)=0;
for k=1:cycles1
j=j+1;
u1(1:n)=u1(1:n)+dat(((j*n-n+1):(j*n)),1);
v1(1:n)=v1(1:n)+dat(((j*n-n+1):(j*n)),2);
end
u(1:n,o)=u1(1:n)/cycles1;
v(1:n,o)=v1(1:n)/cycles1;
j=j+(cycles-cycles1);
end
clear dat
end
a=atan2(v,u);
vel=sqrt((v.^2)+(u.^2));

for i=1:m
clc
disp(['Data Set ' num2str(p) ' of ' num2str(datasets)]);
disp(['Calculating vorticity (' num2str(i) '/' num2str(m) ')...']);
for j=1:n
if (j == 1)
jp2=j+2*n1;
jp=j+n1;
ip2=j+2;
ip=j+1;

```

```

vort(j,i)=(-v(ip2,i)+4*v(ip,i)-3*v(j,i))/(-x(ip2)+4*x(ip)-3*x(j))-(-u(jp2,i)+4*u(jp,i)-
3*u(j,i))/(-y(jp2)+4*y(jp)-3*y(j));
elseif (j == n1)
jp2=j+2*n1;
jp=j+n1;
ip2=j-2;
ip=j-1;
vort(j,i)=(-v(ip2,i)+4*v(ip,i)-3*v(j,i))/(-x(ip2)+4*x(ip)-3*x(j))-(-u(jp2,i)+4*u(jp,i)-
3*u(j,i))/(-y(jp2)+4*y(jp)-3*y(j));
elseif (j == (n-n1+1))
jp2=j-2*n1;
jp=j-n1;
ip2=j+2;
ip=j+1;
vort(j,i)=(-v(ip2,i)+4*v(ip,i)-3*v(j,i))/(-x(ip2)+4*x(ip)-3*x(j))-(-u(jp2,i)+4*u(jp,i)-
3*u(j,i))/(-y(jp2)+4*y(jp)-3*y(j));
elseif (j == n)
jp2=j-2*n1;
jp=j-n1;
ip2=j-2;
ip=j-1;
vort(j,i)=(-v(ip2,i)+4*v(ip,i)-3*v(j,i))/(-x(ip2)+4*x(ip)-3*x(j))-(-u(jp2,i)+4*u(jp,i)-
3*u(j,i))/(-y(jp2)+4*y(jp)-3*y(j));
elseif (j > 1) & (j < n1)
jp2=j+2*n1;
jp=j+n1;
ip=j+1;
im=j-1;
vort(j,i)=(v(ip,i)-v(im,i))/(x(ip)-x(im))-(-u(jp2,i)+4*u(jp,i)-3*u(j,i))/(-y(jp2)+4*y(jp)-
3*y(j));
elseif (j > n1) & ((rem((j-1),n1))==0) & (j < (n-n1))
jp=j+n1;
jm=j-n1;
ip2=j+2;
ip=j+1;
vort(j,i)=(-v(ip2,i)+4*v(ip,i)-3*v(j,i))/(-x(ip2)+4*x(ip)-3*x(j))-(-u(jp,i)-u(jm,i))/(y(jp)-
y(jm));
elseif (j > n1) & (rem(j,n1)==0) & (j <= (n-n1))
jp=j+n1;
jm=j-n1;
ip2=j-2;
ip=j-1;
vort(j,i)=(-v(ip2,i)+4*v(ip,i)-3*v(j,i))/(-x(ip2)+4*x(ip)-3*x(j))-(-u(jp,i)-u(jm,i))/(y(jp)-
y(jm));
elseif (j > (n-n1+1)) & (j < n)
jp2=j-2*n1;

```

```

    jp=j-n1;
    ip=j+1;
    im=j-1;
    vort(j,i)=(v(ip,i)-v(im,i))/(x(ip)-x(im))-(-u(jp2,i)+4*u(jp,i)-3*u(j,i))/(-y(jp2)+4*y(jp)-
3*y(j));
    else
    jp=j+n1;
    jm=j-n1;
    ip=j+1;
    im=j-1;
    vort(j,i)=(v(ip,i)-v(im,i))/(x(ip)-x(im))-(u(jp,i)-u(jm,i))/(y(jp)-y(jm));
    end
end
end

for i=1:m
    time(i)=(to+(i-1)*dt)/1000;
end

if dmax == dmin
    s="";
else
    s=p;
end
b=1;
while b ~= 0
    fid=fopen([fname2 num2str(s) '.dat'],'a');
    fseek(fid,0,1);
    b=ftell(fid);
    if b == 0
        break
    end
    fclose(fid);
    beep;
    fname2=input(['Error creating ' fname2 num2str(s) '.dat. File already exists. Please input
another file name. \n' ...
'(".dat" will be automatically be appended to file name)\n>>'],'s');
end

vars = [' VARIABLES = "' horiz ' (mm)", "Z (mm)", "U (m/s)", "V (m/s)", "Mag (m/s)",
"Ang (rad)", "Vort (s^-1)"];
fprintf(fid,'%s\r\n',vars);
for i=1:m
    clc
    disp(['Creating Output File (Zone ' num2str(i) ' of ' num2str(m) ')...']);
end

```

```

zone=([' zone t="Time = ' num2str(time(i),'%5.4f) 's", i=' num2str(n1) ' j=' num2str(n2)
]);
fprintf(fid,'%s\r\n',zone);
array=[x y u(:,i) v(:,i) vel(:,i) a(:,i) 1000*vort(:,i)];
fprintf(fid,'%8.3ft %8.3ft %8.3ft %8.3ft %8.3ft %8.3ft %8.3ft\r\n',array);
text=([' text x=50, y=93.5, t="&(VARIABLE:8) at &(ZONENAME:' num2str(i) ')",
AN=CENTER, F=COURIER-BOLD, CS=FRAME, H=4, ZN=' num2str(i) ]);
fprintf(fid,'%s\r\n\r\n',text);
end
fclose(fid);
end
%button = questdlg('Convert output file(s) to Tecplot binary file?','ASCII to
Binary','No');
button = 'Yes';
if strcmp(button,'Yes') == 1
for p=dmin:dmax
if dmax == dmin
s="";
else
s=p;
end
fname=[fname2 num2str(s) '.dat'];
dos(['preplot ' fname]);
end
end
e=toc;
hour1=e/3600;
hour=floor(hour1);
e1=e-(3600*hour);
min1=e1/60;
min=floor(min1);
sec=round(e1-(60*min));
clc
disp(['Time Elapsed (h:m:s) - ' num2str(hour) ':' num2str(min) ':' num2str(sec)]);

```

PIVplotsteady.m

```

clear all
blow = '1';
date='041221';
freq=0.5;
dc=50;
%eliminate decimal point in filename reference
freq1=num2str(freq);
freq2=[];
for i=1:(length(freq1))
if strcmp(freq1(i),'.') ~ =1

```

```

freq2=[freq2 freq1(i)]
end
end
%file names to read in (.log file and .txt file) without extension
fname1=['G:\Moore\PIV\FreeJe~1\Crossflow\' date \f freq2 'dc' num2str(dc) 'b' blow
'CLavg'];
%fname1='C:\Docume~1\moorek1\MyDocu~1\test1\test5';
%file name to output (.dat file) without extension
fname2=['G:\Moore\PIV\FreeJe~1\Crossflow\' date \f freq2 'dc' num2str(dc) 'b' blow
'CLavg'];
%fname2='C:\Docume~1\moorek1\MyDocu~1\test1\test5';
%Divide data file into 'div' parts to reduce variable size (to solve "Out of Memory"
errors)
div=2;
%include standard deviations?
stdv='y';
%Title of plots (VARIABLE:8 is either "Velocity (m/s)" or "Vorticity (s^-1)")
title=['&(VARIABLE:8) at ' num2str(freq) 'Hz,' num2str(dc) '%DC,B=1,x=0d'];
tic
clc

% l=length(fname1);
% for i=1:-1:1
% if strcmp(fname1(i),'\')==1
% break
% end
% end
% if (l-i) > 8
% [a,b] = dos(['dir "' fname1 '.txt' /x']);
% fname1a=fname1(1:i);
% for i=1:length(b)
% if strcmp(b(i),'\')==1
% fname1b=(b((i-6):(i+1)));
% clear fname1
% fname1=[fname1a fname1b];
% end
% end
% end

n=0;
n1=1;
n2=1;
flag1=0;
flag2=0;
fname=([fname1 '.txt']);
disp('Reading input data...')

```

```

fid=fopen(fname);
nline = str2num(fgetl(fid));
xline1 = nline(1);
yline1 = nline(2);
while flag2 == 0
    n=n+1;
    f=fgetl(fid);
    if (f ~= -1)
        nline = str2num(f);
        xline = nline(1);
        yline = nline(2);
        if ((xline == xline1) & (flag1 ~= 1))
            flag1=1;
        end
        if ((xline ~= xline1) & (flag1 ~= 1))
            n1=n1+1;
        end
    else
        flag2=1;
        n2=n/n1;
    end
end
fclose(fid);
clc
x=dlmread(fname,'\t',[0 0 (n-1) 0]);
y=dlmread(fname,'\t',[0 1 (n-1) 1]);
u=dlmread(fname,'\t',[0 2 (n-1) 2]);
v=dlmread(fname,'\t',[0 3 (n-1) 3]);
if strcmp(stdv,'y')==1
stdvu=dlmread(fname,'\t',[0 4 (n-1) 4]);
stdvv=dlmread(fname,'\t',[0 5 (n-1) 5]);
stdv2=dlmread(fname,'\t',[0 6 (n-1) 6]);
end
a=atan2(v,u);
vel=sqrt((v.^2)+(u.^2));

for i=1:1
    disp(['Calculating vorticity...']);
    for j=1:n
        if (j == 1)
            jp2=j+2*n1;
            jp=j+n1;
            ip2=j+2;
            ip=j+1;
            vort(j,i)=(-v(ip2,i)+4*v(ip,i)-3*v(j,i))/(-x(ip2)+4*x(ip)-3*x(j))-(-u(jp2,i)+4*u(jp,i)-
3*u(j,i))/(-y(jp2)+4*y(jp)-3*y(j)));

```



```

elseif (j == n1)
  jp2=j+2*n1;
  jp=j+n1;
  ip2=j-2;
  ip=j-1;
  vort(j,i)=(-v(ip2,i)+4*v(ip,i)-3*v(j,i))/(-x(ip2)+4*x(ip)-3*x(j))-(-u(jp2,i)+4*u(jp,i)-
3*u(j,i))/(-y(jp2)+4*y(jp)-3*y(j));
elseif (j == (n-n1+1))
  jp2=j-2*n1;
  jp=j-n1;
  ip2=j+2;
  ip=j+1;
  vort(j,i)=(-v(ip2,i)+4*v(ip,i)-3*v(j,i))/(-x(ip2)+4*x(ip)-3*x(j))-(-u(jp2,i)+4*u(jp,i)-
3*u(j,i))/(-y(jp2)+4*y(jp)-3*y(j));
elseif (j == n)
  jp2=j-2*n1;
  jp=j-n1;
  ip2=j-2;
  ip=j-1;
  vort(j,i)=(-v(ip2,i)+4*v(ip,i)-3*v(j,i))/(-x(ip2)+4*x(ip)-3*x(j))-(-u(jp2,i)+4*u(jp,i)-
3*u(j,i))/(-y(jp2)+4*y(jp)-3*y(j));
elseif (j > 1) & (j < n1)
  jp2=j+2*n1;
  jp=j+n1;
  ip=j+1;
  im=j-1;
  vort(j,i)=(v(ip,i)-v(im,i))/(x(ip)-x(im))-(-u(jp2,i)+4*u(jp,i)-3*u(j,i))/(-y(jp2)+4*y(jp)-
3*y(j));
elseif (j > n1) & ((rem((j-1),n1))==0) & (j < (n-n1))
  jp=j+n1;
  jm=j-n1;
  ip2=j+2;
  ip=j+1;
  vort(j,i)=(-v(ip2,i)+4*v(ip,i)-3*v(j,i))/(-x(ip2)+4*x(ip)-3*x(j))-(u(jp,i)-u(jm,i))/(y(jp)-
y(jm));
elseif (j > n1) & (rem(j,n1)==0) & (j <= (n-n1))
  jp=j+n1;
  jm=j-n1;
  ip2=j-2;
  ip=j-1;
  vort(j,i)=(-v(ip2,i)+4*v(ip,i)-3*v(j,i))/(-x(ip2)+4*x(ip)-3*x(j))-(u(jp,i)-u(jm,i))/(y(jp)-
y(jm));
elseif (j > (n-n1+1)) & (j < n)
  jp2=j-2*n1;
  jp=j-n1;
  ip=j+1;

```

```

im=j-1;
vort(j,i)=(v(ip,i)-v(im,i))/(x(ip)-x(im))-(-u(jp2,i)+4*u(jp,i)-3*u(j,i))/(-y(jp2)+4*y(jp)-
3*y(j));
else
jp=j+n1;
jm=j-n1;
ip=j+1;
im=j-1;
vort(j,i)=(v(ip,i)-v(im,i))/(x(ip)-x(im))-(u(jp,i)-u(jm,i))/(y(jp)-y(jm));
end
end
end

b=1;
while b ~= 0
fid=fopen([fname2 '.dat'],'a');
fseek(fid,0,1);
b=ftell(fid);
if b == 0
break
end
fclose(fid);
beep;
fname2=input(['Error creating ' fname2 '.dat. File already exists. Please input another
file name. \n' ...
'(".dat" will be automatically be appended to file name)\n>>'],'s');
end

if strcmp(stdv,'y')==1
vars = ' VARIABLES = "X (mm)", "Z (mm)", "U (m/s)", "V (m/s)", "Mag (m/s)", "Ang
(rad)", "Vort (s^-1)", "StdvU (m/s)", "StdvV (m/s)", "StdvMag (m/s)";
else
vars = ' VARIABLES = "X (mm)", "Z (mm)", "U (m/s)", "V (m/s)", "Mag (m/s)", "Ang
(rad)", "Vort (s^-1)";
end
fprintf(fid,'%s\r\n',vars);
for i=1:1
clc
disp(['Creating Output File...']);
zone=([' zone t="Steady Jet", i=' num2str(n1) ' j=' num2str(n2) ]);
fprintf(fid,'%s\r\n',zone);
if strcmp(stdv,'y')==1
array=[x y u(:,i) v(:,i) vel(:,i) a(:,i) 1000*vort(:,i) stdvu(:,i) stdvv(:,i) sqrt(stdv2(:,i))];
fprintf(fid,'%8.3ft %8.3ft %8.3ft %8.3ft %8.3ft %8.3ft %8.3ft %8.3ft %8.3ft
%8.3fr\n',array);
else

```

```

array=[x y u(:,i) v(:,i) vel(:,i) a(:,i) 1000*vort(:,i)];
fprintf(fid,'%8.3ft %8.3ft %8.3ft %8.3ft %8.3ft %8.3ft %8.3fr\n',array');
end
text=([' text x=50, y=93.5, t="" title ""', AN=CENTER, F=COURIER-BOLD,
CS=FRAME, H=4, ZN=' num2str(i) ]);
fprintf(fid,'%s\r\n\r\n',text);
end
fclose(fid);
%button = questdlg('Convert output file(s) to Tecplot binary file?','ASCII to
Binary','No');
button = 'Yes';
if strcmp(button,'Yes') == 1
    fname=[fname2 '.dat'];
    dos(['preplot ' fname]);
end
e=toc;
hour1=e/3600;
hour=floor(hour1);
e1=e-(3600*hour);
min1=e1/60;
min=floor(min1);
sec=round(e1-(60*min));
clc
disp(['Time Elapsed (h:m:s) - ' num2str(hour) ':' num2str(min) ':' num2str(sec)]);

```

velvort.mcr

```

#!MC 900
$!VarSet |MFBD| = 'C:\Program Files\TEC90'

$!LOOP 1
$!PROMPTFORYESNO |fclear|
    INSTRUCTIONS = "All frames will be deleted. Continue?"
$!IF "|fclear|" == "No"
$!Continue
$!ENDIF
$!PICK ADDALL
    SELECTFRAMES = YES
$!PICK CLEAR

$!INTERFACE
    AUTOREDRAWISACTIVE = FALSE
$!VarSet |H| = 7
$!VarSet |W| = 11
$!VarSet |ATH| = 4
$!VarSet |ALH| = 4
$!VarSet |YO| = 5

```

```

$!VarSet |TH| = 6
$!VarSet |GX1| = 7.5
$!VarSet |GX2| = 87.5
$!VarSet |GY1| = 8.237
$!VarSet |GY2| = 89.995
$!VarSet |XPOS1| = 14.2
$!VarSet |XPOS2| = 40
$!VarSet |times| = 1
$!VarSet |skip| = 4
$!PROMPTFORTEXTSTRING |plot|
  INSTRUCTIONS = "Enter 1 to plot velocity, 2 for vorticity, or 3 to plot both."

```

```

$!IF |plot| == 1
  $!VarSet |times| = 1
$!ENDIF
$!IF |plot| == 2
  $!VarSet |times| = 2
$!ENDIF
$!IF |plot| == 3
  $!VarSet |times| = 2
  $!VarSet |H| = 4
  $!VarSet |W| = 6.286
  $!VarSet |ATH| = 4
  $!VarSet |ALH| = 4
  $!VarSet |YO| = 5
  $!VarSet |TH| = 6
  $!VarSet |GX1| = 7.5
  $!VarSet |GX2| = 87.5
  $!VarSet |GY1| = 8.237
  $!VarSet |GY2| = 89.995
  $!VarSet |XPOS1| = 14.2
  $!VarSet |XPOS2| = 40
  $!VarSet |skip| = 4
$!PICK ADDALL
  SELECTFRAMES = YES
$!PICK COPY
$!PICK PASTE
$!ENDIF

```

```

$!PROMPTFORTEXTSTRING |R|
  INSTRUCTIONS = "Enter number of data regions to add."

```

```

$!LOOP |times|
$!FRAMECONTROL PUSH TOP
$!IF |LOOP| == 1
$!LOOP |R|

```

```

$!IF |LOOP| == 1
  $!VarSet |data| = "|macrofilepath|\ "
$!ENDIF
$!PROMPTFORFILENAME |data|
  DIALOGTITLE = "Load Data File |LOOP|"
  DEFAULTFNAME = "|data|"
  FILEFILTER = "*.dat;*.plt"
$!IF |LOOP| == 1
  $!VarSet |DN| = ""|data|"
$!ENDIF
$!IF |LOOP| > 1
  $!VarSet |DN| = '|DN| "|data|"'
$!ENDIF
$!ENDLOOP

$!READDATASET "|DN|"

$!IF |plot| == 2
  $!Continue
$!ENDIF
$!VarSet |CONTVAR| = 5
$!VarSet |CONTMIN| = 0.5
$!VarSet |CONTMAX| = 4.0
$!VarSet |NUMLEVELS| = 8
$!VarSet |RS| = 2.5
$!VarSet |RH| = 4
$!VarSet |LX| = 92.3
$!VarSet |LY| = 88.8
$!VarSet |CVARNAME| = "Velocity (m/s)"
$!FRAMENAME = "Velocity"
$!VarSet |CFORMAT| = "FIXEDFLOAT"
$!VarSet |VECTORS| = "YES"
$!VarSet |OVERRIDE| = "NO"
$!VarSet |YPOS| = 0.5
$!ENDIF
$!IF |LOOP| == 2
  $!VarSet |CONTVAR| = 7
  $!VarSet |CONTMIN| = -200
  $!VarSet |CONTMAX| = 200
  $!VarSet |NUMLEVELS| = 9
  $!VarSet |RS| = 2.2
  $!VarSet |RH| = 4
  $!VarSet |LX| = 92.5
  $!VarSet |LY| = 88.8
  $!VarSet |CVARNAME| = "Vorticity (s^-1)"
  $!FRAMENAME = "Vorticity"

```

```

$!VarSet |CFORMAT| = "INTEGER"
$!VarSet |VECTORS| = "NO"
$!VarSet |OVERRIDE| = "YES"
$!VarSet |YPOS| = 0.5
$!IF |plot| == 3
  $!VarSet |YPOS| = 4.5
  $!READDATASET "|DN|"
$!ENDIF
$!ENDIF

```

```

$!FRAMELAYOUT SHOWHEADER = NO
$!FRAMELAYOUT SHOWBORDER = NO
$!FRAMELAYOUT XYPOS{X = 0}
$!FRAMELAYOUT XYPOS{Y = |YPOS|}
$!FRAMELAYOUT HEIGHT = |H|
$!FRAMELAYOUT WIDTH = |W|
$!FIELDLAYERS SHOWMESH = NO
$!FIELDLAYERS SHOWBOUNDARY = NO
$!GLOBALCONTOUR VAR = |CONTVAR|
$!FIELDLAYERS SHOWCONTOUR = YES
$!CONTOURLEVELS DELETERANGE
  RANGEMIN = |MINC|
  RANGEMAX = |MAXC|
$!VarSet |D| = ((|CONTMAX|-|CONTMIN|)/(|NUMLEVELS|-1))
$!LOOP |NUMLEVELS|
$!VarSet |CONT| = (|CONTMIN| + (|LOOP| - 1)*|D|)
$!CONTOURLEVELS ADD
  RAWDATA
  1
  |CONT|
$!ENDLOOP
$!GLOBALCONTOUR LEGEND{SHOW = YES}
$!GLOBALCONTOUR LEGEND{SHOWHEADER = NO}
$!GLOBALCONTOUR LEGEND{ROWSPACING = |RS|}
$!GLOBALCONTOUR LEGEND{TEXTSHAPE{HEIGHT = |RH|}}
$!GLOBALCONTOUR LEGEND{XYPOS{X = |LX|}}
$!GLOBALCONTOUR LEGEND{XYPOS{Y = |LY|}}
$!GLOBALCONTOUR LEGEND{NUMFORMAT{FORMATTING = |CFORMAT|}}
$!GLOBALCONTOUR LEGEND{NUMFORMAT{PRECISION = 2}}
$!GLOBALCONTOUR LEGEND{BOX{BOXTYPE = NONE}}
$!GLOBALTWOVECTOR UVAR = 3
$!GLOBALTWOVECTOR VVAR = 4
$!RESETVECTORLENGTH
$!FIELDLAYERS SHOWVECTOR = YES
$!FIELD [1-|NUMZONES|] VECTOR{IJKSKIP{I = |skip|}}

```

```

$!FIELD [1-|NUMZONES|] VECTOR{JKSKIP{J = |skip|}}
$!FIELD [1-|NUMZONES|] VECTOR{ISTANGENT = YES}
$!FIELD [1-|NUMZONES|] VECTOR{COLOR = BLACK}
$!FIELD [1-|NUMZONES|] VECTOR{PATTERNLENGTH = 5}
$!GLOBALTWOVECTOR RELATIVELENGTH = 1
$!GLOBALTWOVECTOR HEADSIZEASFRACTION = 0.3
$!GLOBALFRAME PRESERVEAXISSCALE = NO
$!TWOVECTOR YDETAIL {RANGEMIN = 0}
$!TWOVECTOR YDETAIL {RANGEMAX = 104}
$!TWOVECTOR XDETAIL {RANGEMIN = 0}
$!TWOVECTOR XDETAIL {RANGEMAX = 160}
$!GLOBALFRAME PRESERVEAXISSCALE = YES
$!TWOVECTOR YDETAIL {AUTOGRID = NO}
$!TWOVECTOR YDETAIL {GRSPACING = 10}
$!TWOVECTOR YDETAIL {AXISPOSITION = |GX1|}
$!TWOVECTOR GRIDAREA {EXTENTS{X1 = |GX1|}}
$!TWOVECTOR GRIDAREA {EXTENTS{X2 = |GX2|}}
$!TWOVECTOR XDETAIL {AXISPOSITION = |GY1|}
$!TWOVECTOR GRIDAREA {EXTENTS{Y1 = |GY1|}}
$!TWOVECTOR GRIDAREA {EXTENTS{Y2 = |GY2|}}
$!TWOVECTOR YDETAIL {TITLE {OFFSET = |YO|}}
$!TWOVECTOR YDETAIL {TITLE {TEXTSHAPE {HEIGHT = |ATH|}}}
$!TWOVECTOR YDETAIL {TICKLABEL {TEXTSHAPE {HEIGHT = |ALH|}}}
$!TWOVECTOR XDETAIL {TITLE {TEXTSHAPE {HEIGHT = |ATH|}}}
$!TWOVECTOR XDETAIL {TICKLABEL {TEXTSHAPE {HEIGHT = |ALH|}}}
$!ALTERDATA
  EQUATION = 'V8 = C'
$!RENAMEDATASETVAR
  VAR = 8
  NAME = "|CVARNAME|"

#dummy geometry to make sure all are clear
$!ATTACHGEOM
  RAWDATA
  1
  1
  1 1
$!PICK ADDALL
  SELECTGEOMS = YES
$!PICK CLEAR

$!PICK ADDALL
  SELECTTEXT = YES
$!PICK EDIT
  TEXTHEIGHTBYPERCENT = |TH|

```

```

$!LOOP 2
$!VarSet |XPOS| = |XPOS1|
$!IF |LOOP| == 2
$!VarSet |XPOS| = |XPOS2|
$!ENDIF
$!ATTACHGEOM
  POSITIONCOORDSYS = FRAME
  XYZPOS
  {
    X = |XPOS|
    Y = |GY1|
  }
  RAWDATA
  1
  2
  0 0
  -7.5 -6.81
$!ENDLOOP

$!FIELDLAYERS SHOWVECTOR = |VECTORS|
$!GLOBALCONTOUR COLORMAPFILTER{COLORMAPOVERRIDEACTIVE =
|OVERRIDE|}
$!GLOBALCONTOUR COLORMAPFILTER{COLORMAPOVERRIDE 1 {INCLUDE
= YES}}
$!GLOBALCONTOUR COLORMAPFILTER{COLORMAPOVERRIDE 1
{STARTLEVEL = 4}}
$!GLOBALCONTOUR COLORMAPFILTER{COLORMAPOVERRIDE 1
{ENDLEVEL = 6}}
$!GLOBALCONTOUR COLORMAPFILTER{COLORMAPOVERRIDE 1 {COLOR =
CUSTOM20}}

$!ENDLOOP
$!ENDLOOP
$!RemoveVar |MFBD|

```

aviexport.mcr

```

#!MC 900
$!VarSet |MFBD| = 'C:\Program Files\TEC90'
$!PROMPTFORTEXTSTRING |R|
  INSTRUCTIONS = "Enter number of data regions"
$!VarSet |Z| = (|NUMZONES|/|R|)
# $!VarSet |S| = 30
$!VarSet |S| = ((3/25)*|Z|)
$!LOOP |NUMFRAMES|
$!FRAMECONTROL PUSHTOP
$!ACTIVEFIELDZONES += [1-|NUMZONES|]

```



```

$!ACTIVEFIELDZONES -= [2-|NUMZONES|]
$!LOOP |R|
$!VarSet |A| = (((|LOOP|-1)*|Z|)+1)
$!ACTIVEFIELDZONES += [|A|]
$!ENDLOOP
$!ENDLOOP
$!EXPORTSETUP BITDUMPREGION = ALLFRAMES
$!EXPORTSETUP IMAGEWIDTH = 751
$!EXPORTSETUP EXPORTFORMAT = AVI
$!EXPORTSETUP ANIMATIONSPEED = |S|
$!PROMPTFORTEXTSTRING |fname|
  INSTRUCTIONS = "Enter file name (avi will be put in |MACROFILEPATH|).
Warning! If file already exists, it will be overwritten."
$!EXPORTSETUP EXPORTFNAME = "|MACROFILEPATH|\|fname|.avi"
$!EXPORTSTART
$!VarSet |N| = (|Z|-1)
$!LOOP |N|
$!VarSet |L|=(|LOOP|+1)
$!LOOP |NUMFRAMES|
$!FRAMECONTROL PUSHTOP
$!LOOP |R|
$!VarSet |A| = (((|LOOP|-1)*|Z|)+(|L|))
$!VarSet |D| = (((|LOOP|-1)*|Z|)+(|L|-1))
$!ACTIVEFIELDZONES += [|A|]
$!ACTIVEFIELDZONES -= [|D|]
$!ENDLOOP
$!ENDLOOP
$!EXPORTNEXTFRAME
$!ENDLOOP
$!EXPORTFINISH
$!RemoveVar |MFBD|

```

APPENDIX H. MATLAB AND TECPLOT CODES USED FOR JET IN CROSSFLOW
PIV EXPERIMENT

velvort2.mcr

```
#!/MC 900
$!VarSet |MFBD| = 'C:\Program Files\TEC90'

$!LOOP 1
$!PROMPTFORYESNO |fclear|
  INSTRUCTIONS = "All frames will be deleted. Continue?"
$!IF "|fclear|" == "No"
$!Continue
$!ENDIF
$!PROMPTFORYESNO |geomplot|
  INSTRUCTIONS = "Indicate jet hole location with lines on horizontal axis?"
$!PROMPTFORYESNO |ramp|
  INSTRUCTIONS = "Mask out area of ramp?"

$!PICK ADDALL
  SELECTFRAMES = YES
$!PICK CLEAR

$!INTERFACE
  AUTOREDRAWISACTIVE = FALSE
$!VarSet |H| = 7
$!VarSet |W| = 11
$!VarSet |ATH| = 4
$!VarSet |ALH| = 4
$!VarSet |YO| = 5
$!VarSet |TH| = 6
$!VarSet |GX1| = 7.5
$!VarSet |GX2| = 87.5
$!VarSet |GY1| = 8.237
$!VarSet |GY2| = 89.995
$!VarSet |XPOS1| = 27.048872180
$!VarSet |XPOS2| = 42.0864661654
$!VarSet |times| = 1
$!VarSet |skip| = 2
$!PROMPTFORTEXTSTRING |plot|
  INSTRUCTIONS = "Enter 1 to plot velocity, 2 for vorticity, or 3 to plot both."

$!IF |plot| == 1
  $!VarSet |times| = 1
$!ENDIF
$!IF |plot| == 2
  $!VarSet |times| = 2
```

```

$!ENDIF
$!IF |plot| == 3
  $!VarSet |times| = 2
  $!VarSet |H| = 4
  $!VarSet |W| = 6.286
  $!VarSet |ATH| = 4
  $!VarSet |ALH| = 4
  $!VarSet |YO| = 5
  $!VarSet |TH| = 6
  $!VarSet |GX1| = 7.5
  $!VarSet |GX2| = 87.5
  $!VarSet |GY1| = 8.237
  $!VarSet |GY2| = 89.995
  $!VarSet |XPOS1| = 27.048872180
  $!VarSet |XPOS2| = 42.0864661654
  $!VarSet |skip| = 4
$!PICK ADDALL
  SELECTFRAMES = YES
$!PICK COPY
$!PICK PASTE
$!ENDIF

$!PROMPTFORTEXTSTRING |R|
  INSTRUCTIONS = "Enter number of data regions to add."

$!LOOP |times|
$!FRAMECONTROL PUSHTOP
$!IF |LOOP| == 1
$!LOOP |R|
  $!IF |LOOP| == 1
    $!VarSet |data| = "|macrofilepath|\ "
  $!ENDIF
  $!PROMPTFORFILENAME |data|
    DIALOGTITLE = "Load Data File |LOOP|"
    DEFAULTFNAME = "|data|"
    FILEFILTER = "*.dat;*.plt"
  $!IF |LOOP| == 1
    $!VarSet |DN| = ""|data|"
  $!ENDIF
  $!IF |LOOP| > 1
    $!VarSet |DN| = '|DN| "|data|"'
  $!ENDIF
$!ENDLOOP

$!READDATASET ""|DN|"

```

```

$!IF |plot| == 2
  $!Continue
  $!ENDIF
  $!VarSet |CONTVAR| = 5
  $!VarSet |CONTMIN| = 0.5
  $!VarSet |CONTMAX| = 3
  $!VarSet |NUMLEVELS| = 8
  $!VarSet |RS| = 2.5
  $!VarSet |RH| = 4
  $!VarSet |LX| = 92.3
  $!VarSet |LY| = 90.3
  $!VarSet |CVARNAME| = "Velocity (m/s)"
  $!FRAMENAME = "Velocity"
  $!VarSet |CFORMAT| = "FIXEDFLOAT"
  $!VarSet |VECTORS| = "YES"
  $!VarSet |OVERRIDE| = "NO"
  $!VarSet |YPOS| = 0.5
  $!ENDIF
  $!IF |LOOP| == 2
    $!VarSet |CONTVAR| = 7
    $!VarSet |CONTMIN| = -200
    $!VarSet |CONTMAX| = 200
    $!VarSet |NUMLEVELS| = 9
    $!VarSet |RS| = 2.2
    $!VarSet |RH| = 4
    $!VarSet |LX| = 92.5
    $!VarSet |LY| = 90.3
    $!VarSet |CVARNAME| = "Vorticity (s^-1)"
    $!FRAMENAME = "Vorticity"
    $!VarSet |CFORMAT| = "INTEGER"
    $!VarSet |VECTORS| = "NO"
    $!VarSet |OVERRIDE| = "YES"
    $!VarSet |YPOS| = 0.5
    $!IF |plot| == 3
      $!VarSet |YPOS| = 4.5
      $!READDATASET "|DN|"
    $!ENDIF
  $!ENDIF

```

```

$!FRAME LAYOUT SHOWHEADER = NO
$!FRAME LAYOUT SHOWBORDER = NO
$!FRAME LAYOUT XYPOS {X = 0}
$!FRAME LAYOUT XYPOS {Y = |YPOS|}
$!FRAME LAYOUT HEIGHT = |H|
$!FRAME LAYOUT WIDTH = |W|

```

```

$!FIELDLAYERS SHOWMESH = NO
$!FIELDLAYERS SHOWBOUNDARY = NO
$!GLOBALCONTOUR VAR = |CONTVAR|
$!FIELDLAYERS SHOWCONTOUR = YES
$!CONTOURLEVELS DELETERANGE
  RANGEMIN = |MINC|
  RANGEMAX = |MAXC|
$!VarSet |D| = ((|CONTMAX|-|CONTMIN|)/(|NUMLEVELS|-1))
$!LOOP |NUMLEVELS|
$!VarSet |CONT| = (|CONTMIN| + (|LOOP| - 1)*|D|)
$!CONTOURLEVELS ADD
  RAWDATA
  1
  |CONT|
$!ENDLOOP
$!GLOBALCONTOUR LEGEND{SHOW = YES}
$!GLOBALCONTOUR LEGEND{SHOWHEADER = NO}
$!GLOBALCONTOUR LEGEND{ROWSPACING = |RS|}
$!GLOBALCONTOUR LEGEND{TEXTSHAPE{HEIGHT = |RH|}}
$!GLOBALCONTOUR LEGEND{XYPOS{X = |LX|}}
$!GLOBALCONTOUR LEGEND{XYPOS{Y = |LY|}}
$!GLOBALCONTOUR LEGEND{NUMFORMAT{FORMATTING = |CFORMAT|}}
$!GLOBALCONTOUR LEGEND{NUMFORMAT{PRECISION = 2}}
$!GLOBALCONTOUR LEGEND{BOX{BOXTYPE = NONE}}
$!GLOBALTWOVECTOR UVAR = 3
$!GLOBALTWOVECTOR VVAR = 4
$!RESETVECTORLENGTH
$!FIELDLAYERS SHOWVECTOR = YES
$!FIELD [1-|NUMZONES|] VECTOR{IJKSKIP{I = |skip|}}
$!FIELD [1-|NUMZONES|] VECTOR{IJKSKIP{J = |skip|}}
$!FIELD [1-|NUMZONES|] VECTOR{ISTANGENT = YES}
$!FIELD [1-|NUMZONES|] VECTOR{COLOR = BLACK}
$!FIELD [1-|NUMZONES|] VECTOR{PATTERNLENGTH = 5}
$!GLOBALTWOVECTOR RELATIVELENGTH = 1
$!GLOBALTWOVECTOR HEADSIZEASFRACTION = 0.3
$!GLOBALFRAME PRESERVEAXISSCALE = NO
$!VarSet |YMAX| = ((CEIL(|MAXV02|/10))*10)
$!VarSet |XMIN| = ((FLOOR(|MINV01|/5))*5)
$!VarSet |XMAX| = ((CEIL(|MAXV01|/5))*5)
$!TWOAXIS YDETAIL{RANGEMIN = 0}
$!TWOAXIS YDETAIL{RANGEMAX = |YMAX|}
$!TWOAXIS XDETAIL{RANGEMIN = |XMIN|}
$!TWOAXIS XDETAIL{RANGEMAX = |XMAX|}
$!GLOBALFRAME PRESERVEAXISSCALE = YES
$!TWOAXIS YDETAIL{AUTOGRID = NO}
$!TWOAXIS YDETAIL{GRSPACING = 10}

```

```

$!TWO DAXIS XDETAIL {AUTOGRID = NO}
$!TWO DAXIS XDETAIL {GRSPACING = 25}
$!TWO DAXIS YDETAIL {AXISPOSITION = |GX1|}
$!TWO DAXIS GRIDAREA {EXTENTS {X1 = |GX1|}}
$!TWO DAXIS GRIDAREA {EXTENTS {X2 = |GX2|}}
$!TWO DAXIS XDETAIL {AXISPOSITION = |GY1|}
$!TWO DAXIS GRIDAREA {EXTENTS {Y1 = |GY1|}}
$!TWO DAXIS GRIDAREA {EXTENTS {Y2 = |GY2|}}
$!TWO DAXIS YDETAIL {TITLE {OFFSET = |YO|}}
$!TWO DAXIS YDETAIL {TITLE {TEXTSHAPE {HEIGHT = |ATH|}}}
$!TWO DAXIS YDETAIL {TICKLABEL {TEXTSHAPE {HEIGHT = |ALH|}}}
$!TWO DAXIS XDETAIL {TITLE {TEXTSHAPE {HEIGHT = |ATH|}}}
$!TWO DAXIS XDETAIL {TICKLABEL {TEXTSHAPE {HEIGHT = |ALH|}}}
$!ALTERDATA
  EQUATION = 'V8 = C'
$!RENAMEDATASETVAR
  VAR = 8
  NAME = "|CVARNAME|"

#dummy geometry to make sure all are clear
$!ATTACHGEOM
  RAWDATA
  1
  1
  1 1
$!PICK ADDALL
  SELECTGEOMS = YES
$!PICK CLEAR

$!PICK ADDALL
  SELECTTEXT = YES
$!PICK EDIT
  TEXTHEIGHTBYPERCENT = |TH|

$!IF "|ramp|" == "Yes"
$!ATTACHGEOM
  POSITIONCOORDSYS = GRID
  XYZPOS
  {
  X = -40
  Y = 0
  }
  FILLCOLOR = BLACK
  ISFILLED = YES
  RAWDATA
  1

```

```
5
0 0
0 14
18.8 23.5
26.3 0
0 0
$!ENDIF
```

```
$!IF "|geomplot|" == "Yes"
$!LOOP 2
$!VarSet |XPOS| = |XPOS1|
$!IF |LOOP| == 2
$!VarSet |XPOS| = |XPOS2|
$!ENDIF
$!ATTACHGEOM
POSITIONCOORDSYS = FRAME
XYZPOS
{
X = |XPOS|
Y = |GY1|
}
RAWDATA
1
2
0 0
0 -6.81
$!ENDLOOP
$!ENDIF
```

```
$!FIELDLAYERS SHOWVECTOR = |VECTORS|
$!GLOBALCONTOUR COLORMAPFILTER{COLORMAPOVERRIDEACTIVE =
|OVERRIDE|}
$!GLOBALCONTOUR COLORMAPFILTER{COLORMAPOVERRIDE 1 {INCLUDE
= YES}}
$!GLOBALCONTOUR COLORMAPFILTER{COLORMAPOVERRIDE 1
{STARTLEVEL = 4}}
$!GLOBALCONTOUR COLORMAPFILTER{COLORMAPOVERRIDE 1
{ENDLEVEL = 6}}
$!GLOBALCONTOUR COLORMAPFILTER{COLORMAPOVERRIDE 1 {COLOR =
CUSTOM20}}

$!ENDLOOP
$!ENDLOOP
$!RemoveVar |MFBD|
```

PIVplot3D.m

```
clear all
close all

for g=1:1
tic
fmax=7;
numx=149;
numy=97;
num=numx*numy;
fname1=['G:\Moore\PIV\FreeJe~1\Crossflow\041221\f05dc50b05y-1\f05dc50b05y-1.dat'];
fname2=['G:\Moore\PIV\FreeJe~1\Crossflow\041221\f05dc50b05y0\f05dc50b05y0.dat'];
fname3=['G:\Moore\PIV\FreeJe~1\Crossflow\041221\f05dc50b05y1\f05dc50b05y1.dat'];
fname4=['G:\Moore\PIV\FreeJe~1\Crossflow\041221\f05dc50b05y2\f05dc50b05y2.dat'];
fname5=['G:\Moore\PIV\FreeJe~1\Crossflow\041221\f05dc50b05y3\f05dc50b05y3.dat'];
fname6=['G:\Moore\PIV\FreeJe~1\Crossflow\041221\f05dc50b05y4\f05dc50b05y4.dat'];
fname7=['G:\Moore\PIV\FreeJe~1\Crossflow\041221\f05dc50b05y5\f05dc50b05y5.dat'];
fname8=['G:\Moore\PIV\FreeJe~1\Crossflow\all3DdataB05.dat'];
b=1;
while b ~= 0
fid=fopen(fname8,'a');
fseek(fid,0,1);
b=ftell(fid);
if b == 0
break
end
fclose(fid);
fndisp=fname8;
l=length(fndisp);
i=1;
while i <= l
if strcmp(fndisp(i),'\')==1
fndisp(i+2:(length(fndisp)+1))=fndisp(i+1:(length(fndisp)));
fndisp(i+1)='\';
i=i+1;
l=l+1;
end
i=i+1;
end
beep;
fname8=input(['Error creating ' fndisp '\nFile already exists. Please input another file name. \n>>'],'s');
end
fname=char(fname1,fname2,fname3,fname4,fname5,fname6,fname7,fname8);
for j=1:100
```



```

time(j)=(j-1)*0.02;
for i=1:fmax
y(i)=(i-2)*25.4;
if i == 4
y(i)=2.25*25.4;
end
if i==fmax
y(i)=5.25*25.4;
end
data=dlmread(fname(i,:),\t',[(2+(num+3)*(j-1)) 0 (((num+3)*j)-2) 6]);
data(:,8)=y(i);
data(:,9)=0;
if ((j == 1) & (i == 1))
vars = [' VARIABLES = "X (mm)", "Z (mm)", "U (m/s)", "W (m/s)", "Mag (m/s)", "Ang
(rad)", "Vort (s^-1)", "Y (mm)", "V (m/s)"];
fid=fopen(fname((fmax+1),:),'a');
fprintf(fid,'%s\r\n',vars);
end
clc
disp(['Creating Output File (Zone ' num2str(j) ' of 100)...']);
if i==1
zone=([' zone t="Time = ' num2str(time(j),'%5.3f') 's", i=' num2str(numx) ' j='
num2str(numy) ' k=' num2str(fmax) ]]);
fprintf(fid,'%s\r\n',zone);
end
fprintf(fid,'%8.3ft %8.3ft %8.3ft %8.3ft %8.3ft %8.3ft %8.3ft %8.3ft
%8.3fr\n',data');
if i==fmax
text=([' text x=50, y=93.5, t="&(VARNAME:10) at &(ZONENAME:' num2str(j) ')",
AN=CENTER, F=COURIER-BOLD, CS=FRAME, H=4, ZN=' num2str(j) ]]);
fprintf(fid,'%s\r\n\r\n',text);
end
end
end
%button = questdlg('Convert output file(s) to Tecplot binary file?','ASCII to
Binary','No');
button = 'Yes';
if strcmp(button,'Yes') == 1
dos(['preplot ' fname((fmax+1),:)' '.dat']);
end
end
fclose(fid);
e=toc;
hour1=e/3600;
hour=floor(hour1);
e1=e-(3600*hour);

```

```
min1=e1/60;  
min=floor(min1);  
sec=round(e1-(60*min));  
disp(['Time Elapsed (h:m:s) - ' num2str(hour) ':' num2str(min) ':' num2str(sec)
```

REFERENCES

1. Lake J.P. *Flow Separation Prevention on a Turbine Blade in Cascade at Low Reynolds Number*. Ph.D. Dissertation, Air Force Institute of Technology, Dayton, OH, 1999.
2. Rivir R., White A., Carter C., and Ganguly B. "AC and Pulsed Plasma Flow Control." *42nd Aerospace Sciences Meeting and Exhibit*, Reno, NV, AIAA 2004-847, 2004.
3. List J., Byerley A., McLaughlin T., and Van Dyken R. "Using a Plasma Actuator to Control Laminar Separation on a Linear Cascade Turbine Blade." *41st Aerospace Sciences Meeting and Exhibit*, Reno, NV, AIAA 2003-1026, 2003.
4. Bons J., Sondergaard R., and Rivir R. "Turbine Separation Control Using Pulsed Vortex Generator Jets." *ASME Journal of Turbomachinery*, Vol. 123, No. 4, pp. 198-206, 2001.
5. Bons J., Sondergaard R., and Rivir R. "The Fluid Dynamics of LPT Blade Separation Control Using Pulsed Jets." *ASME Journal of Turbomachinery*, Vol. 124, No. 1, pp. 77-85, 2002.
6. Johari, H. and McManus, K.R., "Visualization of Pulsed Vortex Generator Jets for Active Control of Boundary Layer Separation," *28th AIAA Fluid Dynamics Conference*, Snowmass Village, CO, AIAA 97-2021, 1997.
7. Compton, D.A. and Johnston, J.P., "Streamwise Vortex Production by Pitched and Skewed Jets in a Turbulent Boundary Layer," *AIAA Journal*, Vol. 30, No. 3, pp. 640-647, March 1992.
8. Bons, J., Sondergaard, R., and Rivir, R. "Control of Low-Pressure Turbine Separation Using Pulsed Vortex Generator Jets," *37th AIAA Aerospace Sciences Meeting and Exhibit*, Reno, NV, AIAA 99-0367, January 1999.
9. Milanovic, I.M., and Zaman, K.B.M.Q. "Highly Inclined Jets in Cross-Flow," *41st Aerospace Sciences Meeting and Exhibit*, Reno, NV, AIAA 2003-0183, January 2003.
10. Heinzen, S., Hall, C. and Chokani, N. "In-Flight Application of Active Separation Control Using Pulsed Jet Blowing," *40th AIAA Aerospace Sciences Meeting & Exhibit*, Reno, NV, 2002-0416, January 2002.
11. McManus, K.R., Legner, H.H., and Davis, S.J. "Pulsed Vortex Generator Jets for Active Control of Flow Separation," *25th AIAA Fluid Dynamics Conference*, Colorado Springs, CO, AIAA 94-2218, June 1994.

12. McManus, K., Ducharme, A., Goldey, C., and Magill, J. "Pulsed Jet Actuators for Suppressing Flow Separation," *34th AIAA Aerospace Sciences Meeting and Exhibit*, Reno, NV, AIAA 96-0442, January 1996.
13. McManus, K. and Magill, J. "Separation Control in Incompressible and Compressible Flows Using Pulsed Jets," *27th AIAA Fluid Dynamics Conference*, New Orleans, LA, AIAA 96-1948, June 1996.
14. McManus, K. and Magill, J. "Airfoil Performance Enhancement Using Pulsed Jet Separation Control," *AIAA 4th Shear Flow Control Conference*, Snowmass Village, CO, AIAA 97-1971, June 1997.
15. Bons, J., Sondergaard, R., and Rivir, R. "Turbine Separation Control Using Pulsed Vortex Generator Jets," *ASME Journal of Turbomachinery*, Vol. 123, No. 4, pp. 198-206, 2001.
16. Bons, J., Sondergaard, R., and Rivir, R. "The Fluid Dynamics of LPT Blade Separation Control Using Pulsed Jets," *ASME Journal of Turbomachinery*, Vol. 124, No. 1, pp. 77-85, 2002.
17. Raffel, M., Willert, C., and Kompenhans, J. *Particle Image Velocimetry: A Practical Guide*, pp. 136-139, Springer-Verlag, Berlin, 1998.
18. Huang H., Dabiri D., and Gharib M. "On Errors of Digital Particle Image Velocimetry." *Measurement Science and Technology*, Vol. 8, No. 12, pp. 1427-1440, 1997.
19. Raffel, M., Willert, C., and Kompenhans, J. *Particle Image Velocimetry: A Practical Guide*, Springer-Verlag, Berlin, 1998.
20. *FlowMap Particle Image Velocimetry Instrumentation, Installation and User's Guide*, Dantec Measurement Technology A/S, Denmark, 2000.
21. Saad, M.A., *Compressible Fluid Flow*, 2nd Ed., p. 98, Prentice Hall, New Jersey, 1993.

BIOGRAPHICAL SKETCH

Kenneth J. Moore, Jr. was born August 2, 1980, in Santa Clara, California. He moved to Columbus, Ohio in 1982. He went to Cedarville University, in Cedarville, Ohio from 1998-2002 and obtained a Bachelor of Science in Mechanical Engineering. Upon graduation, he immediately began work on his Masters of Science in Mechanical Engineering at Wright State in Dayton, Ohio.